EPA 600/3-81-046
July 1981

EARLY DIAGENESIS AND CHEMICAL MASS TRANSFER IN LAKE ERIE SEDIMENTS

by

Gerald Matisoff

J. Berton Fisher

Department of Geological Sciences

Case Western Reserve University

Cleveland, OH 44106

and

Wilbert Lick

Department of Mechanical & Environmental Engineering

University of California

Santa Barbara, CA 93106

Contract No. R805716020

Project Officer

David Dolan

Large Lakes Research Station

Environmental Research Laboratory -- Duluth

Grosse Ile, MI 48138

U.S. ENVIRONMENTAL PROTECTION AGENCY

OFFICE OF RESEARCH AND DEVELOPMENT

ENVIRONMENTAL RESEARCH LABORATORY

DULUTH, MN. 55804

TECHNICAL REPORT DATA
(Please read Instructions on the reverse before completing)

1. REPORT NO. EPA-600/3-81-046	2. ORD Report	3. RECIPIENT'S ACCESSION NO. PB82-247602
4. TITLE AND SUBTITLE Early Diagenesis and Chemical Mass Transfer in Lake Erie Sediments		5. REPORT DATE July 1981
		6. PERFORMING ORGANIZATION CODE
7. AUTHOR(S) Gerald Matisoff, J. Berton Fisher and Wilbert Lick*, Dept. of Mechanical & Environmental Eng., University of California, Santa Barbara, California 93106		8. PERFORMING ORGANIZATION REPORT NO.
9. PERFORMING ORGANIZATION NAME AND ADDRESS Department of Geological Sciences Case Western Reserve University Cleveland, Ohio 44106		10. PROGRAM ELEMENT NO. 1BA769
		11. CONTRACT/GRANT NO. R805716
12. SPONSORING AGENCY NAME AND ADDRESS U.S. Environmental Protection Agency Large Lakes Research Station Environmental Research Laboratory-Duluth 9311 Groh Road, Grosse Ile, Michigan 48138		13. TYPE OF REPORT AND PERIOD COVERED Final
		14. SPONSORING AGENCY CODE
15. SUPPLEMENTARY NOTES		

16. ABSTRACT

Vertical profiles of pore water and sediment solids chemistry were obtained from two sites in Lake Erie. Samples were collected using both gravity coring and pore water "peeper" techniques. In general, concentrations of nutrients and toxic metals in sediment solids decreased with increasing depth. Comparison of pore water "peeper" data to gravity core data showed that "peeper" data provides higher resolution near the sediment-water interface. The thermodynamic tendency of metal phosphate and carbonate mineral phases to precipitate in Lake Erie sediments has been calculated by means of an ion-pair model of the interstitial water chemistry. The calculations suggest that detrital calcite, aragonite, and dolomite should be dissolving in the sediments, but that iron and manganese carbonates should be precipitating. Regenerated phosphate should be reacting with calcium, iron, manganese, and lead to form authigenic mineral phases. Whitlockite ($Ca_3(PO_4)_2$) and not hydroxylapatite ($Ca_5(PO_4)_3OH$) is the predicted mineral phase controlling phosphate solubility. Rates of anaerobic decomposition of Lake Erie sediments from one locality were determined for seven depth intervals at three temperatures. Concentration increases of bicarbonate, phosphate, ammonium, calcium, magnesium, iron, and manganese in pore water within any given depth interval followed zeroth order kinetics and exhibited Arrhenius temperature dependency. The observed release rates decrease exponentially with depth in the sediment due to a corresponding decrease in the amount of oxidizable organic matter and acid hydrolyzable mineral phases.

17. KEY WORDS AND DOCUMENT ANALYSIS

a. DESCRIPTORS	b. IDENTIFIERS/OPEN ENDED TERMS	c. COSATI Field/Group
Diagenesis Sediments Decomposition Reactions	Geological Sedimentation Precipitates Fermentation	08/D 08/H

18. DISTRIBUTION STATEMENT	19. SECURITY CLASS *(This Report)*	21. NO. OF PAGES 197
	20. SECURITY CLASS *(This page)*	22. PRICE

EPA Form 2220-1 (9-73)

DISCLAIMER

This report has been reviewed by the Large Lakes Research Station, U.S. Environmental Protection Agency, and approved for publication. Approval does not signify that the contents necessarily reflect the views and policies of the U.S. Environmental Protection Agency, nor does the mention of trade names or commercial products constitute endorsement or recommendation for use.

Abstract

Vertical profiles of pore water and sediment solids chemistry were obtained from two sites in Lake Erie. Samples were collected using both gravity coring and pore water "peeper" techniques. In general, concentrations of nutrients and toxic metals in sediment solids decreased with increasing depth. Comparison of pore water "peeper" data to gravity core data showed that "peeper" data provides higher resolution near the sediment-water interface. Modifications of the present peeper are required to adequately sample easily oxidizable materials (e.g. ammonia, ferrous iron).

The thermodynamic tendency of metal phosphate and carbonate mineral phases to precipitate in Lake Erie sediments has been calculated by means of an ion-pair model of the interstitial water chemistry. The calculations suggest that detrital calcite, aragonite, and dolomite should be dissolving in the sediments, but that iron and manganese carbonates should be precipitating. Regenerated phosphate should be reacting with calcium, iron, manganese, and lead to form authigenic mineral phases. Whitlockite (Ca_3 $(PO_4)_2$) and not hydroxylapatite (Ca_5 $(PO_4)_3$ OH) is the predicted mineral phase controlling phosphate solubility. Zinc and cadmium are apparently controlled by other mechanisms, perhaps by sulfide phases, mixed mineral phases, adsorption and/or ion exchange equilibria.

Rates of anaerobic decomposition of Lake Erie sediments from one locality were determined for seven depth intervals at three temperatures. Sealed sediment sections were incubated under anoxic conditions and the interstitial waters were sampled over a period of approximately 200 days. Concentration increases of bicarbonate, phosphate, ammonium, calcium, magnesium, iron, and manganese in pore water within any given depth interval followed zeroth order

kinetics and exhibited Arrhenius temperature dependency. The rates and energetics of these fermentation reactions are only slightly less than those reported from sediments undergoing sulfate reduction. The observed release rates decrease exponentially with depth in the sediment due to a corresponding decrease in the amount of oxidizable organic matter and acid hydrolyzable mineral phases.

A stoichiometric model was constructed utilizing the observed release rates and assumed chemical reactions to predict the stoichiometry of the decomposing organic matter and the nature of the hydrogen buffer.

The flux of nutrients and metals from Lake Erie sediments to anoxic overlying water were studied in laboratory microcosms. Three cases were investigated: 1) homogenized sediment without worms, 2) homogenized sediment preconditioned by tubificid worm activities, 3) natural lake cores. Flux estimates were made using both direct (concentration changes in the overlying water) and indirect (pore water concentration gradients) techniques. Tubificids were found to increase the flux of ammonia, and decrease the flux of iron, soluble reactive phosphorous, and soluble reactive silica. The presence of tubificids had no effect on bicarbonate flux. Fluxes observed in the natural lake core experiment were similar to those observed in the homogenized sediment with tubificids. Mineral equilibrium calculations performed for the pore water data collected in these experiments showed that the laboratory microcosms provided a reasonable representation of chemical conditions in Lake Erie sediments. Comparison of direct and indirect flux estimates showed that both types of estimate had high variability. In general, indirect flux estimates were higher than direct flux estimates.

Field measurements and data from the production experiment were used to calculate loads and losses of metals (Cu, Pb, Zn) and nutrients (organic nitrogen) to and from Lake Erie sediments. It was found that man's influence

on metals was Zn>>Pb>Cu. The natural abundance ratio is Zn>Cu>Pb. Further, it was found that the inclusion of organic decomposition in the calculation of apparent anthropogenic nitrogen loading to Lake Erie sediments resulted in a significant decrease (about a factor of two) in the estimate of anthropogenic loading.

The time dependent behavior of ammonia and bicarbonate in the homogenized sediments lacking a tubificid population could be well approximated by a one dimensional time dependent transport-reaction model. More complex models are needed to provide adequate descriptions for other parameters and situations (real lake sediments, homogenized sediments with tubificids).

Contents

	Page
Disclaimer	ii
Abstract	iii
Figures	viii
Tables	xii
1. Introduction	1
2. Conclusions	2
3. Methods and Materials	5
Field Measurements	5
Study Area	5
Core Collection	7
Pore Water Peeper	8
Laboratory Experiments	8
Production Experiment	8
Flux Experiment	11
4. Results	16
Field Measurements	16
Production Experiment	28
Release Kinetics	28
Depth Dependency	33
Temperature Dependency	40
Flux Experiment	44
Overlying Water Chemistry	44
Interstitial Water Chemistry	48
Chemistry of the Sediment Solids	53
5. Discussion	64

Page

Mineral Equilibria 64

Calculation of Activities 66

Calculation of Ion Activity Products 68

Field Measurements 71

Production Experiment 75

Flux Experiment 78

Mineral Equilibria in Anoxic Lake Sediments 86

Stoichiometric Model 92

Solid Phase Prediction 97

Prediction of Pore Water Concentration 100

Direct and Indirect Flux EStimates 102

Laboratory Flux Experiments 103

Lake Core Experiments 107

Field Cores 108

Load and Loss Calculations 108

Metals 108

Nutrients 126

Prediction of Pore Water Chemistry 133

6. References 138

7. Appendices 147

I. Chemical Methods 147

II. Field Core Data 158

III. Production Experiment Data 165

IV. Flux Experiment Data 171

FIGURES

Number		Page
1	Field sampling localities in Lake Erie.	6
2	Apparatus used for the flux experiment: 1. Sampling cover 2. Detachable top 3. Overlying water reservoir 4. Sediment chamber 5. Extruder piston 6. Extruder base 7. Quick connect valve 8. Turbine magnetic stirrer.	13
3	Total and organic carbon versus depth at Station 83	17
4	Total and organic carbon versus depth at Station A1	18
5	Acid volatile sulfide versus depth at Station 83.	19
6	Total sulfur versus depth at Station 83	20
7	Total Kjeldahl nitrogen versus depth at Station 83	21
8	Total Kjeldahl nitrogen versus depth at Station A1.	22
9	Total phosphorous versus depth at Station 83.	23
10	Total phosphorous versus depth at Station A1.	24
11	Vertical profiles of ferrous iron, ammonia, and SRP in the interstitial water of sediments at Station A1 determined by both gravity coring and pore water "peeper" technique.	26
12	Vertical profiles of chloride, alkalinity, and SRS in the interstitial water of sediments at Station A1 determined by both gravity coring and pore water "peeper" technique.	27
13	Ammonia concentration data and derived regression line from the production experiment for three temperatures and four depths.	30
14	Ammonia production rate, R_{NH4}, versus total Kjeldahl nitrogen . . .	32
15	Ammonia production rate at three temperatures as a function of depth.	34
16	Bacterial abundance as a function of depth at Station 83.	39

17 Excess Pb-120 versus depth at Station 83 41

18 Concentration of ammonia, ferrous iron, alkalinity, SRP, and SRS and pH in the overlying water of homogenized mud experiment cores. C-with tubificide, T-without tubificide . . . 45

19 Concentration of ammonia, ferrous iron, alkalinity, SRP, and SRS and pH in the overlying water of a lake core experiment core. (LCE-4) 47

20 Vertical profiles of ammonia, ferrous iron, alkalinity, SRP, and SRS in the homogenized mud experiment cores without worms. . 49

21 Vertical profiles of ammonia, ferrous iron, alkalinity, SRP, and SRS in the homogenized mud experiment cores with worms . . . 50

22 Vertical profiles of ammonia, ferrous iron, alkalinity, SRP, and SRS in the lake core experiment cores 52

23 Total and organic carbon in homogenized mud core R (+72 days). . . 54

24 Total and organic carbon in homogenized mud core T (+169 days) . . 55

25 Total and organic carbon in lake core 6 (+13 days) 56

26 Total Kjeldahl nitrogen in homogenized mud core R (+72 days) . . . 57

27 Total Kjeldahl nitrogen in homogenized mud core T (+169 days) . . 58

28 Total Kjeldahl nitrogen in lake core experiment core 6 (+13 days) 59

29 Total phosphorus in homogenized mud core R (+72 days) 60

30 Total phosphorus in homogenized mud core T (+169 days) 61

31 Total phosphorus in lake core experiment core 6 (+13 days) 62

32 Saturation index versus depth for interstitial water from a typical Station 83 core for calcide ($CaCO_3$), siderite ($FeCO_3$), rhodochrosite ($MnCO_3$), smithsonite ($ZnCO_3$), and cerrussite ($PbCO_3$). 72

33 Saturation index versus depth for interstitial waters from a typical Station 83 core for vivianite ($Fe_3(PO_4)_2 \cdot 8H_2O$), whitelockite ($Ca_3(PO_4)_2$), reddingite ($Mn_3(PO_4)_2 \cdot 3H_2O$), hydroxylapatite ($Ca_5(PO_4)_3OH$), hydroxylpyromorphyte ($Pb_5(PO_4)_3OH$), chlorophyromorphite ($Pb_5(PO_4)_3Cl$), α-hopeite ($Zn_3(PO_4)_2 \cdot 4H_2O$), and struvite ($MgNH_4PO_4 \cdot 6H_2O$). 73

34 Saturation indices over time for siderite, rhodochrosite, calcite and magnesite observed in the production experiment . . 76

35 Saturation indices over time for vivianite, hydroxylapatite, reddingite, whitlockite, fluorapatite, and struvite observed in the production experiment 77

36 Saturation indices for carbonate and phosphate phases observed in the homogenized mud core experiment 82

37 Saturation indices for carbonate phases observed in the lake core experiment 84

38 Saturation indices for phosphate phases observed in the lake core experiment 85

39 Rate of carbonate production ($R'_{HCO\bar{3}}$) versus the sum of the rates of calcium (R'_{Ca}), iron (R'_{Fe}) and manganese (R'_{Mn}) production for three temperatures 95

40 Phosphorus flux estimates versus iron flux estimates (direct and indirect) for the homogenized mud core experiment (with and without worms) and the lake core experiment 109

41 Schematic diagram of the simplified two-compartment model. F_1 represents natural flux to the lake. F_{12} represents the flux of metal from compartment 1, the lake water (dissolved and particulate) to the sediments. F_{21} is the flux of metal in the opposite direction. F_3 represents export from the lake to the Niagara River and the Welland Canal. F_2 is the anthropogenic flux to the lake 116

42 Model predictions of Zn, Pb, and Cu concentrations in Lake Erie water to the year 2075 124

43 Model predictions of Zn, Pb, and Cu concentrations in Lake Erie sediments (Station 83) to the year 2075 125

44 Water content (%H_2O) versus depth at Station 83 129

45 K_1 as a function of time of sediment deposition at Station 83 . . 130

46 Present day particulate organic nitrogen concentration (Np) and calculated organic nitrogen concentrations at the time of deposition (N_{pO}) plotted versus depth and time of deposition at Station 83 132

47 Observed and calculated concentration profiles of ammonia and alkalinity ($HCO\bar{3}$) for the homogenized mud core experiment (without worms). 137

TABLES

Number		Page
1	Apparent rates of release of nutrients and metals observed in the production experiment. All units are millimoles/l/yr.	29
2	Depth dependencies of rates of production from the equation $R'(Z,T) = R'_o(T) \exp(-\alpha(T) \cdot A)$. Units are R'_o (millimoles/l/yr) and α (cm^{-1})	35
3	Temperature dependencies of the rates of production from the equation $R'_o(T) = A_o \exp(-E^*/RT)$. $R'_o(T)$ (millimoles/l/yr) is the production rate at the sediment water interface; A_o (millimoles/l/yr) is the pre-exponential factor, E^* (KCal/mole) is the activation energy; and R (1.9872 cal/mole/^oK) is the gas constant	42
4	Comparision of averaged concentrations (-log molality) and one standard deviation of major species given in Nordstrom et al. (1979) and those of our model ASAME	69
5	Solubility constants of potential authigenic mineral phases.	70
6	Major ion data used in the mineral equilibrium calculations for the homogenized mud core experiment.	79
7	Major ion data used in the mineral equilibrium calculations for the lake core experiment	80
8	Stoichiometric model of decomposing Lake Erie sediments.	93-94
9	Comparison of calculated solids distribution based on eq. (12) to observed data. Depth interval 0-7 cm.	99
10	Diffusion coefficients used for indirect flux calculations	104
11	Direct and indirect flux estimates obtained from the lake core experiment and the homogenized mud core experiment. SRP flux is reported as moles P/m^2/day. *tubificid population present, **zero values not considered in calculation of mean and variance (before anoxia). n.d. = not determined.	105

12 Indirect flux estimates determined from field measurements at Station 83 and Station A1. Units are $x10^{-6}$ moles/m^2/day . . 110

13 Summary of the direct flux calculations for Stations 83 and A1. Negative fluxes indicate a flux to the sediments. Units are $x10^{-6}$ moles/m^2/day 111

14 Inventory of sources and sinks of heavy metals in Lake Erie . . . 118

15 Values for D, K, R, Co, and Ci used in the time dependent ammonia and bicarbonate transport-reaction calculations 136

Introduction

Lacustrine sediments are known to play an active role in the biogeochemical cycling of materials. Freshwater sediments act as both a source and a sink for many biologically important materials, notably nutrients, such as phosphorous, carbon, nitrogen, sulfur, and silicon. Further, sediments are known to play an important role in resulting cycles of trace metals, radionuclides, and xenobiotics. Because of this, knowledge of the early chemical diagenesis of sediments, that is those reactions occuring during and after burial, is essential to an understanding of materials cycling in freshwater environments.

The present study has focused on the chemistry of nutrient and metal release during early diagenesis, rates of nutrient and metal regeneration, rates of materials' movement across the sediment-water interface, and the effects of bioturbation on materials' cycling.

An experimental approach has been used in this study; the chemistry of nutrient and metal regeneration has been studied in laboratory microcosms. In addition, field observations of pore water chemistry and sediment solids chemistry have been used to verify and test results obtained in the laboratory.

Conclusions

Thermodynamic modeling of interstitial waters is a useful technique for suggesting possible mineralogical controls on trace metals. Application of such a model to Lake Erie pore waters reveals that iron and manganese carbonates, phosphates, and sulfides are all forming in the sediments as well as chlorophyromorphite, a lead phosphate. No mineralogical controls for zinc and cadmium were clearly identified. The inclusion of organic complexes or complexes yet to be discovered in the thermodynamic model will not significantly improve the results. Additional complexing only serves to lower the ion activity products, and hence the saturation indices. Predicted supersaturation would be decreased, but not by more than about a factor of two. Undersaturation of zinc and cadmium phases would increase. Mixed and sulfide mineral phases are the most likely mineralogical controls on zinc and cadmium. It is also possible that the controlling reactions could be adsorption or ion exchange equilibrium. Until more sophisticated techniques for examining sediment solids are employed and until existing thermodynamic data is critically compiled and adopted, no further progress on this problem can be made.

Knowledge of the rate of anaerobic decomposition of organic matter and subsequent release of nutrients and metals to pore waters is essential to an understanding of early diagenesis and chemical mass transfer in sediments. In Lake Erie, anaerobic decomposition proceeds via fermentation reactions, primarily methane fermentation. The rates and energentics of these fermentation reactions are only slightly less than those reported from sediments in which sulfate reduction is the primary diagenetic pathway.

Both direct and indirect estimates of the flux of ammonia, iron, soluble reactive phosphorous (SRP), soluble reactive silica (SRS), and bicarbonate from lake sediments to anoxic overlying water exhibit a high degree of vari-

ability. Further, indirect flux estimates for redox sensitive materials (i.e. ferrous iron and SRP) may grossly underestimate the actual flux. The initial flux of iron and phosphorous from sediments to anoxic overlying water is strongly dependent on conditions at the sediment-water interface prior to anoxia in the overlying water. Sediments preconditioned by the activities of tubificid oligochaetes exhibited a higher flux of ammonia, but a lower flux of iron, SRP, and SRS. The presence of worms had no effect on bicarbonate flux. The higher flux of ammonia in the presence of worms appeared to be due to a worm-caused ammonia source in the upper zone of sediment. Reduced fluxes of iron and phosphorous in the presence of tubificids is most likely due to their continuous subduction of surficial oxidized material prior to anoxia. The reduction of SRS flux in the presence of worms cannot be presently explained.

Inclusion of diffusive loss of trace metals from sediments in mass balance calculations shows that Cu, Pb, and Zn are lost from sediments in roughly the same molar ratio as they accumulate in sediments. Even if the loading of Cu, Pb, and Zn to Lake Erie were to increase exponentially for the next 100 years, the concentration of these metals in the lake's waters would increase by only a factor of three to five.

Consideration of organic decomposition in the calculation of anthropogenic loading of nitrogen to Lake Erie sediments decreases the estimate of anthropogenic loading by about a factor of two. Estimates of anthropogenic loadings of labile materials (carbon, phosphorous, sulfur) to lake sediments cannot ignore organic decomposition.

A one-dimensional time dependent reaction-transport model which considers only production, adsorption, and diffusion was found to adequately predict ammonia and bicarbonate profiles in laboratory microcosms containing homogenized Lake Erie sediment and no tubificids. More complex models are

required for other parameters (iron, phosphorous silicon) and situations (homogenized sediment with tubificids, real lake sediments).

METHODS AND MATERIALS

Field Measurements

Study Area

The data reported in this study were collected from stations 83 and A1 in the central basin of Lake Erie (Fig. 1). Station 83 is located in about 16 meters of water. The 1-3 meter thick hypolimnion is often anoxic in August and September. The sediments are derived from the eastward transport of sediment from the western basin and from shoreline erosion. They consist primarily of silt sized quartz with minor amounts of illite, kaolinite, dolomite, magnetite, and feldspar. Cesium-137 and lead-210 profiles at this site yield a sedimentation rate of 0.077 $g/cm^2/yr$, and exhibit a biogenically mixed zone 4.5 cm thick (J.A. Robbins, pers. comm.). Porosity decreases exponentially from about 90% at the surface to about 60% at 20 cm. The macrobenthic community at Station 83 consists primarily of tubificid oligochaetes ($\sim 9500/m^2$), sphaerid clams ($\sim 2000/m^2$), and chironomid larvae ($\sim 1600/m^2$) (Fisher and Matisoff, in press). These organisms live in the top 5 cm of sediment and are capable of producing the observed mixed zone (top 4.5 cm) and of increasing chemical exchange between sediments and lake water (McCall and Fisher, 1980; Fisher *et al.*, 1980). Station A1 is located in about 24 meters of water. The 3 - 5 meter thick hypolimnion in often anoxic in August and September. Sediments at this locale are derived from the eastward transport of sediment from the western basin and from shoreline erosion. They consist of approximately equal amouts of silt sized quartz and illite. Minor amounts of kaolinite, dolomite, magnetite, and feldspar are also present. Sedimentation rates determined from cores taken in the vicinity of station A1 yield sedimentation rates of 0.119 $g/cm^2/yr$ (Kemp, *et. al*, 1976). Porosity decreases

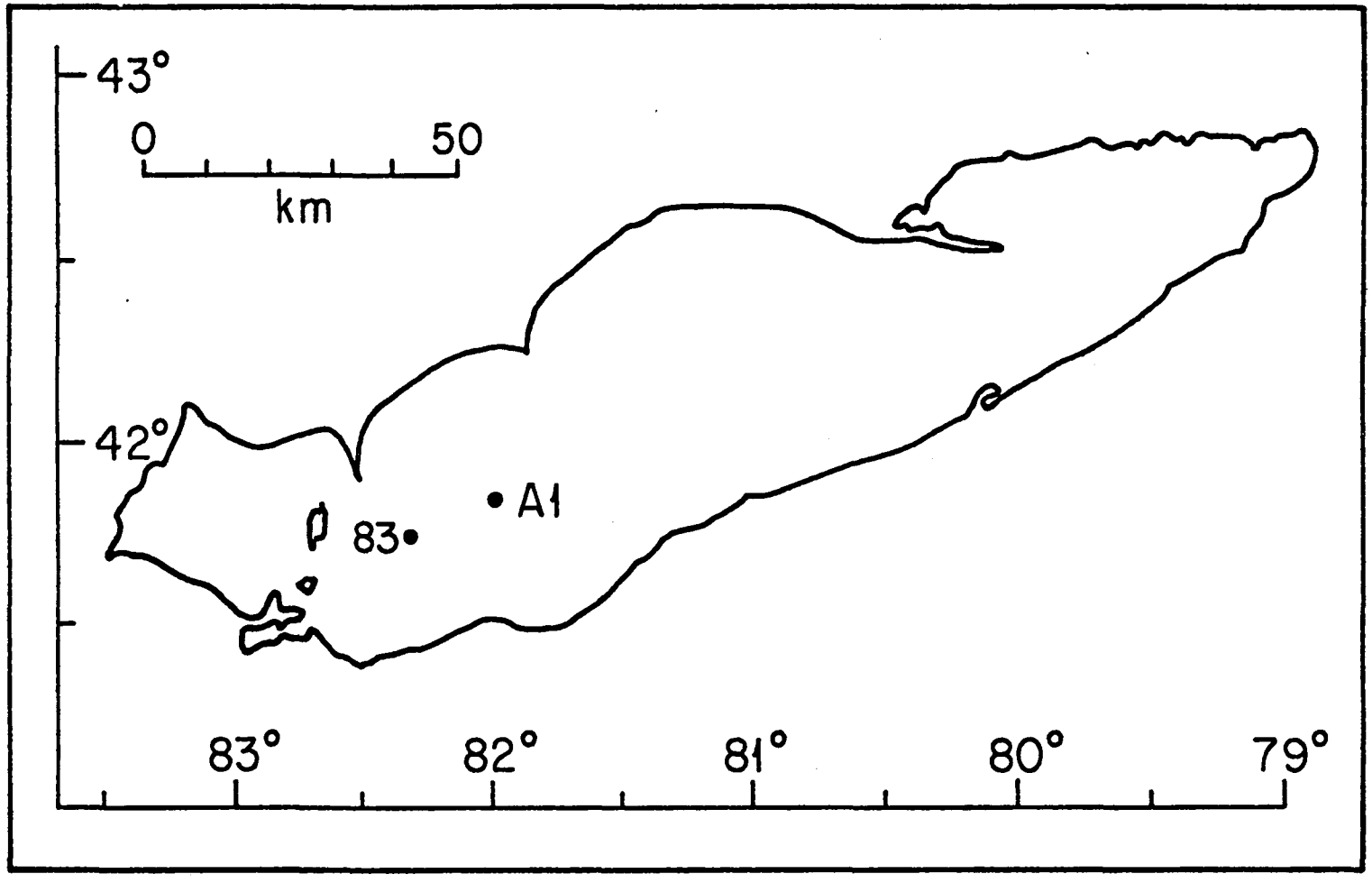

Figure 1. Field sampling localities in Lake Erie.

linearly with depth from about 95% at the surface to about 85% at 20 cm. the benthos at this site is dominated by tubificid oligochaetes (~4400/m^2), sphaerid clams (~4000/m^2), and chironomid larvae (~100/m^2). The biogenically mixed zone at this site is ~2 to 3 cm in thickness.

Core Collection

Cores were collected in a plastic core liner (cellulose-acetate-butyrate, 7.3 cm O.D., 7.0 cm I.D.) with a Benthos gravity corer or by SCUBA divers. The collected core was then capped and held in a vertical position, measured and described. A 125 ml sample of overlying water was collected immediately above the sediment-water interface. This water sample was capped and filtered. The remaining overlying water was then siphoned off. To minimize oxygen contact, a plastic bag was taped over the end of the core liner and nitrogen was continuously blown into the core liner during these manipulations. A hydraulically driven rubber piston was inserted into the bottom of the core liner and the top of the core liner was placed in a N_2-filled glove bag. Sediment samples were sliced off as the core was pushed up by the rubber piston. Ten samples were taken at five consecutive 2 cm intervals in the upper 10 cm, a 3.5 cm layer at about 15 cm, and 5-6 cm intervals at about 20, 30, 40 cm and deeper depending upon the length of the core. Samples were transferred to nylon squeezers which were covered and clamped into a squeezing rack. A 3.4 atm (3.45 x10^6 dynes/cm^2) pressure of N_2 acting against a thin rubber diaphragm ("Dental Dam") (Reeburgh, 1967) forced the interstitial water through two circles of nylon mesh supports overlain by two 0.45 μm Whatman Filters and one 0.22μm Millipore filter (75 mm diameter). Since the sample was not exposed to oxygen at any time, the intersitital water closely approximated the natural system.

Pore Water Peeper

Intersititial waters were collected at Station A-1 by both the preceeding gravity core technique and with a pore water peeper, (originally designed by Hesslein (1976)). The pore water peeper consisted of a thick, meter long plexiglass plate with machined slots filled with deionized water and covered with a polycarbonate membrane filter. The slots were located at 1 cm intervals near the sediment-water interface. The distance between slots increased as one moves further away from the interface. Diffusion of chemical substances across the membrane proceeds until the concentration of all species inside the slots equals their concentrations in the surrounding sediment pore water, usually 10-30 days. Long-term natural disturbances in the upper part of the sediment column, such as biotrubation and sediment mixing due to bottom currents, would create changes in the concentration gradient near the sediment-water interface; these would be reflected in the peeper data. An accurate representation of the effects of bottom disturbances could then be assesed in greater detail.

The peeper was deployed at Station A-1 in August, 1979 and retrieved for a comparison with gravity core data in September, 1979.

Laboratory Experiments

Production Experiment

The chemistry of intersitital waters is driven by the decomposition of organic matter (Berner, 1974). Bacterially mediated decomposition of organic matter in recent sediments releases nutrients to interstitial waters (Siever *et al.*, 1965; Murray *et al.*, 1978; and others). These regenerated nutrients undergo diffusion, advection, and chemical reaction. Nutrients escape across

the sediment-water interface, undergo ion exchange and adsorption with sediments, and precipitate as authigenic mineral phases (Nriagu and Dell, 1974; Holdren et al., 1975; Bricker and Troup, 1975; Emerson and Widmar, 1978; Rosenfeld, 1979; Suess, 1979; and others). Quantitative description of chemical mass transfer in recent sediments requires knowledge of the kinetics and rates of material regeneration (Berner, 1974; Lerman, 1975; Aller, 1977).

In nearly all recent organic rich sediments, the so-called oxidized zone, i.e., the zone in which iron is present as FeOOH, is never more than a few centimeters thick unless the sediment is actively bioturbated (Siever et al., 1965; Sholkovitz, 1973; Emerson, 1976, Bricker et al., 1977; Aller, 1977; Murray et al., 1978; McCall and Fisher, 1980; and others). Thus, a major portion of the observed sediment column falls within the zones of sulfate reduction, methane fermentation, and CO_2 reduction (Martens and Berner, 1974; Reeburgh and Heggie, 1977; Goldhaber et al., 1977.)

Nutrient regeneration in anoxic waters by bacterial sulfate reduction has been described by Richards (1965):

$$(CH_2O)_{106}(NH_3)_{16}H_3PO_4 + 53SO_4^{-2} \rightarrow 106CO_2 + 53S^{-2} + H_3PO_4 + 106H_2O + 16NH_3 \quad (1)$$

In previous work, rates of organic decomposition in sediments were measured by the rate of sulfate reduction or ammonium production (Gunkel and Oppenheimer, 1974; Goldhaber et al., 1977; Aller, 1977; Rosenfeld, 1977). These workers incubated sediments in jars under anoxic conditions and analyzed serially taken samples for sulfate and/or ammonium. Concentration changes in a given depth interval are used to determine reaction rate and kinetics at that depth. Sulfate concentrations in Great Lakes' waters (~200 μM) are much lower than that of seawater (~27,600 μM) (Weiler and Chawla, 1968; Weiler, 1973; Nriagu, 1975; Tisue, 1980). Consequently, sulfate is not a important electron

acceptor in Great Lakes' sediments. In this regard, the decomposition of orgainic matter in Great Lakes sediments is significantly different from that occuring in marine and estuarine sediments. This report presents the first experimental results from jar experiments on the rates of release of nutrients and metals during anaerobic decompositon of freshwater sediments.

Twenty-five gravity cores were collected on September 18, 1978, at Station 83 in the central basin of Lake Erie (Fig. 1). No attempt was made to remove organisms before preparing the sealed jars. The effects of entombment on pore waters has been discussed by Goldhaber et al. (1977).

The cores were sectioned in a helium-filled glovebag. Each of the depth intervals (0-2, 2-4, 4-6, 6-10, 10-14, 14-18, and 35-39 cm) were pooled in separate plastic buckets. After all the cores were collected and sectioned, the mud in each bucket was completely homogenized. Aliquots of sediment from each depth interval were placed in screw capped glass specimen jars (140 ml). The jars were sealed with electrical tape and paraffin. The sealed jars were submerged in mud-filled plastic containers to prevent oxidation and evaporation. Jars were stored at 5°C, 10°C, and 18°C, and serially sampled over a period of approximately 200 days.

Pore waters were expressed under a nitrogen atmosphere using a Reeburgh-type squeezer (Reeburgh, 1967). Expressed pore waters were analyzed for pH, soluble reactive phosphorous (SRP), carbonate alkalinity, ammonium, chloride, ferrous iron, manganese, calcium, and magnesium. Standard analytical methods were modified for small sample volumes, and all analyses, except calcium, magnesium, and manganese, were performed on the day of collection. The analytical proceedures are given in Appendix I.

Flux Experiment

The flux experiment represents part of an attempt to understand in detail the mechanisms that control the flux of nutrients and other materials from lake sediments. The experiments conducted were similar to Mortimer's classic laboratory experiment (Mortimer, 1941; 1942), i.e., sediments and overlying water were placed in a container; the container was sealed and the overlying water was allowed to become anoxic; various chemical parameters were measured as a function of time. In our experiments, however, chemical parameters were measured not only in the overlying water (as done by Mortimer) but also in the interstital waters and sediment solids. Thus, flux estimates using both direct (overlying water concentrations) and indirect (interstital water concentration profiles) techniques could be made. Further, data from these experiments and the production experiment could be used to develop and test time dependent production-transport models for various chemical species in the sediment pore waters.

Two series of flux experiments were conducted. In the first series of experiments (Homogenized Mud Core Experiment), well mixed Lake Erie (Station 83) sediment was used. This was done to eliminate depth variations in the chemistry of the solid phase and reduce core to core variablilty. In this experiment, half (10) of the cores received a population (10^5 individuals $/m^2$) of tubificid Oligochaetes so that the effects of their activities (bioturbation, excretion, etc.) on materials release and pore water chemistry could be investigated. In the second series of experiments (Lake Core Experiment) intact sediment cores recovered from Station 83 were used. This allowed investigation of the processes occuring in naturally deposited Lake Erie sediments.

Apparatus

Microcosms used in the experiments are illustrated in Fig. 2. These devices were comprised of four main components: 1) an overlying water reservoir, 2) a sediment chamber, 3) an extruder base, and 4) an extruder piston. Coupling of components 1,2, and 3 was accomplished by O-ring (Viton) and silicon grease sealed threaded connections. The extruder piston was moveable and a Viton O-ring was used to provide a seal between the piston and the sidewalls of the sediment chamber. The minimum wall thickness of any component was 0.635 cm. Materials used for construction of the microcosms were acrylic, PVC, Viton, Teflon, and stainless steel. The contained water and sediment contacted only non-metallic surfaces.

The overlying water reservoir was a cylindrical acrylic container having an inside diameter of 25.4 cm and a height of 10.16 cm. The total contained volume of the overlying water reservoir was ~5 l. This volume corresponds to a water column ~100 cm in height having the diameter of the sediment chamber. The top of the overlying water reservoir was sealed by an O-ring fitted detachable top and sampling cover. The detachable top was secured to a flange on the overlying water reservoir using eight ¼-20 x 2" stainless steel cap screws. while the sampling cover was secured to the detachable top by eight ¼-20 x 2½" PVC cap screws. Water within the overlying water reservoir was constantly stirred using a well-mounted Nalge 6600 series Star Head magnetic stirbar (2.22 x 1.59cm) driven by a water turbine magnetic stirrer.

The sediment chamber was a cylindrical acrylic container having an inside diameter of 7.62 cm and a height of 50 cm. The extruder base was a solid block of acrylic 15.28 x 15.28 x 7.62cm machined to accept the threaded base of the sediment chamber. The extruder based was fitted with a Swagelock "Quick-Connect" valve. When a microcosm was sacrificed for analysis, the over-

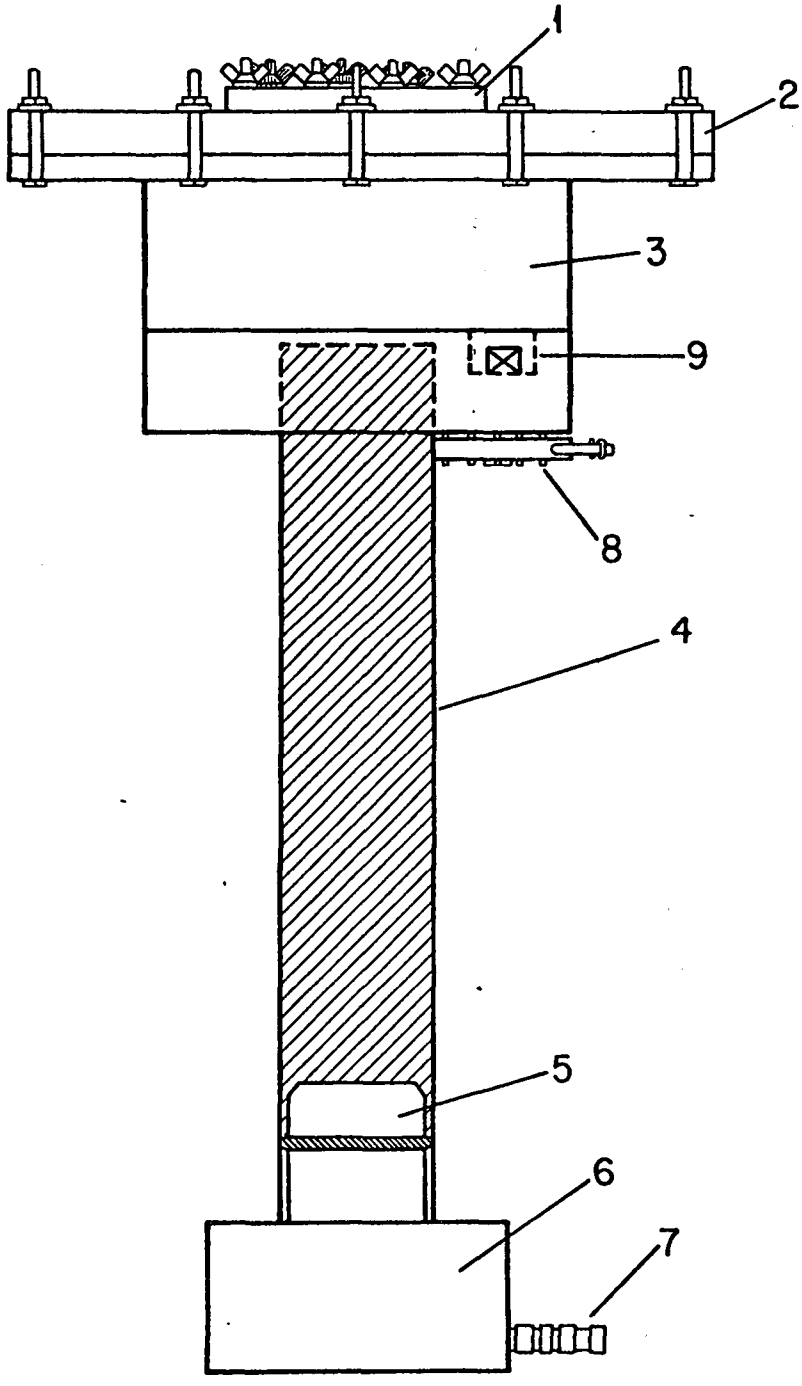

Figure 2. Apparatus used for the flux experiment: 1. Sampling cover 2. Detachable top 3. Overlying water reservoir 4. Sediment chamber 5. Extruder piston 6. Extruder base 7. Quick connect valve 8. Turbine magnetic stirrer.

lying water reservoir was emptied and removed from the sediment chamber and extruder base assembly. A pressurized water line was then corrected to the "Quick-Connect" valve of the extruder base. By admitting water through this valve, the extruder piston was forced upwards and the desired intervals of sediment were collected by means of a slicer fitted to the top of the sediment chamber.

Preparation of Homogenized Mud Cores

In the Homogenized Mud Core Experiment well mixed Lake Erie (Station 83) sediment was used. This sediment was collected with a grab sampler and sieved through a 250μm mesh screen to remove benthic macrofauna and large debris. Before the sediment was placed in the microcosms, it was homogenized by stirring. In all, twenty microcosms were prepared. Tubificids (456 *Limnodrilus spp.*/microcosm) collected from Cleveland Harbor were added to ten of the microcosms to simulate a population density of 10^5 individuals $/m^2$. The remaining microcosms were maintained without worms. The tubificids were allowed to rework the sediments for thirty days before all microcosms were sealed and helium purged. The concentrations of nutrients and other materials in the overlying water of each microcosm was monitored regularly. At intervals, two microcosms (one with worms and one without) were sacrificed to determine pore water gradients of dissolved materials. The water used to fill the overlying water reservoirs was deionized.

Preparation of Lake Cores

In the Lake Core Experiment, undisturbed sediment cores were collected by SCUBA drivers at Station 83. The cores were collected using the sediment chambers of the microcosm apparatus as coring tubes and the PVC extruder pistons as bottom caps. In all, twelve cores were collected. The cores were

returned to the laboratory, sealed and helium purged. In this experiment, the water used to fill the overlying water reservoirs was filtered (0.45 μm) Lake Erie water collected 1m above the bottom at Station 83. Again, the concentrations of nutrients and other materials in the overlying water were monitored regularly. Individual microcosms were sacrificed at intervals to determine pore water gradients of dissolved materials.

In both experiments, the temperature of the microcosms was maintained by immersing them in a large, specially constructed water bath. During both experiments, microcosm temperature was maintained between 14° and 16°c.

Sampling Procedures

Overlying water samples were withdrawn using a syringe. In the Homogenized Mud Core Experiment, the sampling cover was removed, and the samples were withdrawn by inserting a tygon sampling tube into the central part of the overlying water reservoir. During sampling, a helium atmosphere was maintained by enclosing the apparatus in a glove bag. In the Lake Core Experiment, the sampling covers were modified so that helium under a small positive pressure was admitted to the overlying water reservoir. Admission of the helium expelled water through a sampling tube into the sampling syringe. With this arrangement, the sampling cover could remain in place during sampling.

When a core was sacrificed for pore water analysis, the sediment was gently extruded using the indwelling extruder piston. The desired depth intervals were collected, homogenized, and placed in Reeburgh type squeezers (Reeburgh, 1967). Sediment collection and squeezing were carried out using the techniques described for the field cores. Chemical parameters measured in the interstitial water were pH, soluble reactive phosphorous (SRP), carbonate alkalinity, ammonium, chloride, ferrous iron, soluble reactive silica (SRS),

manganese, calcium, and magnesium. Standard analytical methods were modified for small sample volumes, and all analyses except calcium, magnesium, and manganese, were performed on the day of collection. Analytical proceedures are given in Appendix I. After the necessary pore fluids were collected, sediment remaining in the squeezers was collected into plastic bags. These sediment samples were stored in a frozen condition until they were analyzed.

Results

Field Measurements

The chemistry of sediment solids reflects the chemical depositional history of sediments and the post-depositional processes affecting them. Since small changes in sediment solid chemistry can often cause large changes in pore water chemistry, the chemistry of interstitial fluids is studied to identify mineral reactions taking place in sediments. Knowledge of both sediment solid and pore fluid chemistry is required for a complete understanding of chemical processes taking place in sediments.

Chemical data obtained from both Station 83 and A1 is given in Appendix II.

Sediment solids data includes total C, organic C, Kjeldahl N, total P, total S, acid volatile S, and total Ca, Mg, Mn, Fe, Zn, and Cu. Pore water data includes Fe^{+2}, Mn^{+2}, Na^{+}, K^{+}, Ca^{+2}, Mg^{+2}, Zn^{+2}, Cd^{+2}, Pb^{+2}, Cu^{+2}, HCO_3^-, SRP, SRS, NO_2^--NO_3^-, Cl^-, NH_4^+, and pH. In addition, pore water concentrations at station A1 obtained by both the gravity coring technique and the pore water peeper technique are given in Appendix II.

In general, concentrations of nutrients and toxic metals in the sediment solids decrease with depth (Appendix II, Figs. 3 to 10). This may be due to

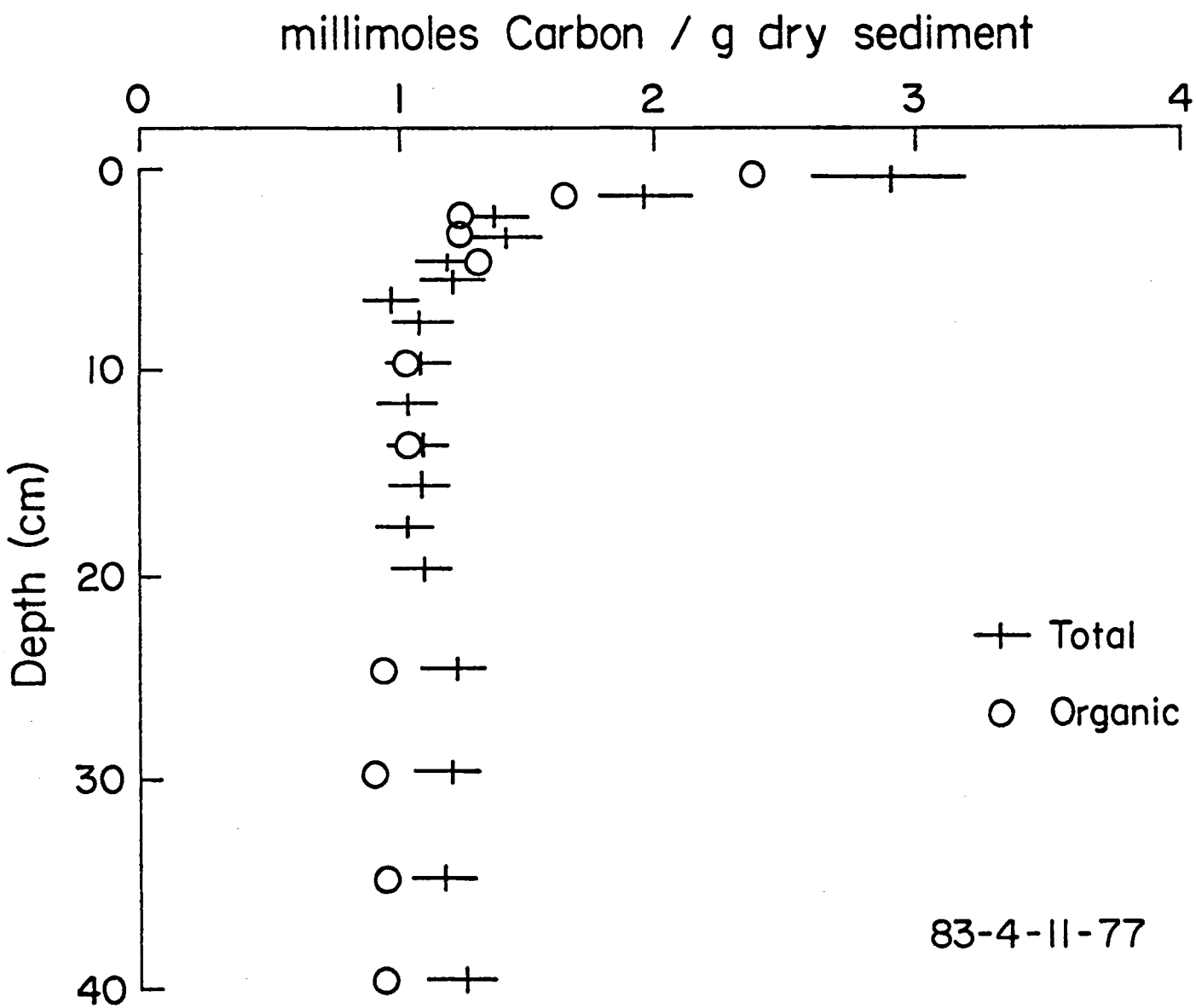

Figure 3. Total and organic carbon versus depth at Station 83.

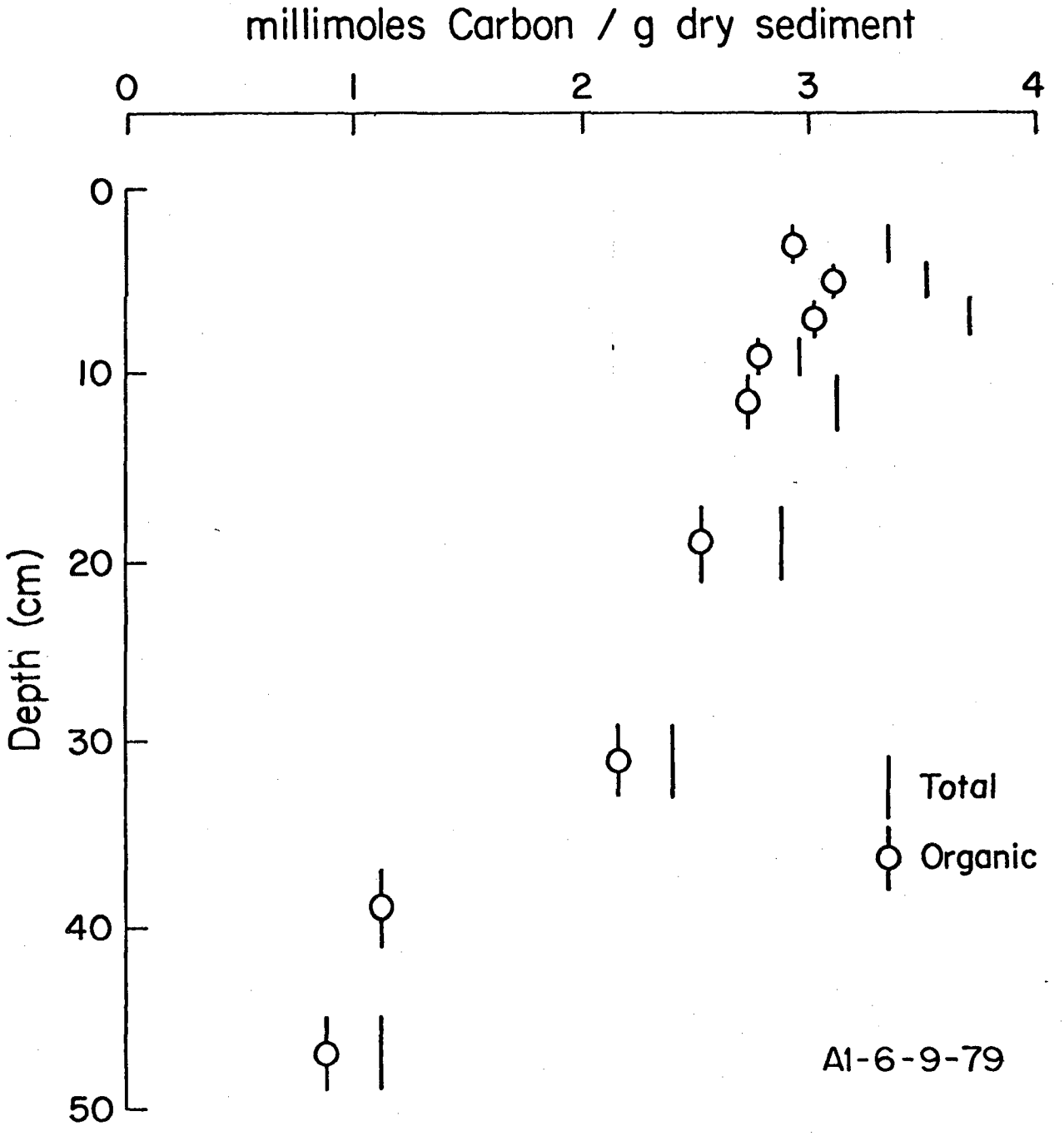

Figure 4. Total and organic carbon versus depth at Station A1.

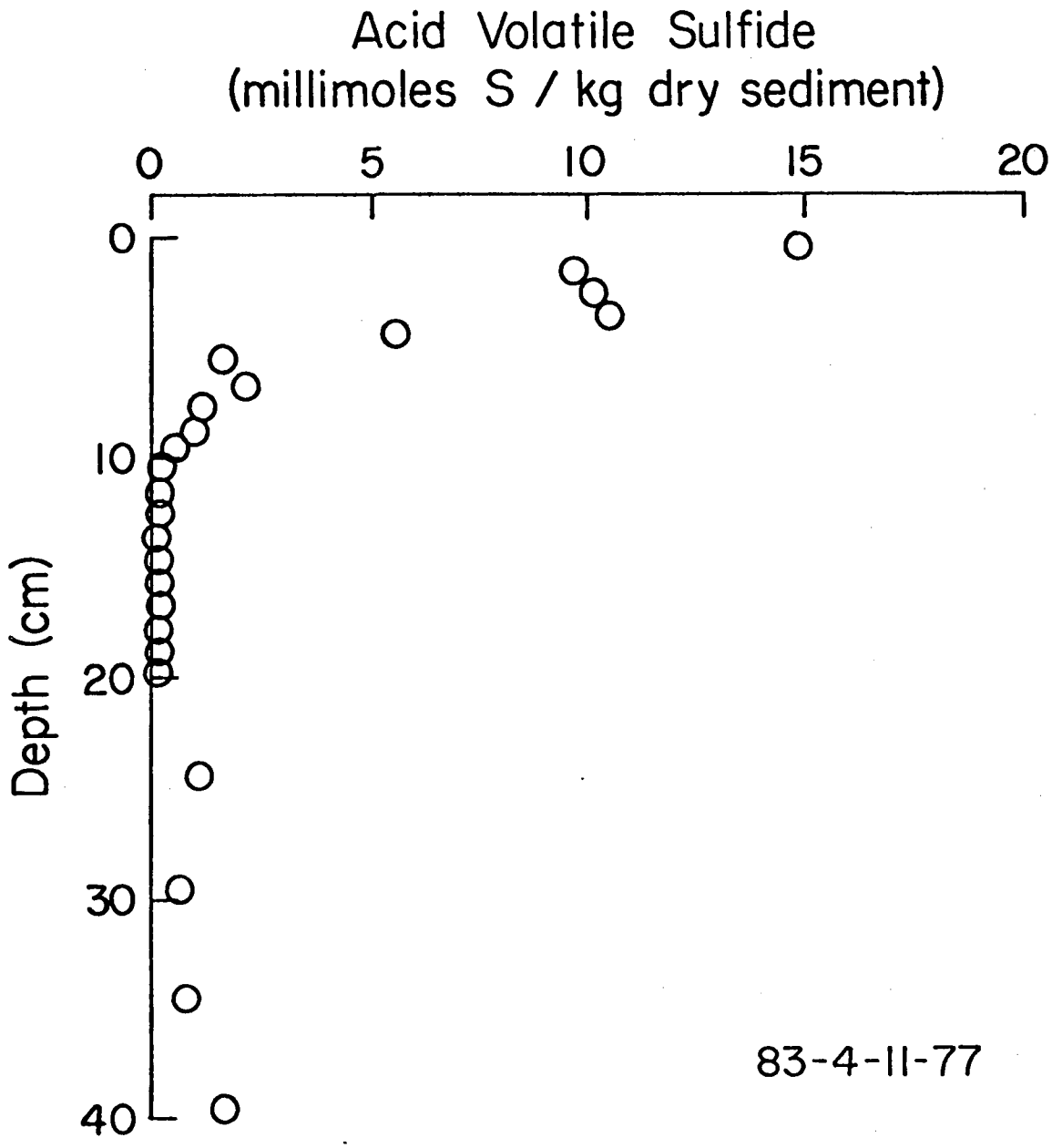

Figure 5. Acid volatile sulfide versus depth at Station 83.

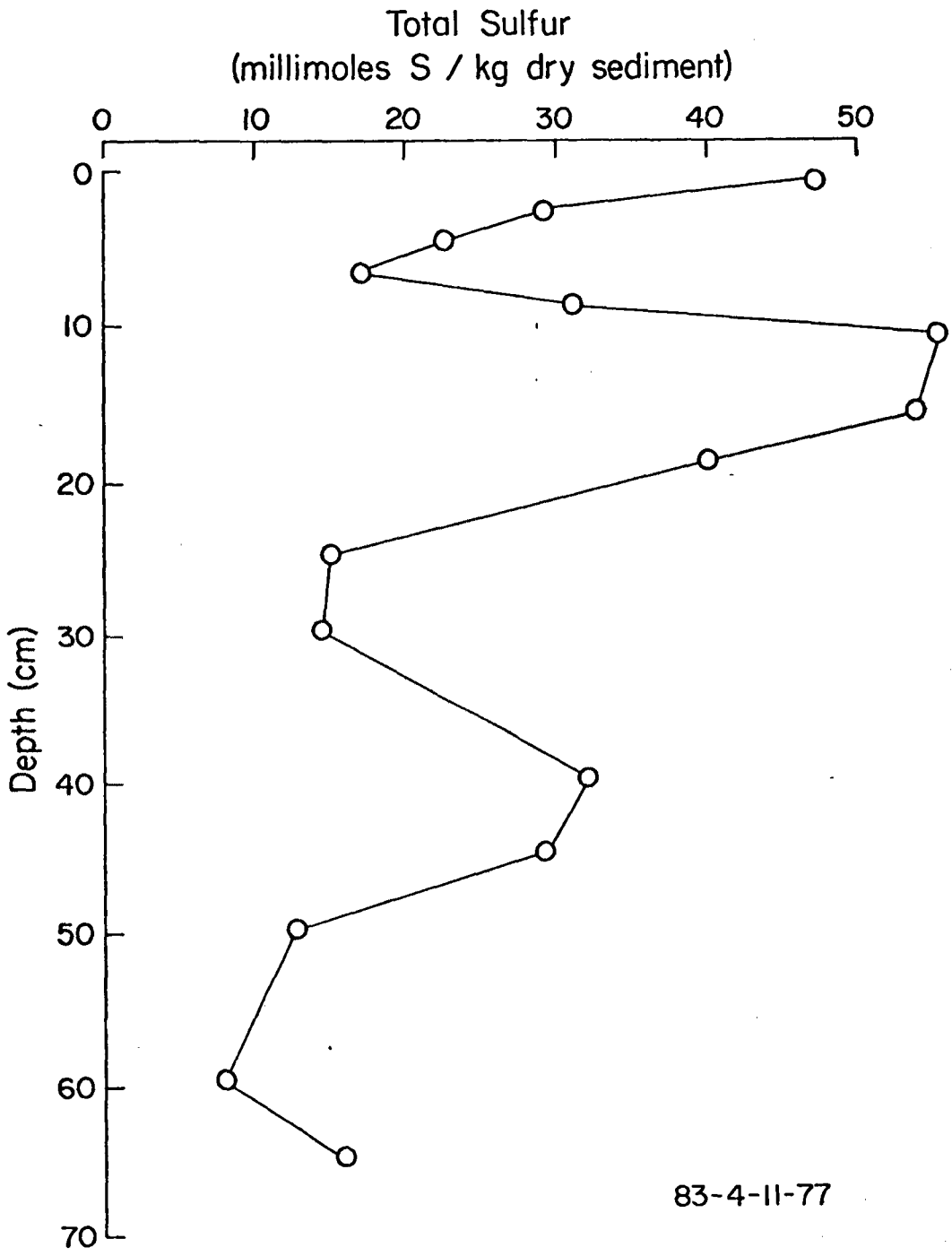

Figure 6. Total sulfur versus depth at Station 83.

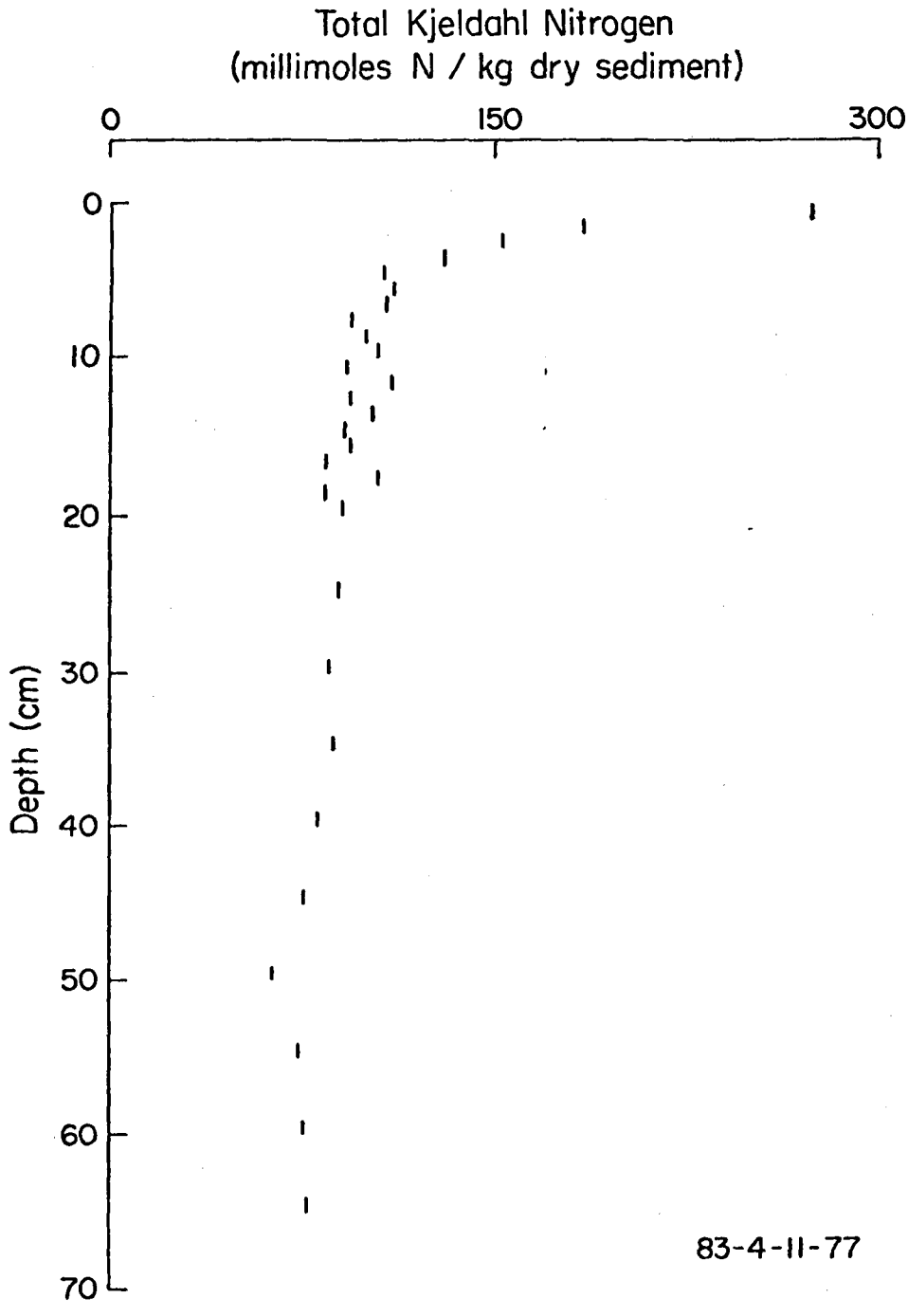

Figure 7. Total Kjeldahl nitrogen versus depth at Station 83.

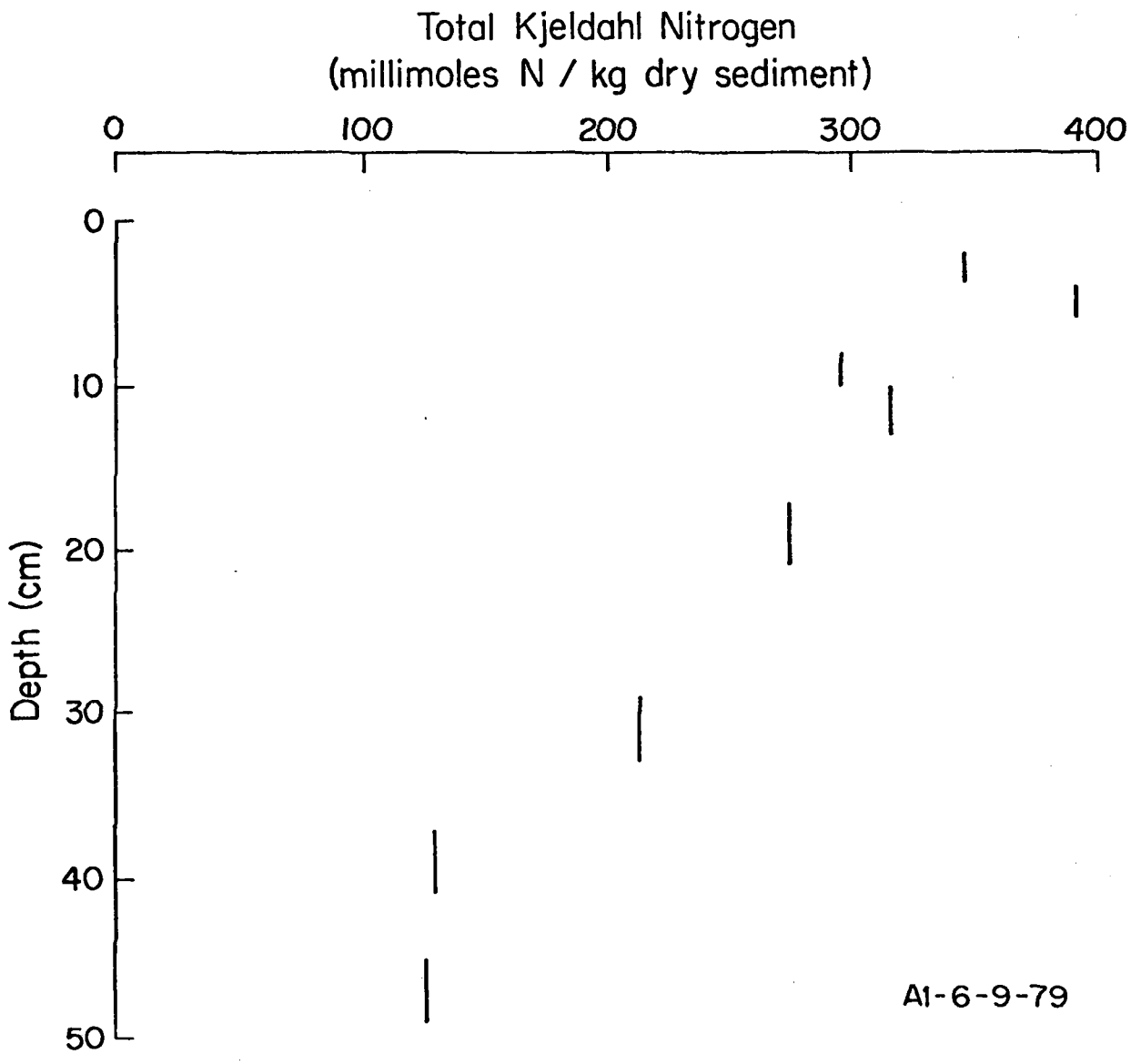

Figure 8. Total Kjeldahl nitrogen versus depth at Station A1.

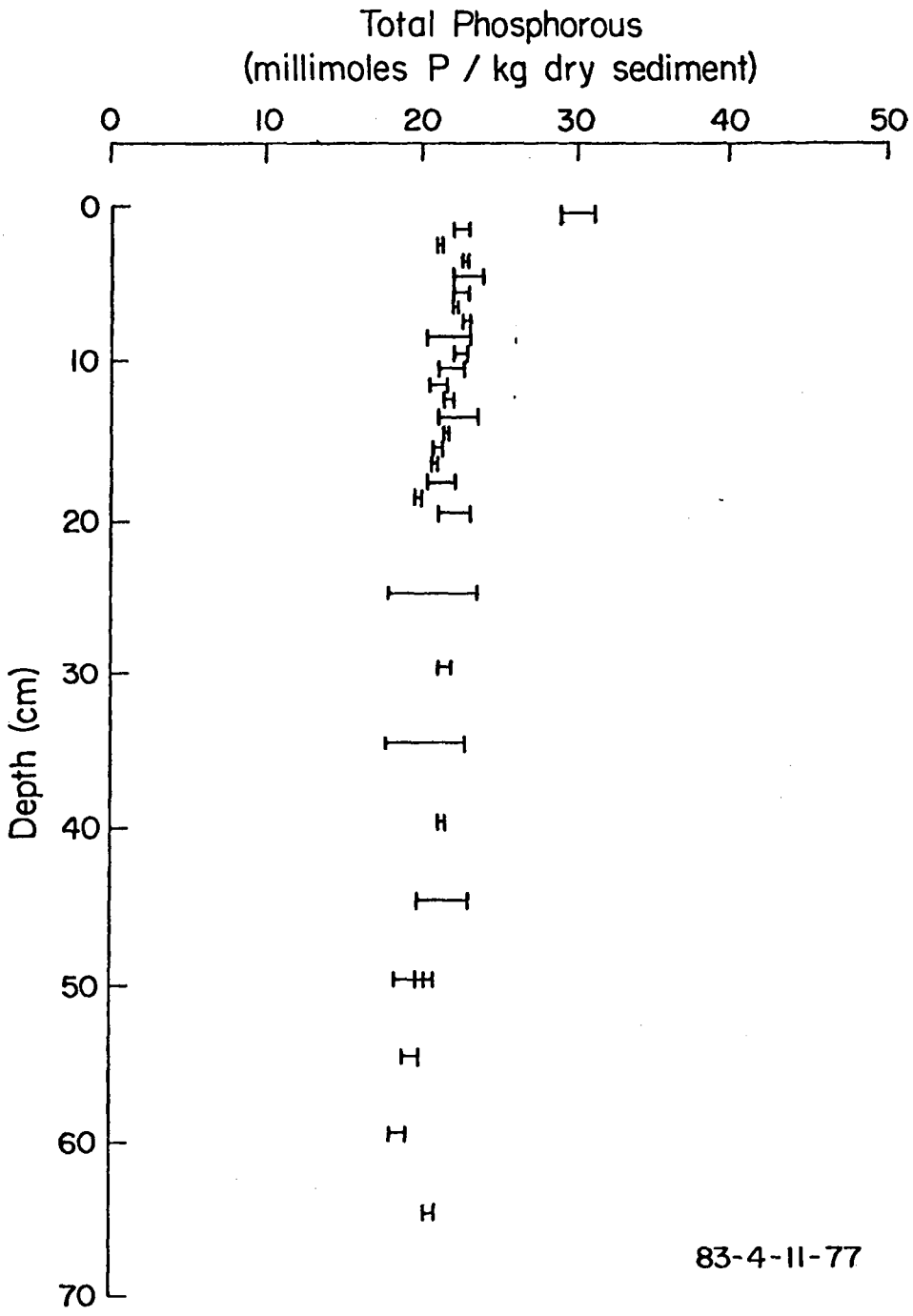

Figure 9. Total phosphorous versus depth at Station 83.

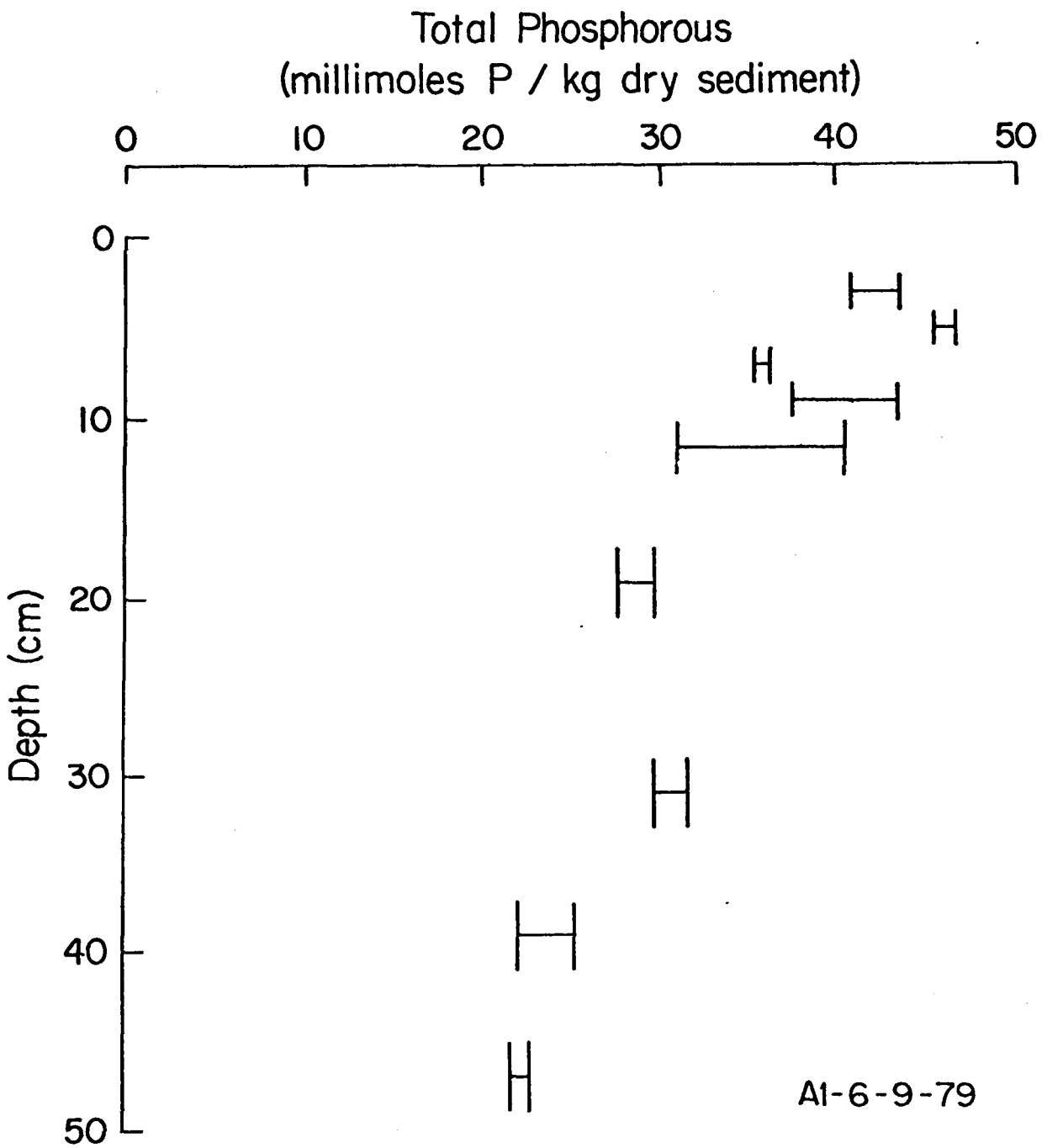

Figure 10. Total phosphorous versus depth at Station A1.

increased loading of these materials over time and/or due to post-depositional chemical mass transfer (see p. 125ff). The concentrations at station 83 of those species undergoing increased loading or post-depositional alteration to 5-7 cm generally decrease rapidly to 5-7 cm and are approximately constant below 7 cm. At station A1, the concentrations increase nearly linearly from a depth of about 40-50 cm. This would imply that the sedimentation rate at station A1 is substantially higher than at station 83.

Calcium and magnesium decrease in the top 10-40 cm at station 83 and then increase at depths greater than 40 cm. Inorganic carbon (Fig. 3) shows a similar increase below about 40 cm. This would imply that calcium and magnesium carbonates are precipitating in the sediments below about 40 cm.

The results of the interstitial water comparison between the gravity coring technique and the pore water peeper technique are shown in Appendix II and Figs. 11 and 12. The pore water peeper permits higher resolution around the sediment-water interface and thus enables a more accurate evaluation of the concentration gradient at the sediment-water interface. This may represent the fact that the pore water peeper collects data that is an average over the time interval of deployment, while a gravity core collects data that is an instantaneous representation of the system. Thus storm wave activity stirring up the bottom is averaged in the peeper case and appears anomalous in gravity coring case. Sampling of reduced species such as Fe^{2+} and NH_4^+ and gases such as CH_4 requires modification of our peeper, since oxidation and loss to the atmosphere occurred for these species.

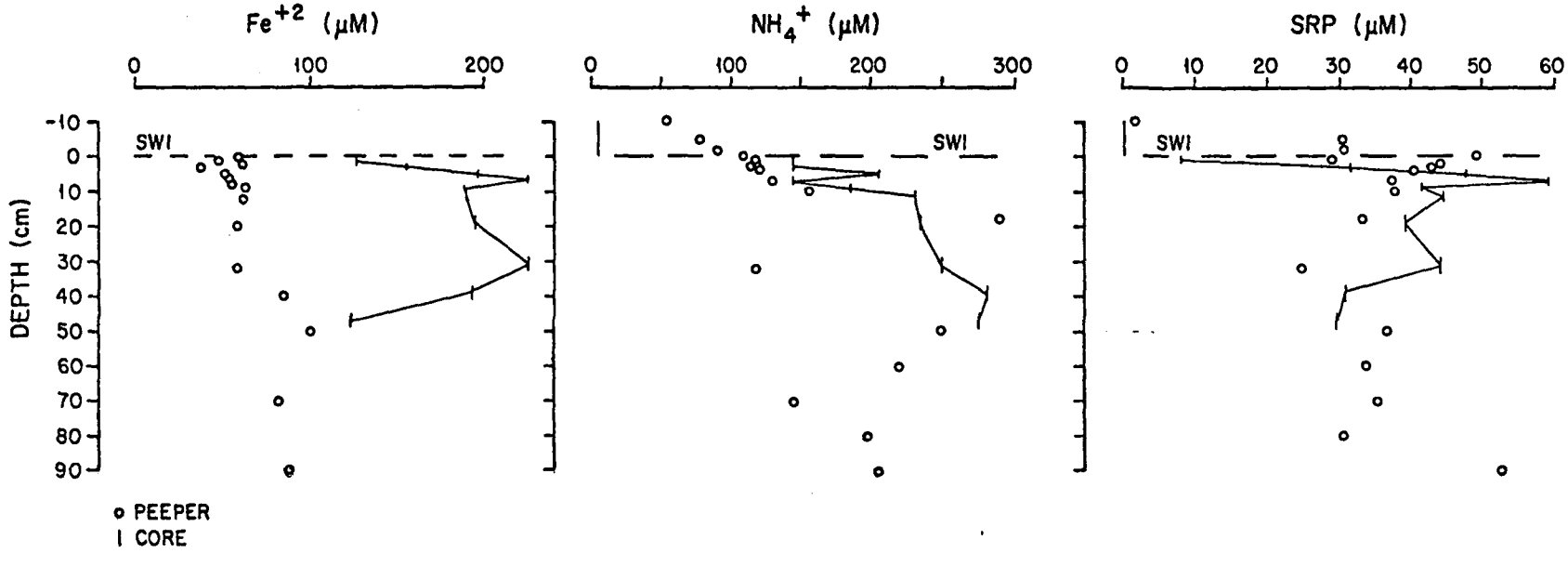

Figure 11. Vertical profiles of ferrous iron, ammonia, and SRP in the interstitial water of sediments at Station A1 determined by both gravity coring and pore water "peeper" technique.

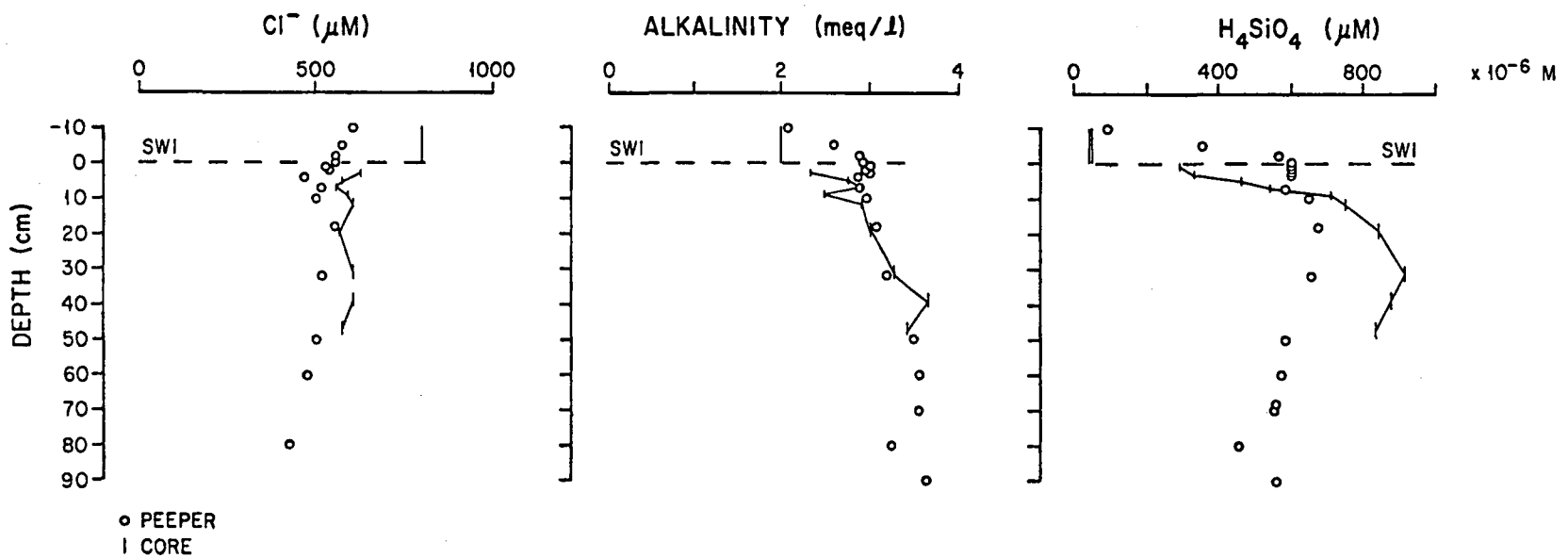

Figure 12. Vertical profiles of chloride, alkalinity, and SRS in the interstitial water of sediments at Station A1 determined by both gravity coring and pore water "peeper" technique.

Production Experiment

Release Kinetics

Concentrations of all nutrients and metals in the jar pore waters in any given depth interval increased with time, and the rate of increase was greater at higher temperatures. Over the course of the experiment, pH remained at approximately 7.2 (Fisher and Matisoff, in press). Initial review of the data (Appendix III) indicated that a linear relationship existed between concentration and time. Accordingly, linear regressions were calculated for all concentration versus time plots. The ammonium data and the derived regression lines are presented in Fig. 13. The results of the regression analysis are given in Table 1. Bicarbonate, calcium, iron, and magnesium all display concentration versus time behavior similar to that shown for ammonium. Soluble reactive phosphorous was the only parameter studied which displayed a significant deviation from this trend. The concentrations of SRP from the 2 day and sometimes the 22-24 day 0-2 cm and 2-4 cm depth samples were higher than those determined at all succeeding times from these depths. These elevated levels of SRP probably result from release of sorbed phosphorous from dissolving ferric oxyhydroxides. Iron does not show a similar pattern because of the concurrent dissolution of other iron phases (See Stoichiometric Model). The reduction in SRP concentration after this initial release is not well understood, although it probably represents the precipitation of a phosphorous phase. After 71-73 days, the concentration of phosphorous increased linearly.

The apparent linearity of the concentration versus time plots suggests zeroth order kinetics for the decomposition:

$$\frac{\partial C}{\partial t} = R'(Z,T) \qquad (2)$$

Temp.	Depth Interval	NH_4^+	HCO_3^-	ΣPO_4	Ca	Fe^{++}	Mn	Mg
18°C	0-2cm	4.93	19.8	.045	4.08	.992	.187	1.50
	2-4	2.38	17.6	.055	4.49	1.32	.168	1.70
	4-6	1.38	15.0	.075	4.15	.710	.128	1.42
	6-10	.323	12.3	.148	3.35	.578	.105	1.30
	10-14	.137	12.1	.030	3.55	.656	.107	1.33
	14-18	.483	7.05	.003	3.02	.179	.069	.858
	35-39	.373	7.45	.033	1.96	.148	.052	.861
10°C	0-2cm	2.59	15.5	.062	2.80	.988	.137	1.15
	2-4	1.48	11.2	.035	2.41	.613	.100	1.03
	4-6	.946	10.1	.049	2.69	.638	.091	.993
	6-10	.190	8.80	.099	2.53	.576	.083	1.07
	10-14	.359	10.9	.038	1.69	.435	.054	.791
	14-18	.467	3.54	.006	1.75	.372	.045	.676
	35-39	.188	6.25	.041	1.59	.230	.041	.679
5°C	0-2cm	1.16	7.82	.064	1.69	.580	.071	.729
	2-4	1.45	10.6	.062	2.34	.571	.074	1.14
	4-6	.783	9.75	.067	2.47	.373	.074	.977
	6-10	.209	4.82	.037	1.59	.130	.040	.731
	10-14	.123	5.08	.022	1.40	.116	.013	.573
	14-18	.319	4.60	.007	1.25	.116	.030	.562
	35-39	.255	7.20	.026	1.30	.135	.032	.464

Table 1. Apparent rates of release, R'(Z,T), of nutrients and metals from the jar experiments. All units are millimoles/year.

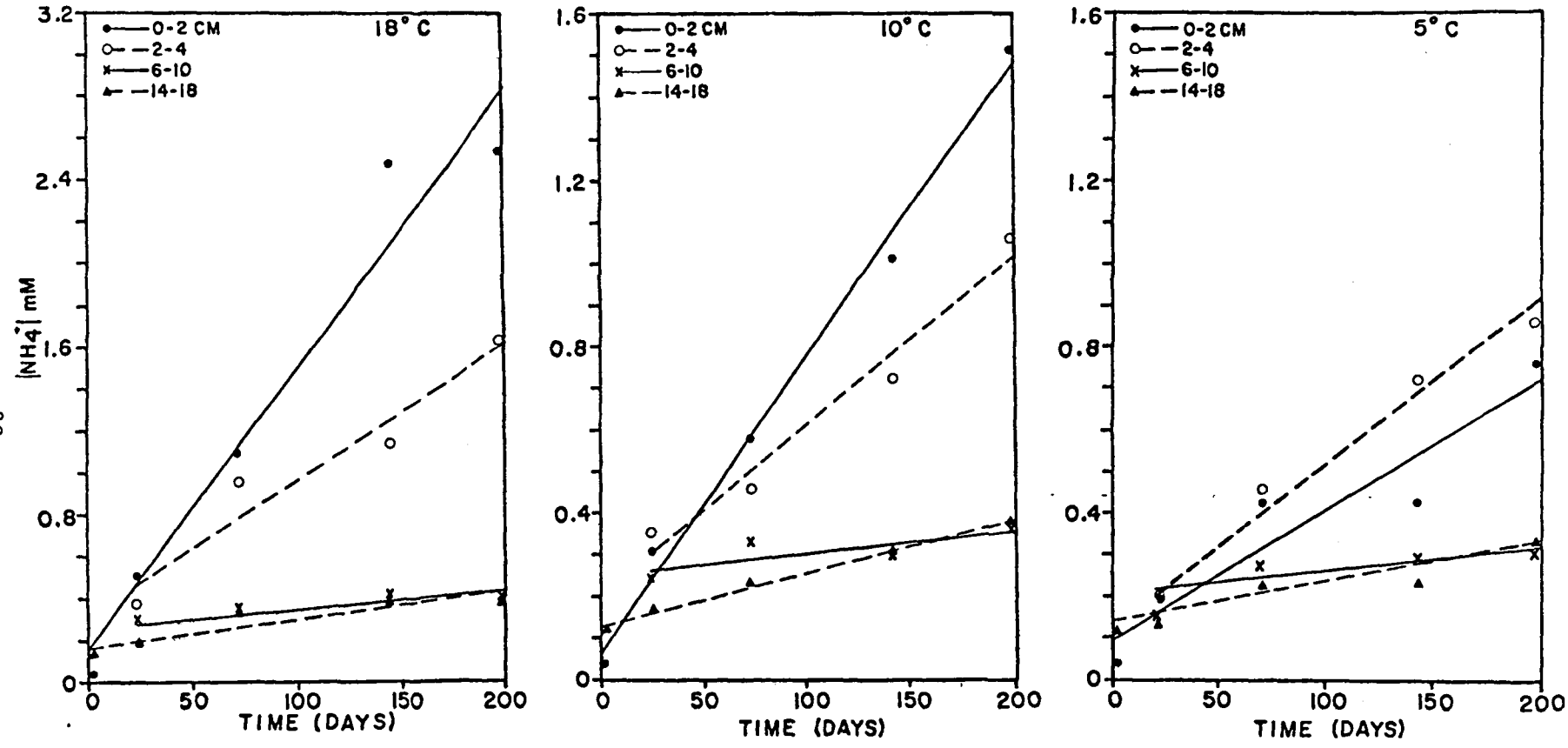

Figure 13. Ammonia concentration data and derived regression line from the production experiment for three temperatures and four depths.

where C is concentration, t is time, R' is the apparent rate of release, Z is depth in the sediment (positive downward), and T is temperature. Integrating

$$C = R'(Z,T) * t + \text{constant} \quad (3)$$

The slope of the linear regression line is interpreted as the apparent rate of release, and the intercept of the regression line represents the pore water concentration at t=0. The intercepts for any given parameter/depth interval should not be and are not significantly different among the different temperatures. Maganese displays the best degree of linearity (r = .85 - .999) while SRP exhibits the greatest deviation from linearity (r = .5 - .95).

The production rate of ammonia is also directly proportional to the amount of organic nitrogen in the sediment (Fig. 14). Kjeldahl nitrogen measures organically bound nitrogen in the trinegative state plus ammonia nitrogen. It does not include nitrate, nitrite, or organic nitrogen in highly refractory heterocyclic compounds such as nicotinic acid and pyridine and certain compounds containing N-N and N-O linkages. These are all minor fractions of organic nitrogen in sediments (Bremner, 1965). Hence, Kjeldahl nitrogen is approximately total organic nitrogen. The linear relationship in Fig. 14 indicates that the overall decomposition kinetics for nitrogen is first order, and that the observed zeroth order release rates (Fig. 13) are only an approximation of the overall kinetics. Sequential zeroth order reactions such as microbial degradation often result in an overall reaction that is first order (Berner, 1974, 1980). A similar relationship exists for organic carbon.

It must be remembered that the observed rates of release in our experiments (apparent rates) are less than the "true" rates of release (Berner, 1976; Rosenfeld, 1979). Some of the regenerated material may absorb onto

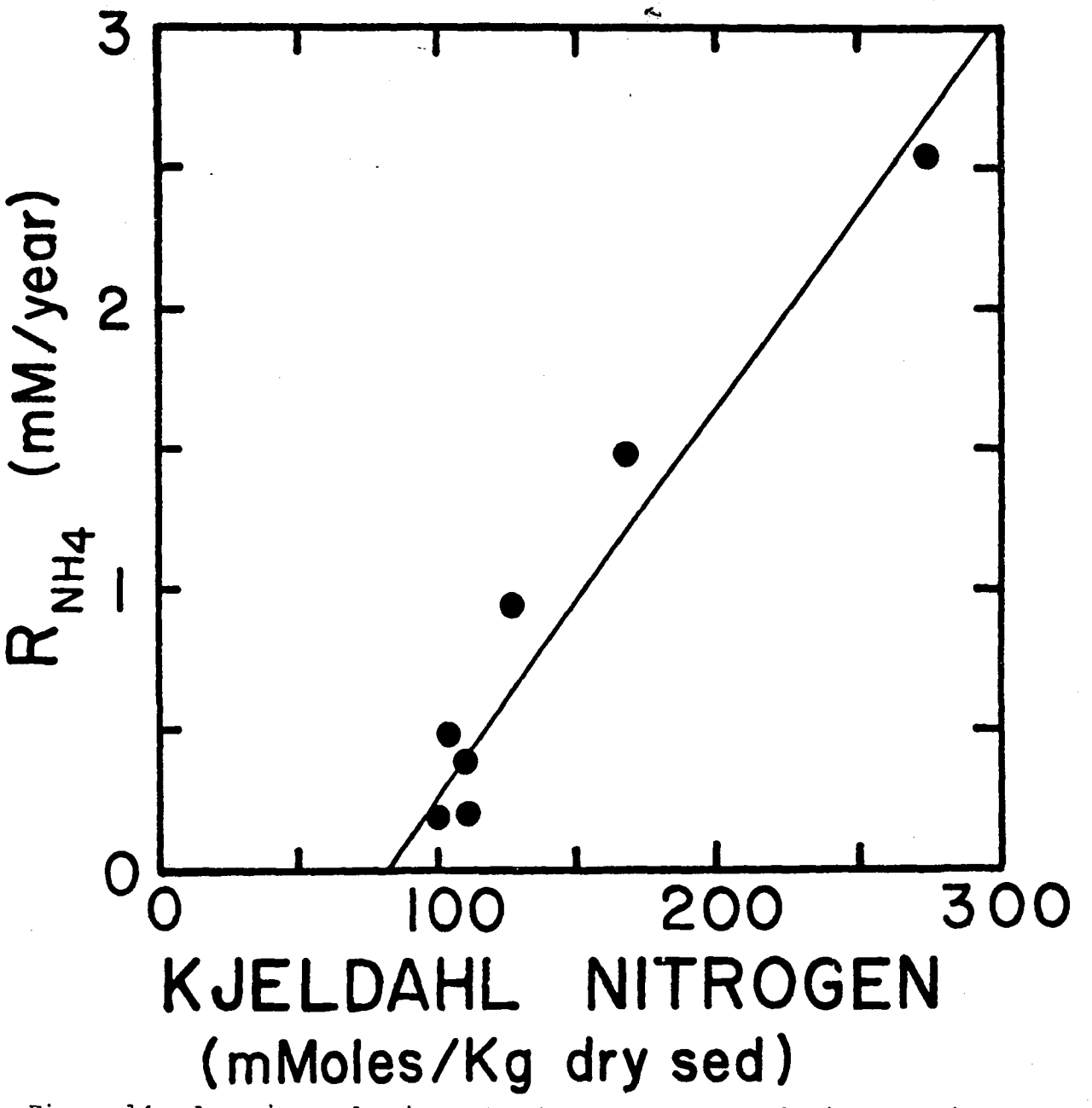

Figure 14. Ammonia production rate, R_{NH_4}, versus total Kjeldahl nitrogen.

sediment particles, undergo ion exchange, and/or precipitate as authigenic mineral phases. The net result is that some of the released material does not appear as an increase in concentration. The rates reported here are not corrected for any of these processes.

Depth Dependency

The release rate for most parameters decreased rapidly with depth. This is illustrated in Fig. 15 where the rates of ammonium release have been plotted as a function of depth for each temperature. Release rates tend to decrease exponentially with depth. This depth denpendency is a function of temperature and may be described by an equation of the form

$$R'(Z,T) = R'_o(T)\, e^{-\alpha(T)*Z} \qquad (4)$$

where $R'_o(T)$ is the apparent release rate at Z=0 and α is a constant. These parameters may be estimated by an exponential fit to the R'(Z,T) versus depth data.

Equation (4) results from the steady-state requirement that the rate of burial of potentially oxidizable organic matter be equal to the rate at which it is decomposed (Berner, 1974, 1980). The distribution of oxidizable organic matter thus decreases exponentially with depth in the sediment (Berner, 1974). Since production rates depend directly upon the amount of oxidizable organic matter, they too must decrease exponentially with depth.

Results of the exponential fits to the apparent release rate data are given in Table 2. Included for comparison in Table 2 are results from similar studies conducted in estuarine sediments. The greatest difference between the two environments is the process of sulfate reduction in the estuarine sediments. Data from Tisue (1980) indicates that sulfate in the Great Lakes is also undergoing reduction in the sediments. Applying the model of Berner

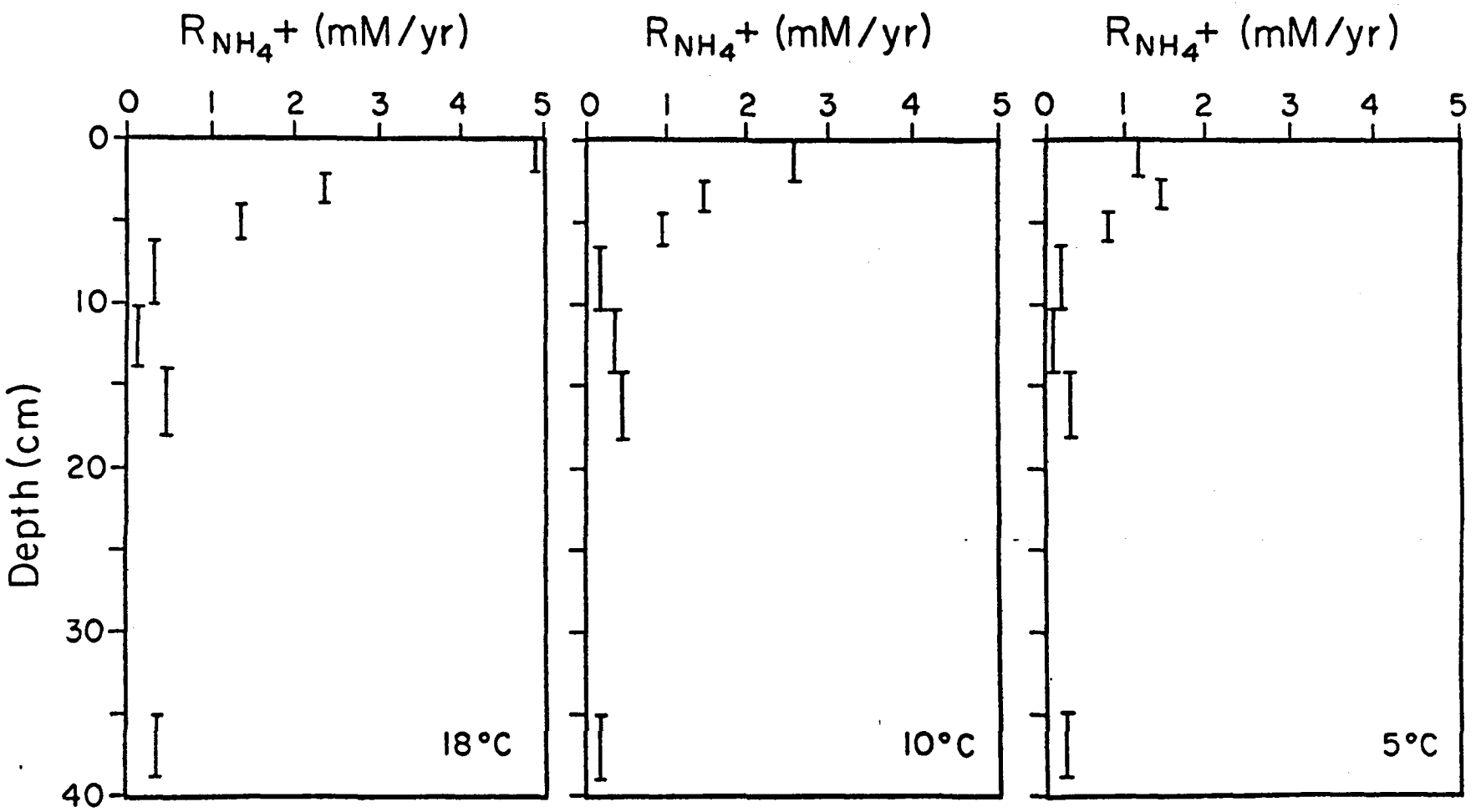

Figure 15. Ammonia production rate at three temperatures as a function of depth.

Temperature	Fit Parameter	NH_4^+	HCO_3^-	ΣPO_4	Ca	Mg	Fe^{++}	Mn	$SO_4^=$	Location Reference
22°C	R_o'								-81.	Long Island Sound
	α								0.24	Goldhaber *et al* (1977)
22°C	R_o'	23.							-129.	Long Island Sound
	α	0.405							0.33	Aller (1977)
20°C	R_o'	22.8		2.41					-96.0	Long Island Sound
	α	0.419		0.410					0.344	Rosenfeld (1977)
18°C	R_o'	6.90	19.2	0.796	4.44	1.60	1.25	0.185		Lake Erie
	α	0.342	0.042	0.315	0.022	0.021	0.079	0.052		This Study
10°C	R_o'	3.31	13.5	0.266	2.71	1.10	0.879	0.130		Lake Erie
	α	0.259	0.038	0.205	0.019	0.018	0.053	0.059		This Study
5°C	R_o'	1.60	8.17	0.189	2.09	0.954	0.727	0.082		Lake Erie
	α	0.149	0.013	0.198	0.018	0.025	0.143	0.069		This Study

Table 2. Depth dependencies of rates of production from the equation $R'(Z,T) = R_o'(T) \exp(-\alpha(T)Z)$. Units are R_o' ($\times 10^{-3}$ moles/yr) and α (cm^{-1}).

(1974) to his data, one may calculate $K_s \sim 9 \times 10^{-8}$ sec^{-1} for Lake Erie sediments. Berner (1974) calculates K_s of 7.5×10^{-11} sec^{-1} and 5.6×10^{-9} sec^{-1} for Santa Barbara Basin and Sommes Sound sediments, respectively. Although sulfate reduction is more rapid in Lake Erie sediments than in these two environments, the small quantities of sulfate do not enable sulfate reduction to be a quantitatively major process of decomposition in the sediments. Hence, methane fermentation would be expected to be the dominant reaction in Lake Erie sediments. Production rates for ammonium and phosphorous are only about a factor of three less in Lake Erie sediments. This is not particularly surprising since Stumm and Morgan (1970) indicate that sulfate reduction is only slightly more energetic than methane fermentation.

The behavior of ammonium is well described by equation (4). This is not true for all of the parameters. Phosphorous displays a suppressed release rate in surficial sediments. As suggested earlier, this may be the result of the precipitation of a phosphorous phase. The large increases in calcium and ferrous iron in surface samples probably supresses the apparent production of phosphorous via precipitation of whitlockite, apatites, and/or vivianite (Nriagu and Dell, 1974; Troup, 1974; Matisoff et al., ms). Other species, such as bicarbonate, have release rates which are greater than zero at depth. The depth dependency of bicarbonate release is better described by

$$R'(Z,T) = R'_{\infty}(T) + R'_{sed}(T)e^{-\alpha(T)*Z} \qquad (5)$$

where $R'_{\infty}(T)$ is the apparent rate of release at $Z=\infty$, and $R'_{\infty}(T) + R'_{sed}(T) = R'_0(T)$ = the apparent production rate at Z=0. At depth, diffusive transport is small for short time intervals. Consequently, the contribution of $R'_{\infty}(T)$ will result in a large, continuous increase in concentration with depth. This is not observed. Accordingly, the true $R'_{\infty}(T)$ must be a very small positive number. The higher values observed in the jar experiments may be an experimental artifact (Goldhaber et al., 1977). A small amount of oxidation of

sulfide minerals during preparation of the jars could easily generate an initial excess bicarbonate release by sulfate reduction upon sealing the jars. This would appear as a positive value of $R'_{\infty}(T)$. Hence, eq. (4) will be used to represent the experimental data.

Regeneration of metals during the decomposition experiment is interpreted as pH buffering mechanisms resulting from the dissolution of carbonate and sulfide phases. Calcite, aragonite, and dolomite have been clearly identified in these sediments by optical and x-ray diffraction studies. A substantial acid volatile sulfide phase is also present. As shown in Fig. 5, the amount of acid volatile sulfide decreases rapidly with depth. The pattern is probably the result of conversion of acid soluble monosulfide phases to less reactive disulfides as shown by Berner (1970). Although $FeCO_3$ and $MnCO_3$ might also be dissolving, because of the high levels of acid volatile sulfide in the surface samples, we have interpreted the production of ferrous iron and maganese in these experiments resulting from dissolution of mackinawite (FeS) and alabanite (MnS) in response to H^+ production during decomposition (Pankow and Morgan, 1980). Accordingly, the production rates of iron and manganese should follow the distribution of acid volatile sulfide, and they do (Appendix II).

The profiles of total and organic carbon at the study site are shown in Fig. 3 . Organic carbon comprises 75% - 100% of the carbon present. Carbon content decreases exponentially with depth to a constant value of approximately 1.2% (~1 x 10^{-2} mole/gram dry sediment) at a depth of 7 cm. The term oxidizable carbon will refer to total carbon less the observed 1.2% constant at depth. Under a steady-state approach, we conclude that below 7 cm the decomposition reactions are probably incomplete and proceeding at a much slower rate than those above this depth. Production rates of metals and nutrients follow the distriubtion of oxidizable carbon (Fig. 3; Tables 1

and 2). The distribution of bacterial abundance (Fig. 16) at this site is also correlated with the vertical profile of oxidizable carbon. The coincidence of these two profiles is not due to the carbon content of the bacteria population. Assuming a weight of 10^{-8} to 10^{-7} μgC/bacterium (Bancroft et al., 1976), the bacteria themselves account for only 0.1-1% of the organic carbon found in the sediment. The depth profile of bacterial abundance probably also reflects the profile of metabolic activity of the bacterial population at this site. Tobin and Anthony (1978) used tritiated thymidine incorporation to measure DNA synthesis in a sediment core from this part of Lake Erie and took DNA synthesis as an indicator of cell proliferation and microbial activity. They found that microbial activity was highest in the top 7 cm of the core, decreasing exponentially by about a factor to ten from the sediment-water interface to a depth of 7 cm. This is similar to the pattern we report here for bacterial number. They also found a high correlation of activity with bacterial biomass and cell numbers.

The observed decreases with depth for carbon and bacteria are sharper than those of the production rates. In part, this may be the result of sampling procedures. Total carbon, organic carbon, and bacterial abundance were all determined at 1 cm intervals on single cores. In contrast, production rates were determined over large intervals on homogenized sediment sections obtained from 25 different cores. Homogenization might tend to diminish the sharpness of depth variation.

Sediment homogenization, however, cannot account for the weak exponential decrease in calcium production. Calcium is released to the pore waters by a two-stage process. Hydrogen ion and organic acids are produced by the proposed decomposition reaction. Calcium is released when the excess acid is

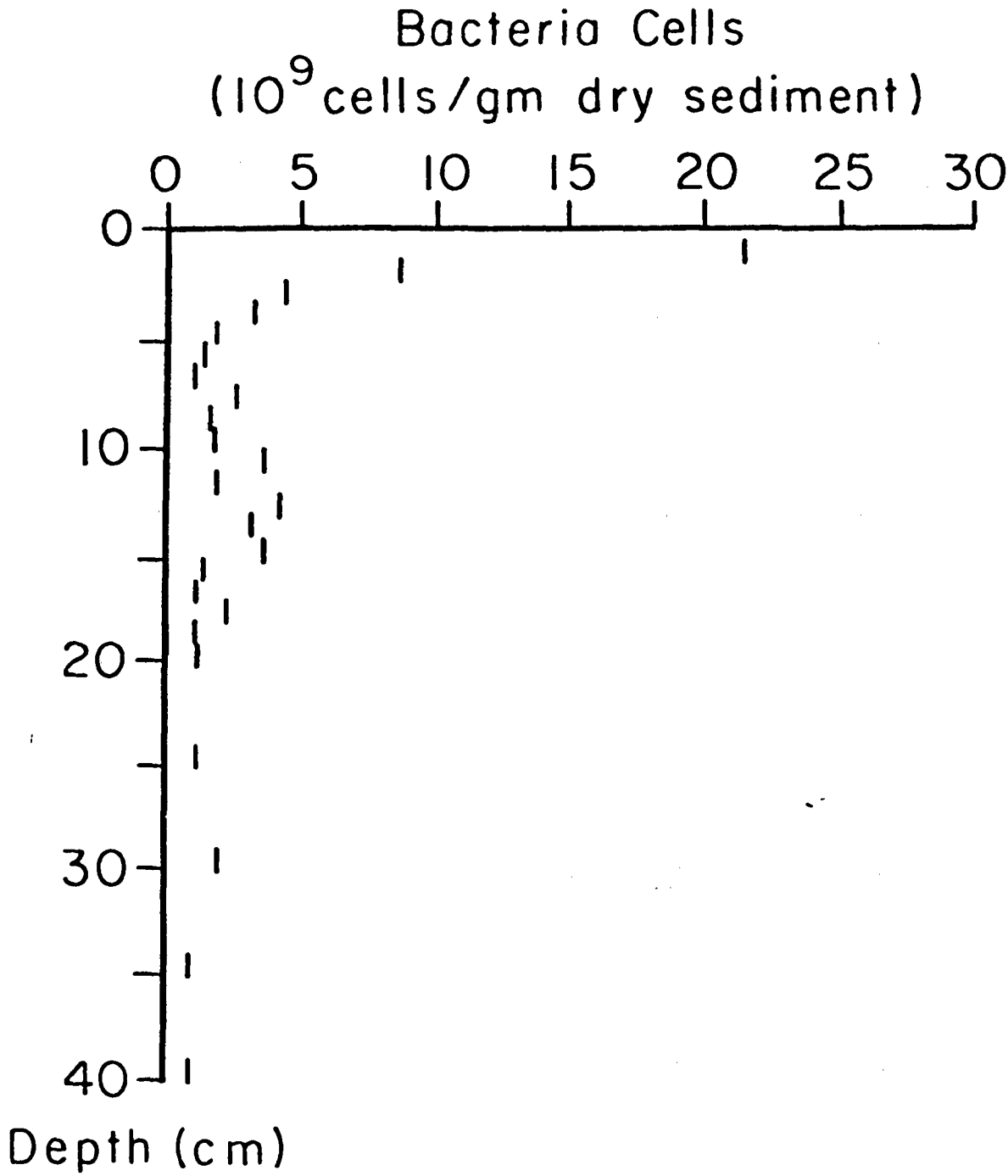

Figure 16. Bacterial abundance as a function of depth at Station 83.

neutralized by dissolution of calcuim-bearing carbonate phases. Thus, mineral equilibria, ion exchange, and adsorption all tend to modify the effects of the decomposition reactions. When coupled with the result that the composition of the sediment and the decomposition reaction rates are approximately uniform below 7 cm, it is reasonable that some of the parameters have rate distributions that are only partially described by equation (4).

It is interesting to note that the profiles of some parameters such as Pb^{210} (Fig. 17) show a mixed zone 4.5 cm thick, while other parameters such as organic carbon and total Kjeldahl nitrogen do not indicate mixing. The reason that the two observations are still consistent lies in the relative rates of mixing, decomposition, and loading of the parameters. Pb^{210} has a 22 year half life and has a constant supply to the sediment while loading of organic carbon has increased by about a factor of two since 1947. Apparently, the increased loading of organic carbon swamps the biogenic mixing signal.

Temperature Dependency

The rates of release of all parameters studied increased with increasing temperature. The temperature dependency of a single chemical reaction may be described by an Arrhenius rate law. The release of nutrients and metals during decomposition is clearly the result of numerous biotic and abiotic reactions, both partial and complete. Nevertheless, the temperature data may be characterized by the Arrhenius function, "apparent activation energies" calculated, and some information about the kinetics of reactions extracted. Table 3 gives the results of applying the Arrhenius rate law to the production rate data.

The apparent activiation energy for ammonium production is slightly larger than the 16.6 KCal/mole value calculated from ammonium data given by Rosenfeld (1977) and is only slightly less than those reported for sulfate

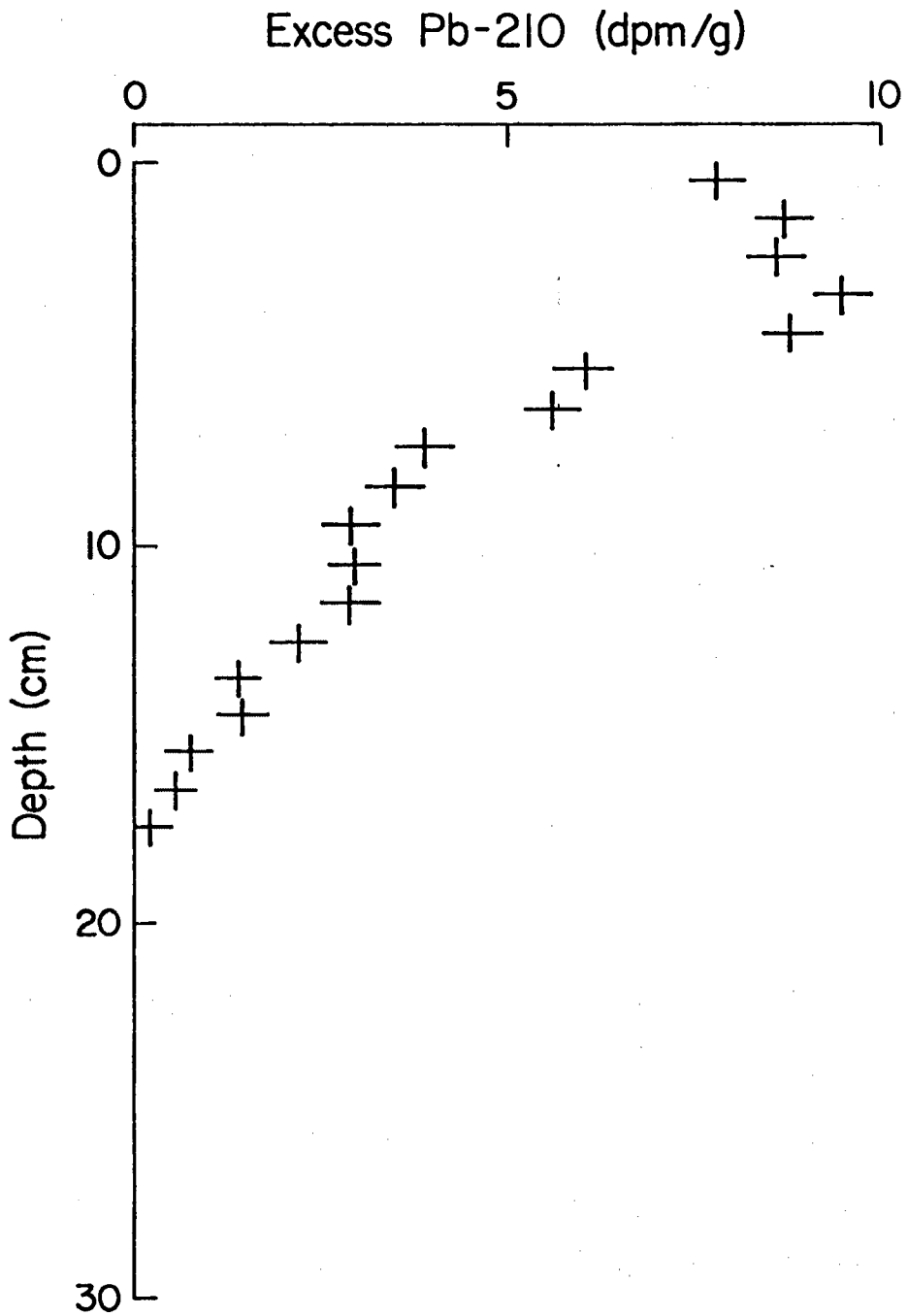

Figure 17. Excess Pb-210 versus depth at Station 83.

	NH_4^+	HCO_3^-	PO_4	Ca	Mg	Fe^{++}	Mn
A_o	32.78	20.79	31.13	17.71	11.69	11.88	15.34
E*	17.82	10.29	18.17	9.38	6.50	6.74	9.83

Table 3. Temperature dependencies of the rate of production from the equation $R_o'(T) = A_o \exp(-E^*/RT)$. $R_o'(T)$ ($x10^{-3}$ moles/yr) is the production rate at the sediment-water interface; A_o ($x10^{-3}$ moles/yr) is the pre-exponential factor; E* (KCal/mole) is the activation energy; and R (=1.9872 cal/mole · °K) is the gas constant.

reduction (Vosjan (1974), 22 KCal/mole; and Rosenfeld (1977), 24.6 KCal/mole). This suggests that bacterial energetics in Lake Erie sediments are comparable to those of estuarine and marine sediments. This agrees well with our previous conclusion that the energetics of methane fermantation are only slightly less than those of sulfate reduction. The lower apparent activation energies for bicarbonate, calcium, magnesium, ferrous iron, and manganese suggest that these species may also be involved in chemical reactions, such as mineral dissolution, that are much less energetic. The high activation energy determined for phosphate is based upon depth dependencies which assume no loss of phosphate to mineral reactions in the surface sediments. The agreement in activation energies between ammonium and phosphate supports this assumption for phosphate.

If the effects of adsorption are considered, the rates obtained are greater than the observed "apparent rates" (Rosenfeld, 1979):

$$R'(A,T) = \frac{R_T(Z,T)}{1 + K} \qquad (6)$$

where $R_T(Z,T)$ is the total or true release rate. Using a value of K ~1-2 for ammonium (Rosenfeld, 1979), the calculated true rates of release are a factor of 2-3 greater than the reported apparent rates, but the activation energy remains essentially unchanged. Thus, adsorption does not affect the previous conclusion that of the species studied only ammonium does not significantly enter into mineral dissolution or precipitation reactions.

Flux Experiment

Overlying Water Chemistry

Homogenized Mud Core Experiment Typical concentration versus time plots for ammonium, alkalinity, pH, SRP, SRS, and ferrous iron in the homogenized mud experiment (with and without worm cases) are given in Fig. 18. On the whole, changes observed in the overlying water are those expected from the work of Mortimer (1941; 1942). The overlying water, which was initially deionized, quickly reached an apparent steady state composition with respect to both SRP and alkalinity. After the microcosms were sealed and purged with helium (+44 days), alkalinity in the overlying water increased markedly. Alkalinity reached somewhat higher values in microcosms with tubificid populations. Immediately prior to (or concurrent with) the rapid increase in ferrous iron in the overlying water, alkalinity decreased slightly. The exact time at which dissolved oxygen in the overlying water was totally depleted was uncertain. Electrode measurements of dissolved oxygen indicated no dissolved oxygen present prior to other chemical changes (e.g. increase in ferrous iron concentration) known to accompany anoxia. Consequently, the presence of detectable level of ferrous iron was taken to indicate anoxia in the overlying water. Ammonia was first detected in the overlying water after the microcosms were sealed and helium purged. In general, the concentration of ammonia increased with time. Microcosms with tubificid populations exhibited higher ammonia concentrations compared to that of those microcosms lacking a worm population. Silica concentrations increased with time. The pattern of silica increase, however, appeared to be unrelated to anoxia or the presence of tubificids. In contrast, Mortimer (1941) observed a large increase in silica

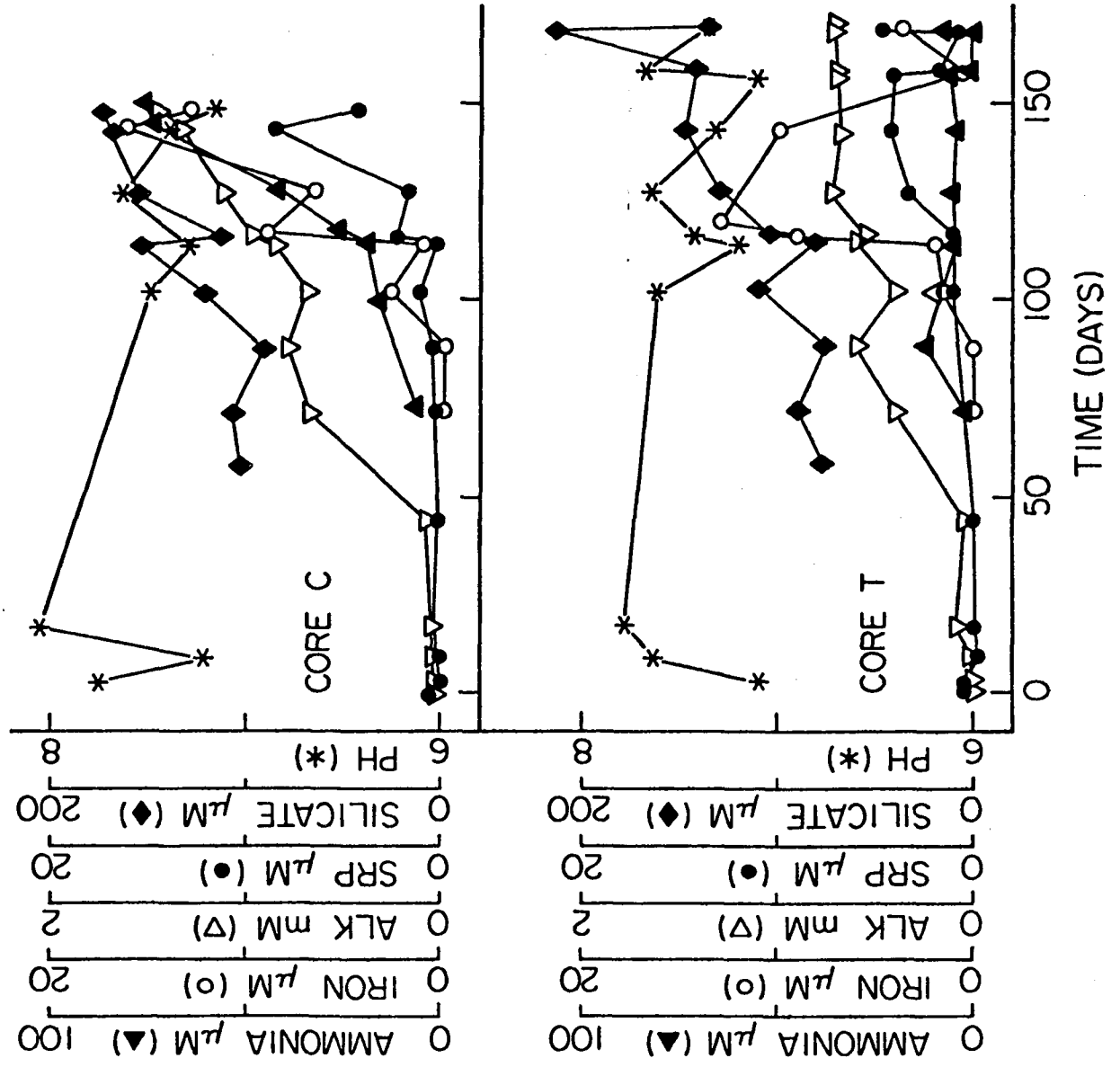

Figure 18. Concentration of ammonia, ferrous iron, alkalinity, SRP, and SRS and pH in the overlying water of homogenized mud experiment cores. C-with tubificids, T-without tubificids.

concentration concurrent with anoxia. Ferrous iron remained at low levels (i.e. below detection) then sharply increased in concentration. Microcosms lacking a tubificid population tended to experience a sharper initial rise in ferrous iron concentration compared to those microcosms having a tubificid population. The concentration of SRP increased after the microcosms were sealed. The pattern of SRP concentration increase, however, did not necessairly mirror that of ferrous iron. Often, SRP concentration increased sharply prior to the detection of ferrous iron in the overlying water. The pH of the overlying water exhibits an initial increase (first 20 days). After this, pH appeared to decrease. Reasonably sharp pH decreases occurred concurrently with the initial rise in ferrous iron concentration .

Lake Core Experiment A typical concentration versus time plot for ammonium, alkalinity, pH, SRP, SRS, and ferrous iron in the lake core experiment is given in Fig. 19. Again, the observed chemical changes are similar to those described by Mortimer (1941; 1942). After sealing, ammonium increases sharply. Alkalinity tends to increase, but not to the same extent as seen in the Homogenized Mud Experiments. Silica displays a strong increase over time. Again, the pattern of silica concentration increase appears to bear no relationship to anoxia (i.e. presence of ferrous iron). Ferrous iron displays a pattern of sharp concentration increase. SRP concentration changes appear to coincide with the increases and decreases of ferrous iron concentration. Again, pH of the overlying water tends to decrease with time.

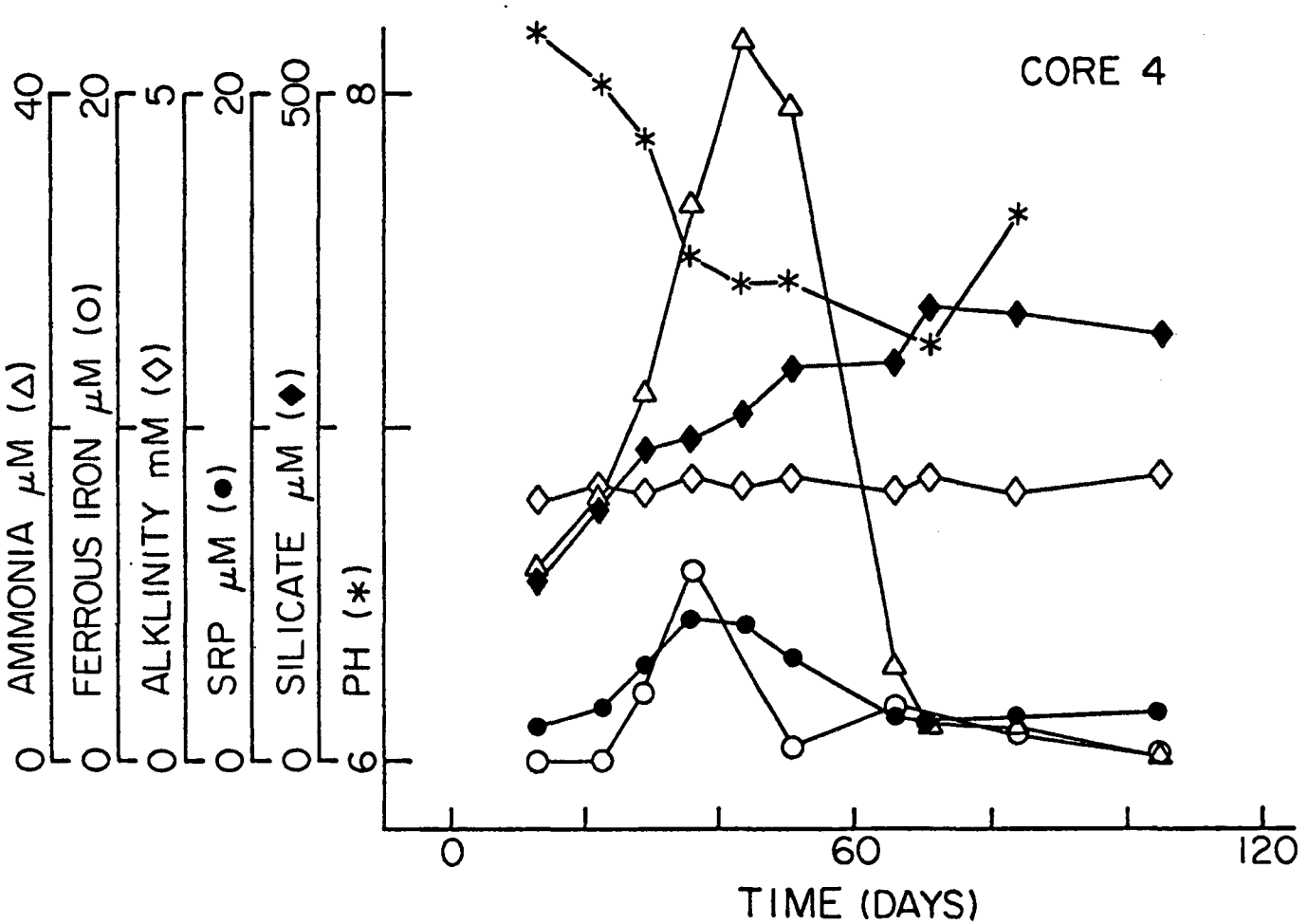

Figure 19. Concentration of ammonia, ferrous iron, alkalinity, SRP, and SRS and pH in the overlying water of a lake core experiment core. (LCE-4).

Interstitial Water Chemistry

Homogenized Mud Core Experiment

Interstitial water profiles of ammonia, ferrous iron, alkalinity, SRP and SRS determined in the homogenized mud experiment for microcosms lacking a tubificid population are shown in Fig. 20. Chemical profiles from microcosms with a tubificid population are shown in Fig. 21. (Numerical data are given in Appendix IV).

Ammonium. In microcosms lacking worms, ammonia concentration increased exponentially to a depth of ~10cm then remained constant. In these microcosms, ammonia profiles did not exhibit a strong time dependency. Ammonia concentration at depth did tend to increase slightly with time. The absolute value of ammonia concentration at depth is similar to that observed in cores collected at Station 83. In microcosms with a tubificid population, the observed ammonia profiles are strikingly different. Ammonia concentrations exhibit far less depth variation and there is some evidence that a subsurface source of ammonia is present. The ammonia concentration at depth is similar to that observed in Lake Erie cores (station 83).

Ferrous Iron. In both with and without worm microcosms, ferrous iron concentration profiles show an increasing trend with depth, and there is no consistent evidence for time dependency. Ferrous iron profiles from microcosms with tubificids are somewhat more chaotic than those from microcosms without worms.

Alkalinity. Depth profiles of alkalinity from both with and without worm microcosms are very similar. Alkalinity profiles exhibit an exponential increase with depth to ~10cm then increase monotonically with depth. Profiles of alkalinity do exhibit substantial evidence of time dependency.

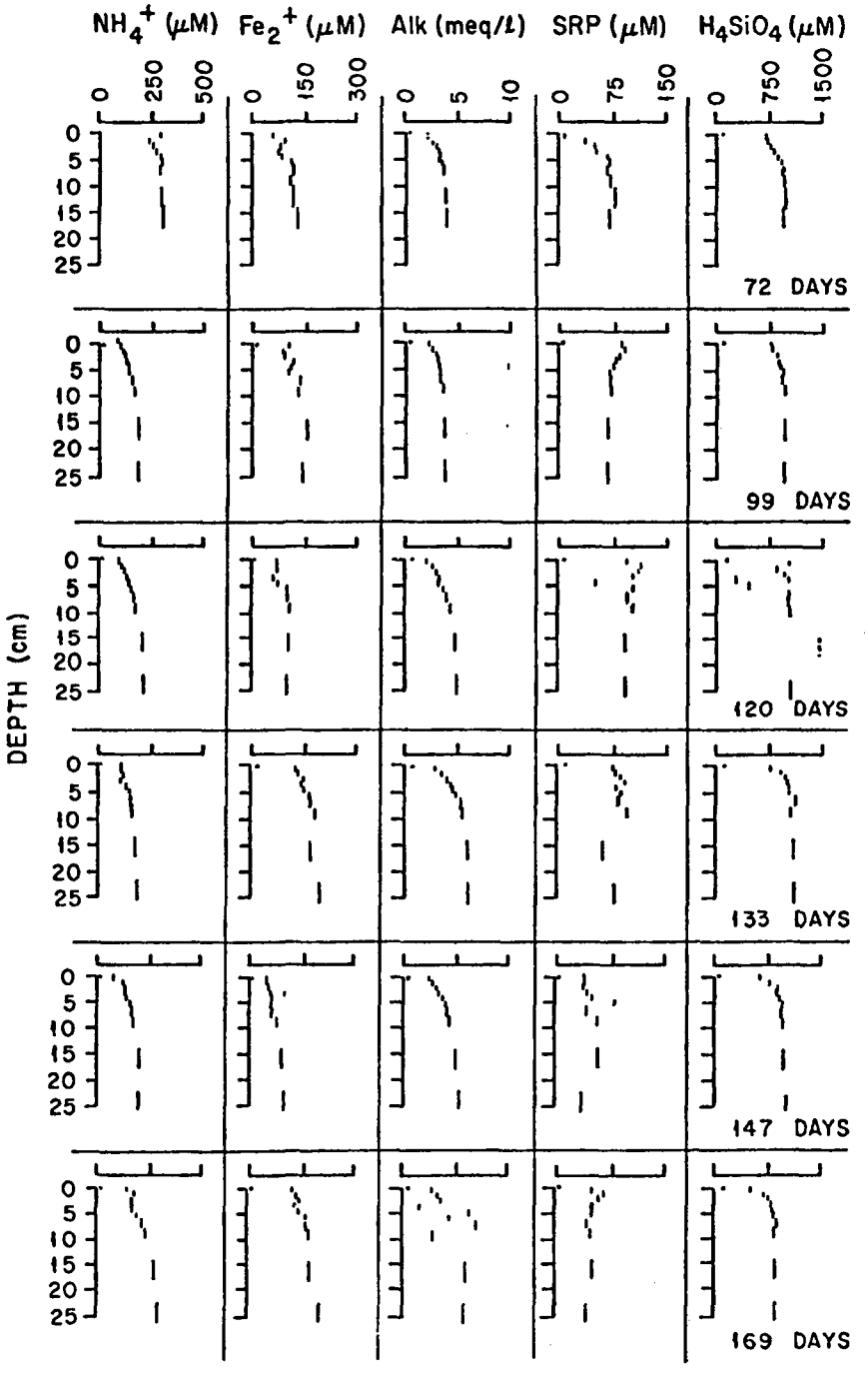

Figure 20. Vertical profiles of ammonia, ferrous iron, alkalinity, SRP, and SRS in the homogenized mud experiment cores without worms.

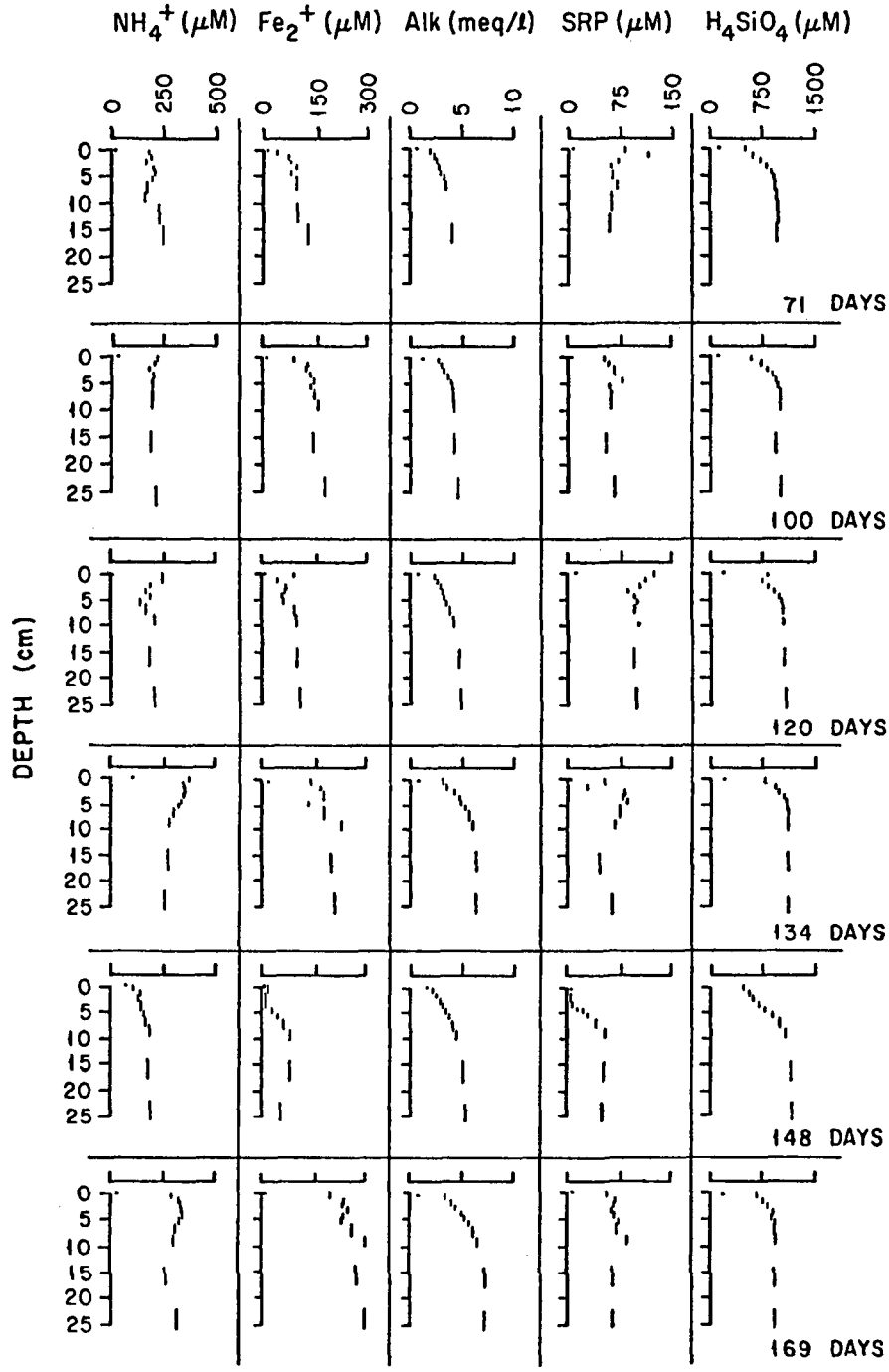

Figure 21. Vertical profiles of ammonia, ferrous iron, alkalinity, SRP, and SRS in the homogenized mud experiment cores with worms.

Profile curvature changes with time and the alkalinity at depth increases with time.

SRP. Profiles of SRP show no consistent trend with either depth or time for either with or without worm cases.

SRS. Silica concentrations in microcosms both with and without tubificids generally exhibit a decrease with depth to a depth of ~ 5cm and thereafter maintain a fairly constant concentration. Silica concentration at depth tends to increase with time in both with and without worm casas.

Lake Core Experiment

Interstitial water profiles of ammonia, ferrous iron, alkalinity, SRP, and SRS obtained in the lake core experiment are given in Fig. 22. (Numerical data are given in Appendix IV).

Ammonia. Ammonia profiles observed in the lake cores exhibit a subsurface maximum indicating subsurface production of ammonia. Below the subsurface maximum, ammonia concentrations are fairly constant with both depth and time. The lake core experiment ammonia profiles are similar to the homogenized mud core (with worms) ammonia profiles, but show greater consistency.

Ferrous Iron. Depth profiles of ferrous iron obtained from the lake core experiment exhibit a subsurface concentration maximum with increases in magnitude with time. Ferrous iron concentrations at depth are constant over time.

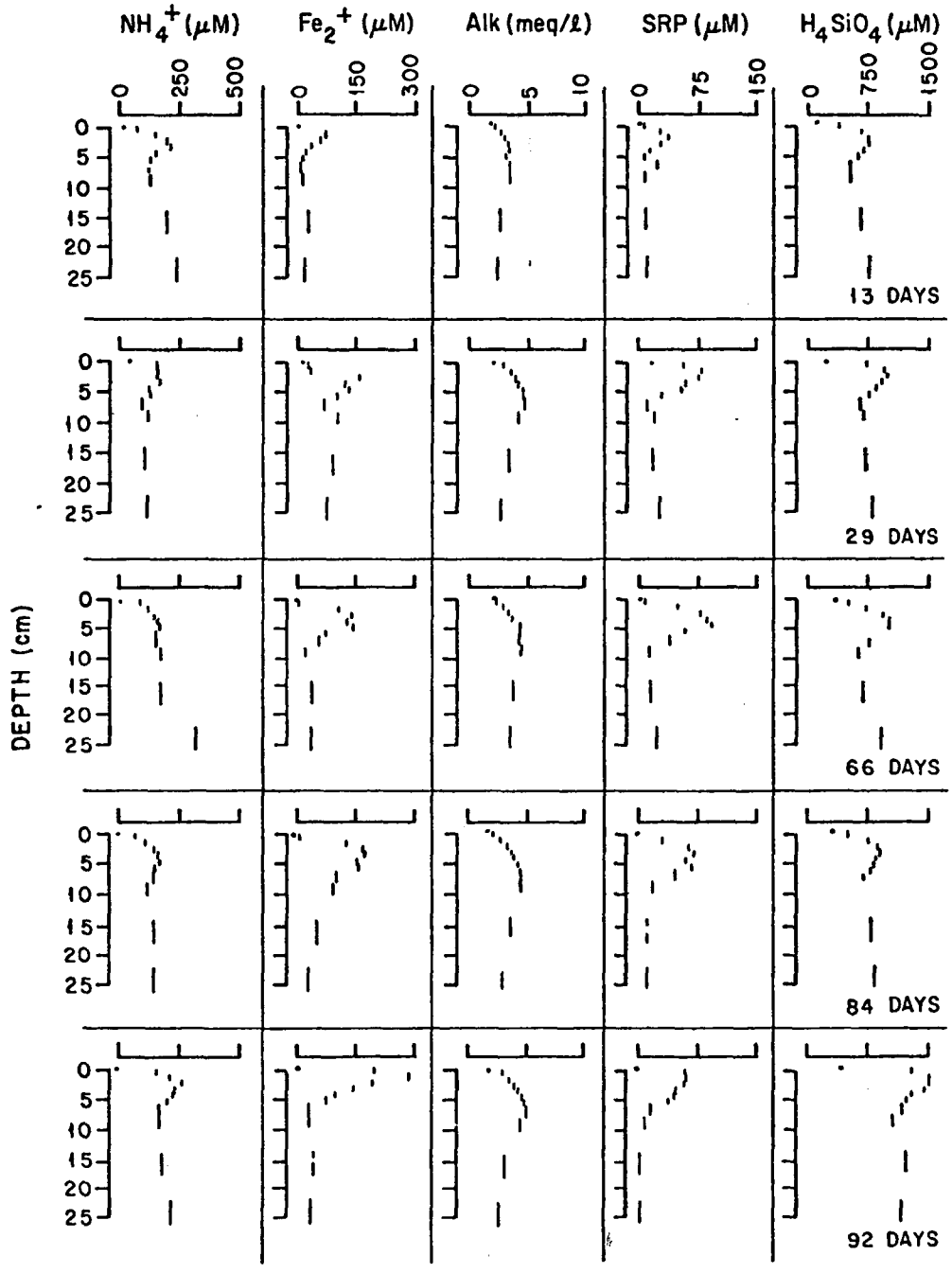

Figure 22. Vertical profiles of ammonia, ferrous iron, alkalinity, SRP, and SRS in the lake core experiment cores.

Alkalinity. Vertical profiles of alkalinity also show a subsurface maximum which increases with time. Alkalinity at depth in the cores is constant with time. The location of the alkalinity maximum coincides with the depth at which ferrous iron reaches a constant value.

SRP. Vertical profiles of SRP appear to follow those of ferrous iron. The location of the SRP subsurface maximum coincides with that of the ferrous iron, and SRP concentration is reasonably constant at depth in all cores. The magnitude of the SRP maximum increases up to 66 days, then decreases. This is in contrast to the ferrous iron maximum which consistenly increases.

SRS. As in the cases of the other parameters, silica profiles also exhibit a subsurface maximum. The vertical location of the maximum is coincident with those of ferrous iron and SRP. Unlike the other parameters, silica concentrations tend to increase with both depth and time below the maximum.

Chemistry of the Sediment Solids

Results of chemical analysis of the sediment solids from two homogenized mud core experiment cores, HMC-R and HMC-T (both without worms, +71 days and +169 days after settling in the microcosms, respectively), and one lake core experiment core LCE-6 (+13 days after collection) are presented in Figures 23-31 (numerical data is given in Appendix IV). The measured parameters include total carbon, organic carbon, Kjeldahl nitrogen, total phosphorous, and total calcium, magnesium, manganese, zinc, and copper.

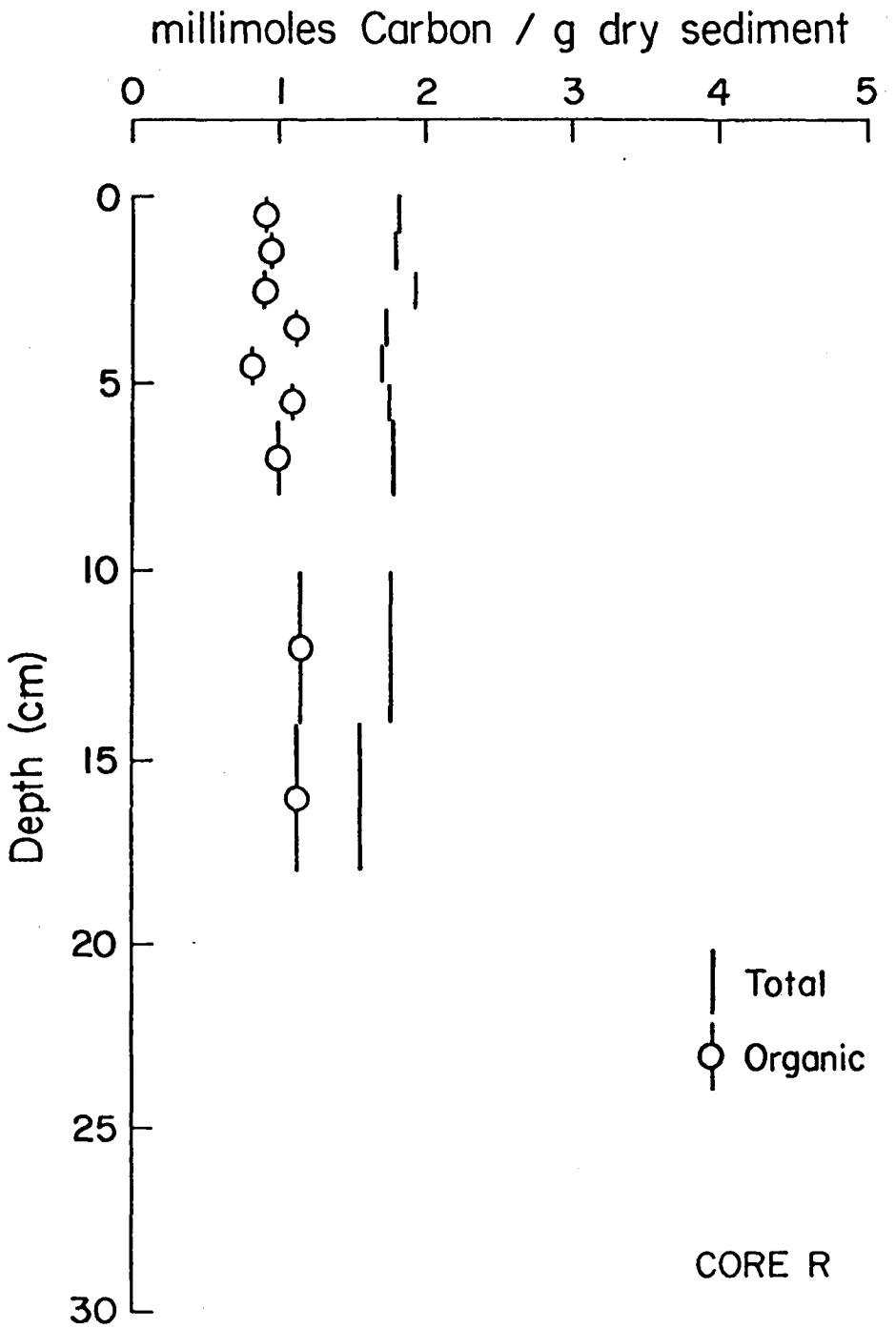

Figure 23. Total and organic carbon in homogenized mud core R (+72 days).

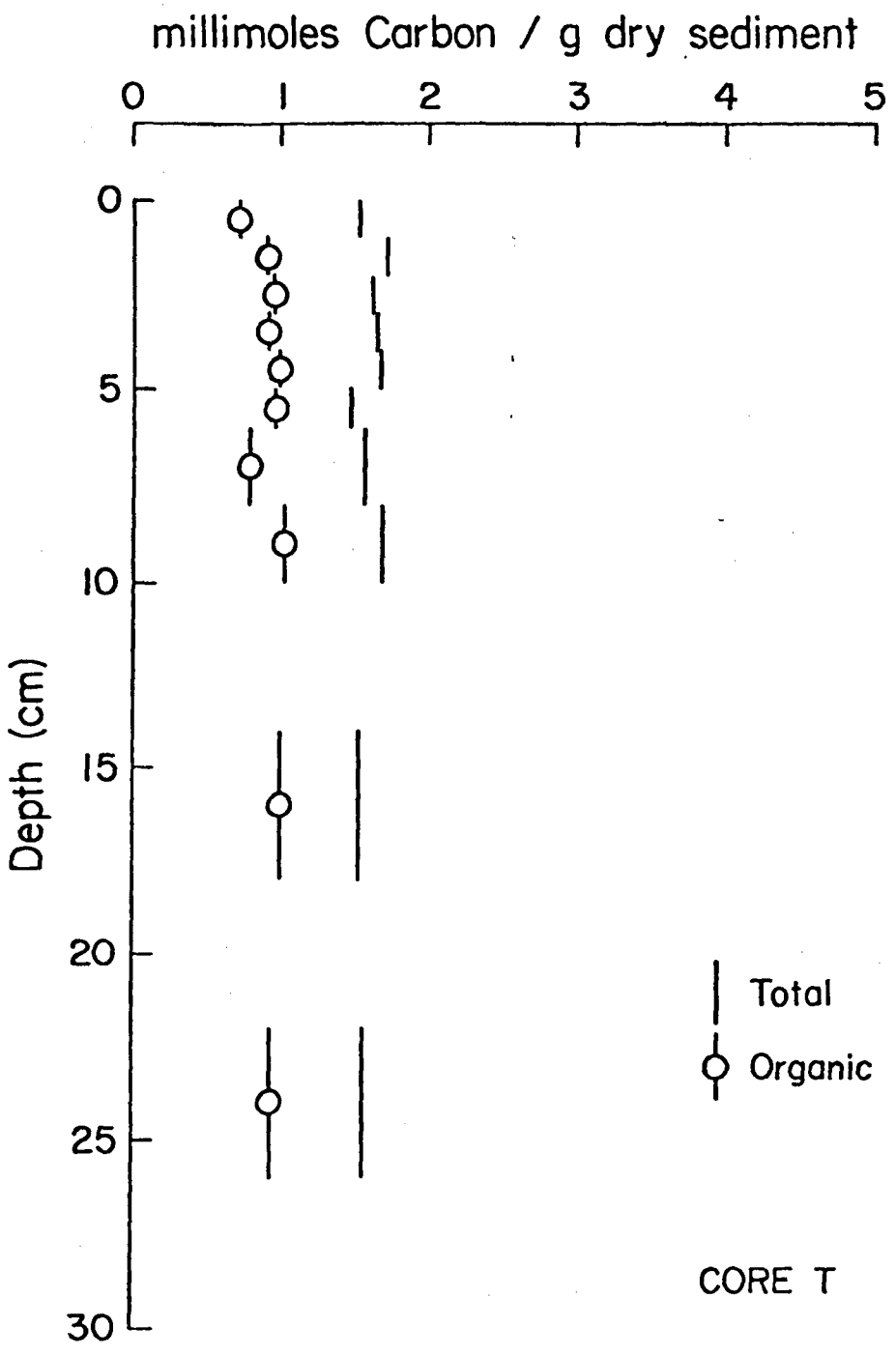

Figure 24. Total and organic carbon in homogenized mud core T (+169 days).

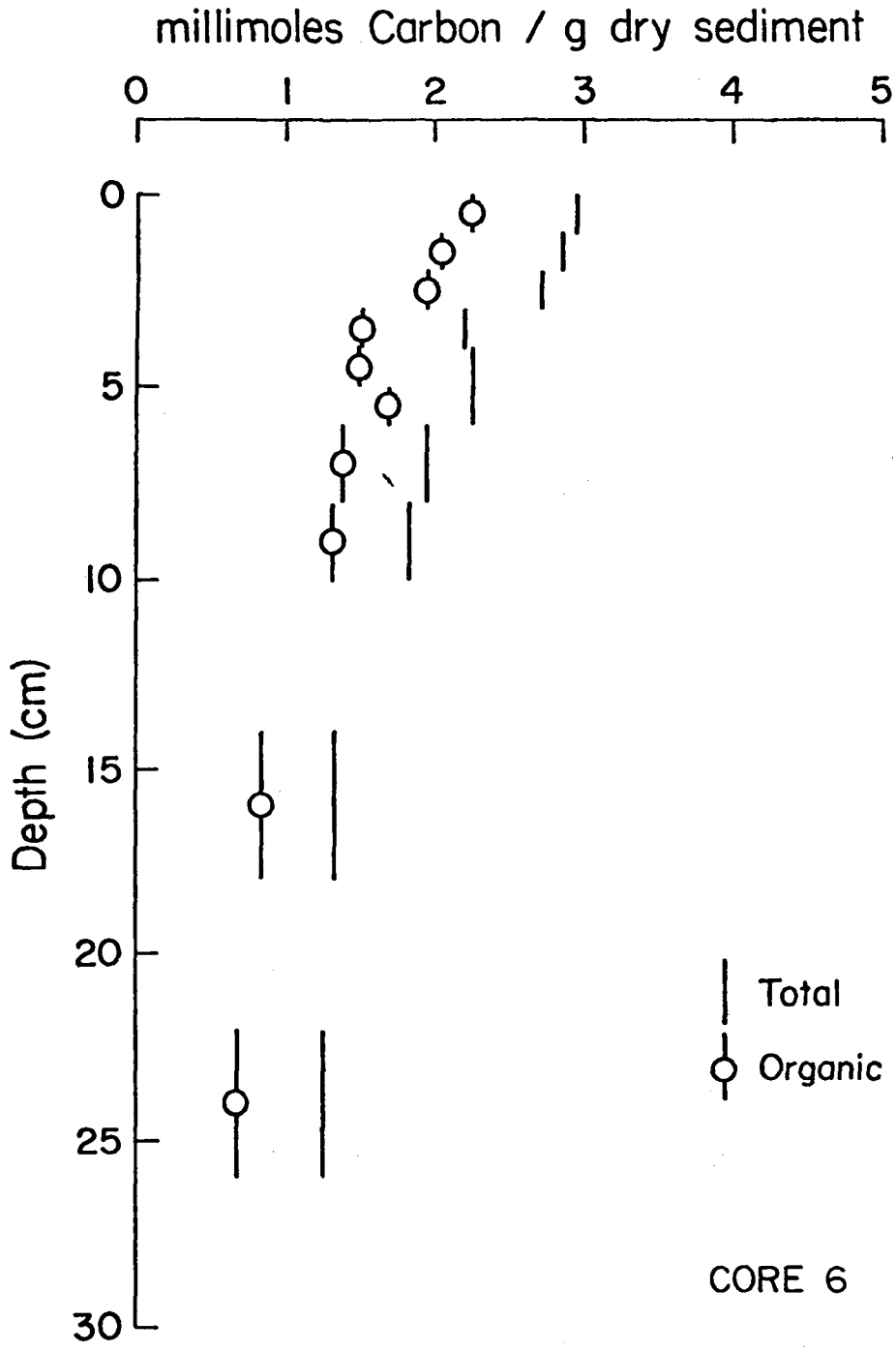

Figure 25. Total and organic carbon in lake core 6 (+13 days).

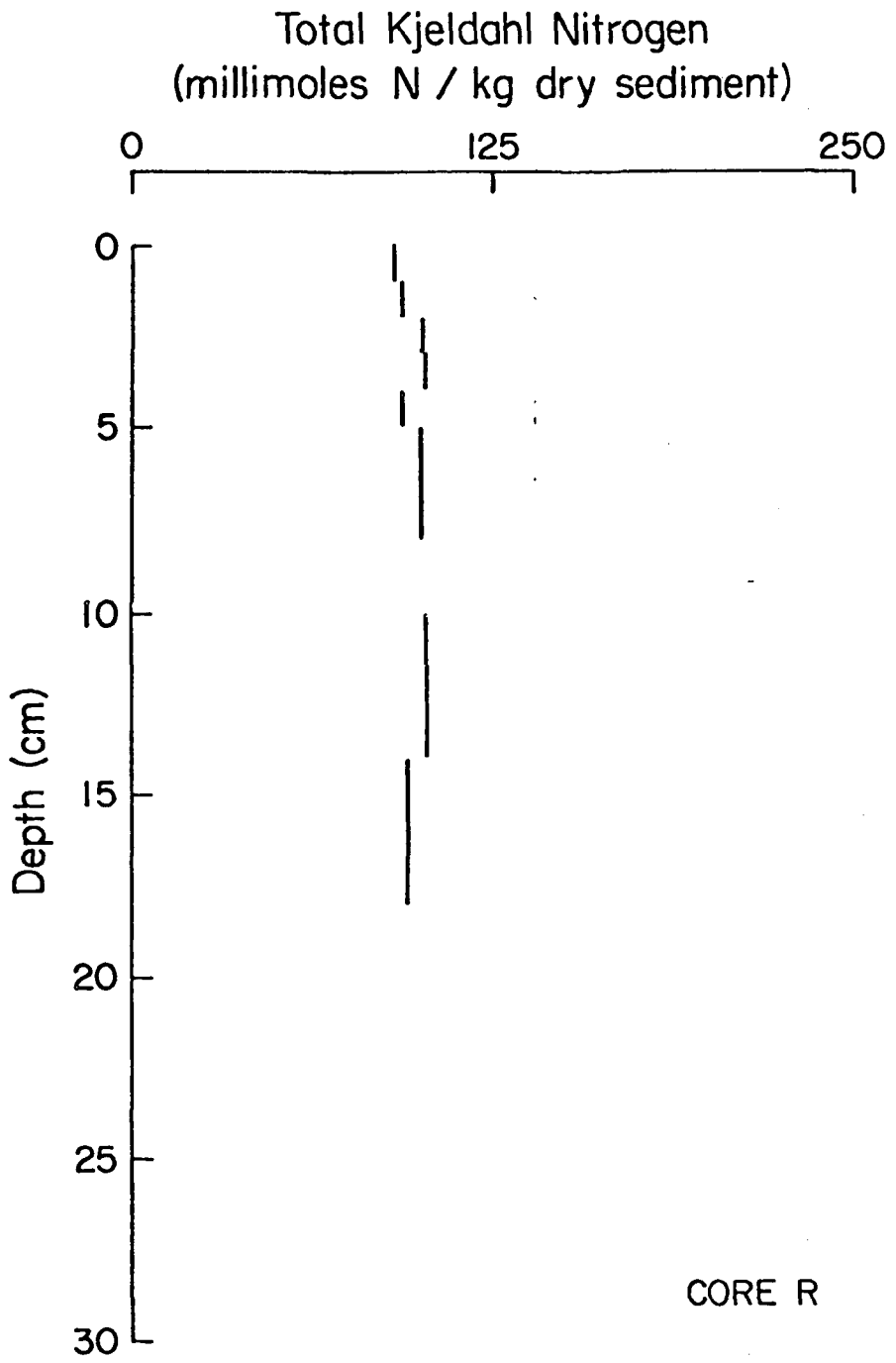

Figure 26. Total Kjeldahl nitrogen in homogenized mud core R (+72 days).

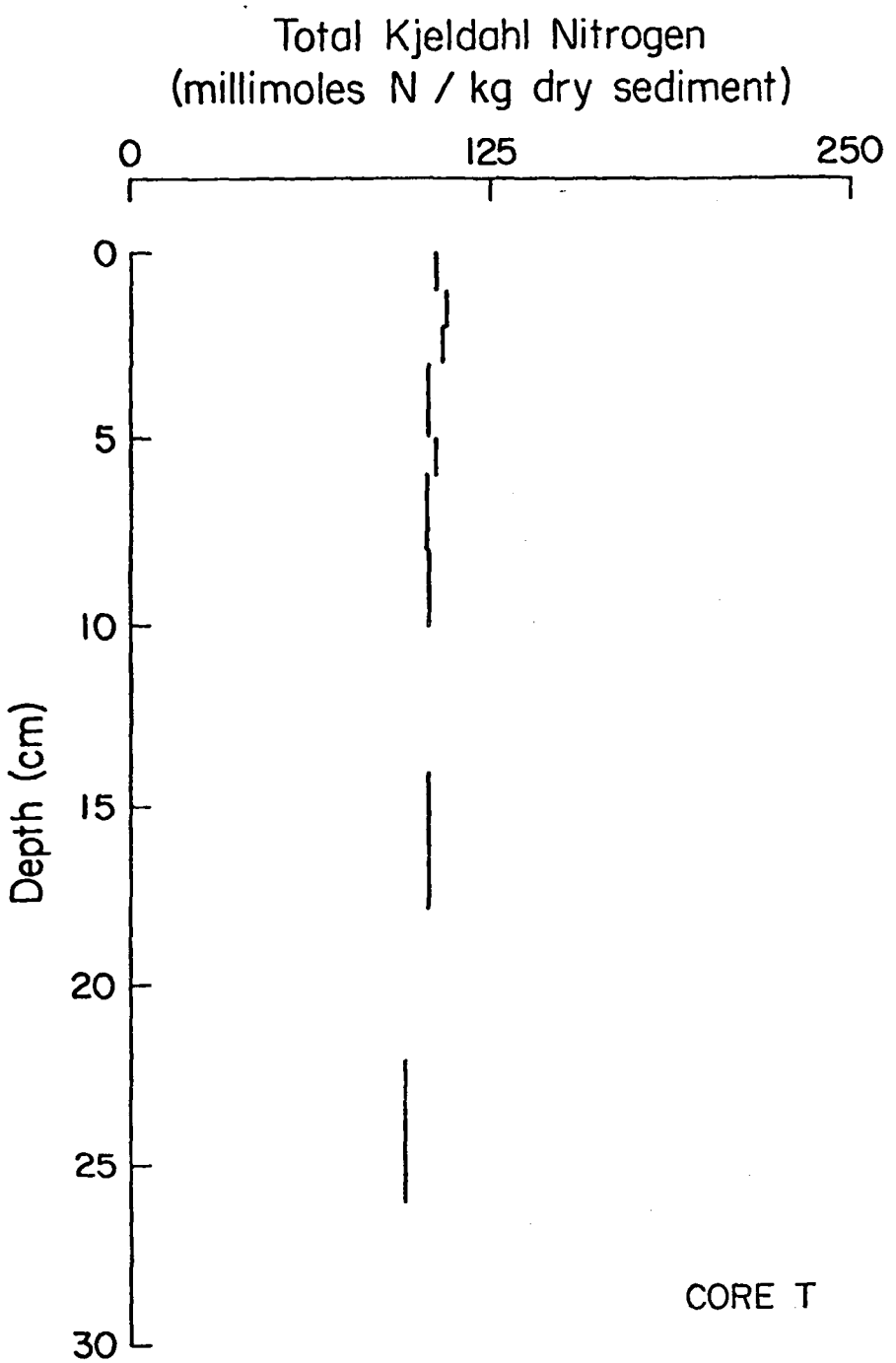

Figure 27. Total Kjeldahl nitrogen in homogenized mud core T (+169 days).

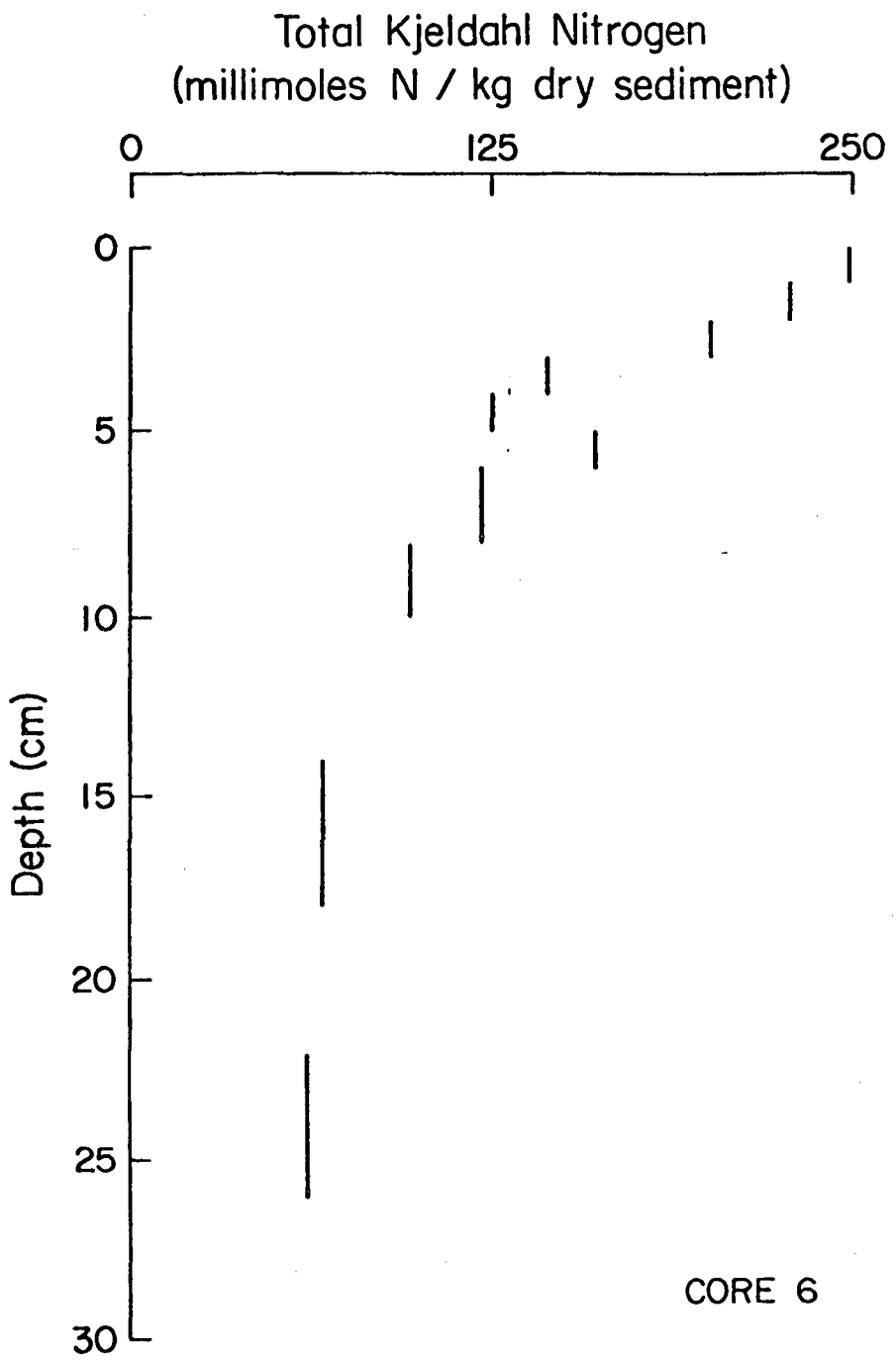

Figure 28. Total Kjeldahl nitrogen in lake core experiment core 6 (+13 days).

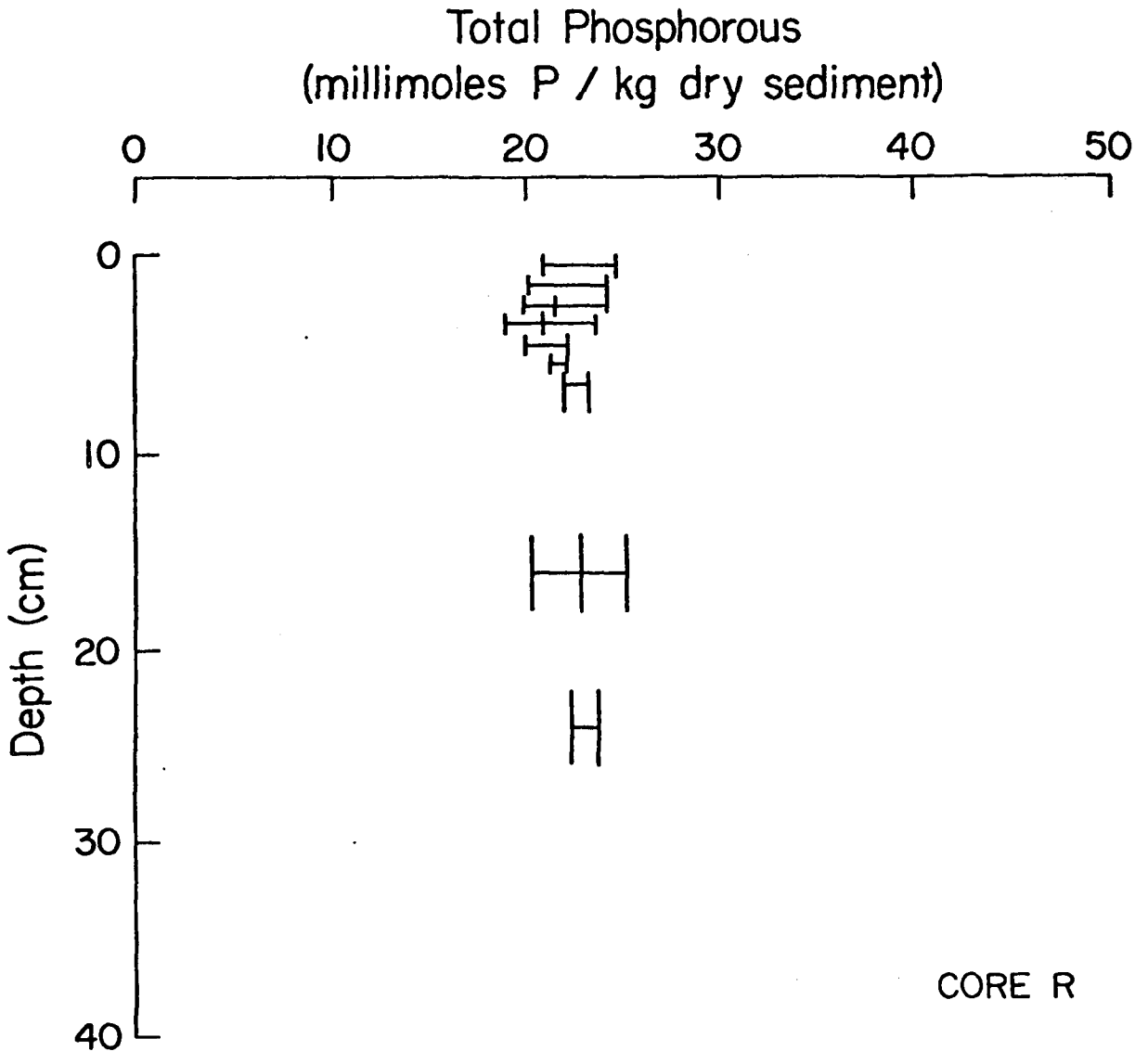

Figure 29. Total phosphorous in homogenized mud core R (+72 days).

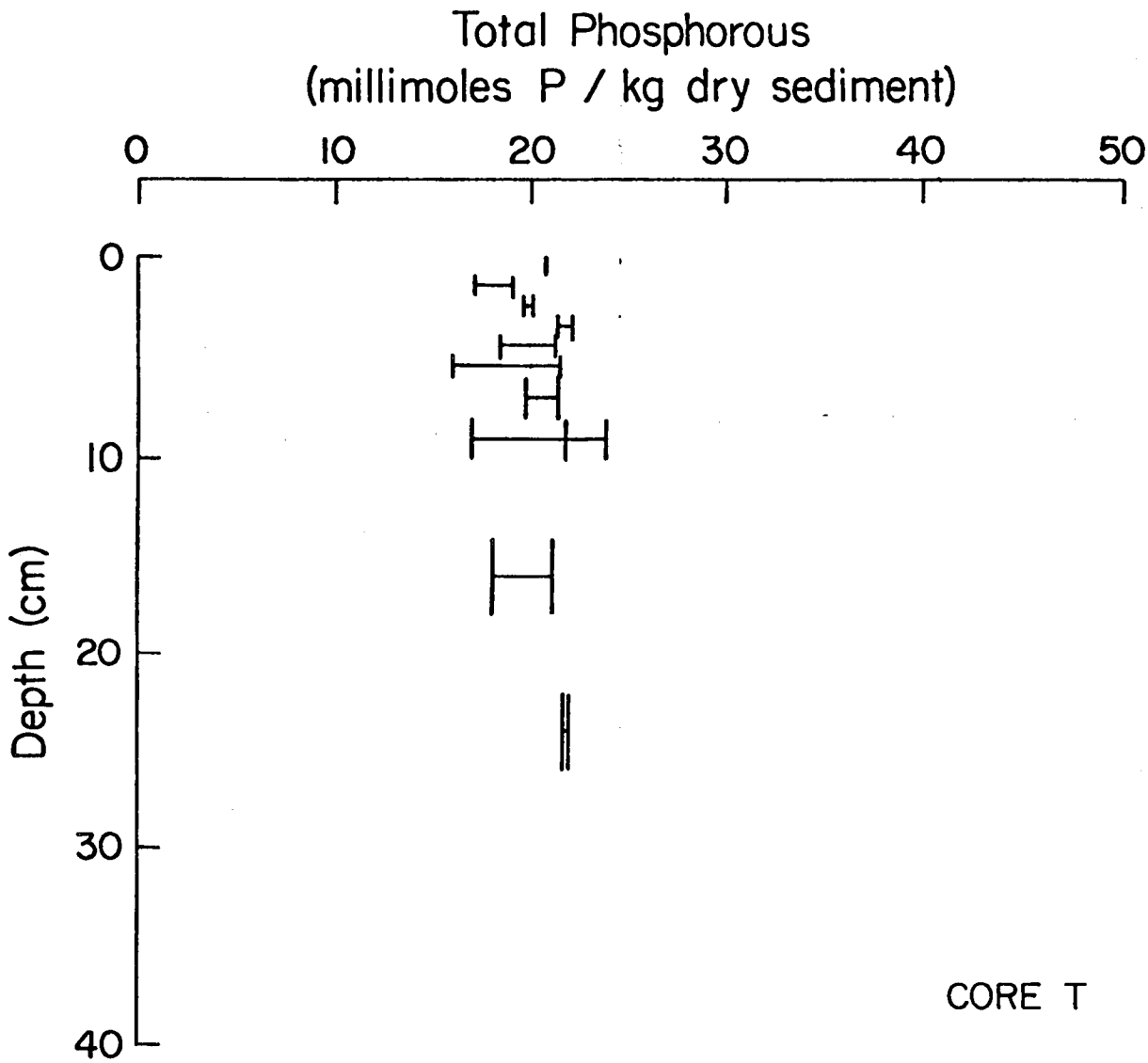

Figure 30. Total phosphorous in homogenized mud core T (+169 days).

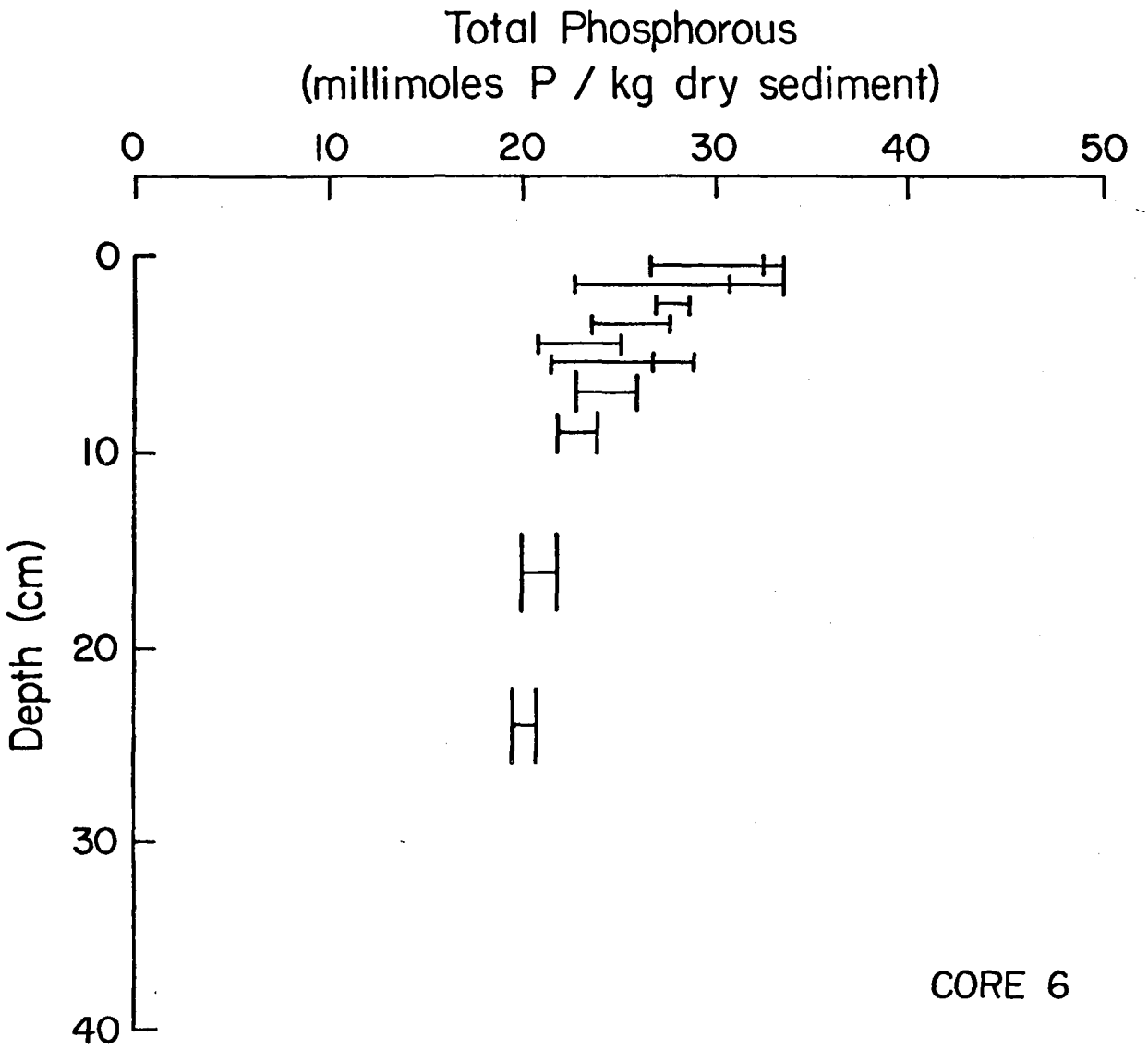

Figure 31. Total phosphorous in lake core experiment core 6 (+13 days).

Homogenized Mud Core Experiment

In the homogenized mud cores, there is no depth variation in total carbon, organic carbon, Kjeldahl nitrogen, total phosphorous, calcium, magnesium, or iron. This result indicates that sediments in the homogenized mud core experiment were well mixed. Vertical profiles of total manganese, zinc, and, to some extent, copper exhibit significant departures from homogeneity. Solid phase manganese shows an exponential decrease in abundance moving from the sediment surface to depth, while both zinc and copper have surface and subsurface maximum. These patterns are observed in both HMC-R and HMC-T. The only possible explanation of such patterns is the mobilization of those metals and their precipitation as authigenic minerals. The specific mineralogy of these precipitates could not be identified, and results from the mineral equilibria calculations did not indicate a large degree of supersaturation for any pure carbonate or phosphate phase for manganese, zinc, or copper at the depths their solid phase maxima are observed.

Lake Core Experiment

Solid phase analyses of the lake core experiment core, LCE-6 show no significant departure from other observations made for cores at station 83. The suite of cores collected at station 83 for the lake core experiment are representative of the locale.

Comparison of Homogenized Mud Cores to Lake Cores

Comparison of solid phase data for the homogenized mud cores and the lake cores shows that the homogenized mud core sediments are significantly lower in water content and exhibit a smaller gradient in porosity change with depth. The homogenized mud cores vary in water content from ~60% at the sediment-

water interface to ∿52% at 22-26 cm. In contrast, the lake cores vary in water content from ∿86% at the sediment-water interface to ∿56% at 22-26 cm. Examination of the total carbon, organic carbon, and Kjedahl nitrogen data indicates that the homogenized mud core sediments are chemically similar (gross comparison) to sediments from a depth of 10 to 15 cm.

Discussion

Mineral Equilibria

Many trace metals can be toxic if their concentrations reach sufficiently high levels in living plants and organisms. It is necessary to understand their behavior and transport to determine the magnitude of their threat in a specific environment. In order to understand chemical behavior, concentrations and reactivities must be determined in the different physical compartments--overlying water, sediments, and interstitial waters --before exchange between the systems can be investigated. In this section, the interstitial waters in Lake Erie sediments were investigated in an effort to identify post-depositional mineral equilibria of calcium, magnesium, maganese, iron, zinc, cadmium and lead carbonate and phosphate minerals.

The formation of these mineral phases results in an increased removal and storage of trace metals and phosphate pollutants in sediments. Thus the indentification of authigenic mineral phases increases our understanding of the lake's response to chemical stress and aids managers in quantitatively evaluating pollutant loading rates.

Little work has been done on the interstitial water chemistry of zinc, cadmium, and lead. A large body of data has accumlated describing their distribution in solid sediments (Wheeler and Duriming, 1976; Presley, et al.,

1972; Semkin and Kramer, 1976; Jenne, 1968) and surface waters (Chawla and Chau, 1969; Zirino and Healy, 1970; Riley and Taylor, 1972; Bachmann, 1963; Bradford, 1972; O'Connor and Renn, 1964; Hem, 1972), but these studies were not able to elucidate their chemical behavior in the sediment-interstitial water system. Several investigators have attempted to determine the controlling mechanisms responsible for the distribution of zinc, cadmium and lead by analyzing their concentrations in various aqueous and solid fractions in one system (Walters et al., 1974; O'Connor and Renn, 1964; Bachmann, 1963; Cline and Upchurch, 1973; Gardiner, 1974a, 1974b). These studies have made headway towards understanding the relative reactivities of metals with organics and their adsorption on ferric hydroxides and clay mineral surfaces. Such methods, however, could not identify individual mineral phases. Therefore, these studies only conclude that the metals were complexed by other dissolved species or were in equilibrium with an unidentified mineral phase (Presley et al., 1972). Analysis of metals in the sediment fraction alone cannot be used to discern processes controlling their distribution.

More recently, researchers have studied interstitial water chemistry (Muller, 1969; Brooks et al., 1968; Troup 1974; Duchart et al., 1973) in the hope of understanding the processes controlling the behavior of the metals in sediments. The interstitial water is the medium connecting the solid phases in the sediments and the soluble species in the overlying water. Because any change in metal behavior will alter the chemical composition of the pore waters, pore water chemistry is a sensitive indicator of chemical reactions and equilibria between solid phases and dissolved species (Berner, 1971). The residence time of metals in interstitial water is greater than in overlying water. Consequently, metals in pore waters are more apt to approach a state of equilibrium with solid phases in the sediments. Thus, the chemical

composition of the interstitial waters can be used to identify and study mineral-water equilibrium reactions in sediments. Once these reactions are determined, chemical mass transport can be studied.

A thermodynamic equilibria approach has been used successfully to study the behavior of ferrous iron in pore waters (Troup, 1974; Bray, 1973; Nriagu, 1972a; Emerson, 1976). Siderite ($FeCO_3$), vivianite ($Fe_3(PO_4)_2 \cdot 8H_2O$) and mackinawite ($Fe_{1+x}S$) were found to be supersaturated in many intersitital waters, and their presence has been confirmed by x-ray diffraction studies. This supports the conclusion that these minerals control the dissolved ion centrations of ferrous iron, carbonate, and phosphate, and that thermodynamic studies of the interstitial waters may be used to predict the controlling mineral equilibria. Lu and Chen (1977) examined the seawater overlying sediments for release of trace metals under oxidizing and reducing conditions. They concluded that solid phase sulfides, carbonates, and silicates were controlling trace metal behavior.

Since zinc, cadmium, lead, and manganese share some chemical properties with ferrous iron, a thermodynamic approach may be applicable to the study of these trace metals. These metals (like ferrous iron) may form relatively insoluble metal carbonates and/or phosphates under conditions found in anoxic lake sediments. Hence, the thermodynamic approach that has been used study ferrous iron behavior was followed in this study.

Calculation of Activities

The ionic strength, activity coefficients, and activities of calcium, magnesium, ferrous iron, manganese, zinc, cadmium, and lead were calculated by a computer program, ASAME (Aquatic Speciation And Mineral Equilibria), to determine the speciation of the metals and the ion activity products of the metal carbonates and phosphates. The computer program developed in this study

is based on procedures outlined by Garrels and Thompson (1962) and is of the 'continued fraction' type discussed in Nordstrom et al. (1979). In this study, all the measured species (Na^+, Ca^{2+}, Mg^{2+}, K^+, Zn, Cd, Pb, Fe^{2+}, Mn^{+2}, NH_4^+, CL^-, NO_3^-, ΣPO_4, and HCO_3^- and estimated values for SO_4^{2-} (Weiler, 1973)) were used to calculate the initial ionic strength, I, of each pore water sample:

$$I = \frac{1}{2} \Sigma m_i Z_i^2 \tag{7}$$

where m_i is the measured analytical concentration and Z_i is the charge of a species i. Activity coefficients were then calculated from the Debye-Hückel, the Guntelberg, or the Davies equations, according to the ionic strength limits given in Stumm and Morgan (1970).

The details of the calculation procedure are given in Garrels and Thompson, (1962), and Nordstrom et al. (1979). Briefly, the activities of the free ions were calculated by a successive approximation. A mass balance equation is written for each analyzed species. Each measured concentration (e.g. total) is equal to the sum of the free ion concentration and the concentrations of all ion pairs containing that species. Mass action equations (at 25°C) for all the ion pairs are substituted into the mass balance equations. The mass balance equations are rearranged and solved for the concentration of the free species in terms of association constants, activity coefficients, and the uncomplexed concentrations of the other species. For the first iteration, the total concentrations are set equal to the free concentrations, and the complexed concentrations are calculated from the mass action equations for use in recalculating a new ionic strength. New activity coefficients are then calculated. The concentrations of the complexed species calculated in the previous iteration are included in the mass balance equations, and a new solution is obtained for the mass balance and mass action equations. Approximately six iterations are required for convergence.

ASAME incorporates 93 aqueous species; these include the free species, acids and bases of these species, and all known inorganic ion pairs. The effects of organic complexes are not considered in ASAME. Table 4 compares standard river water and sea water data calculated by ASAME with the results given for the same data in Nordstrom et al. (1979). In general, results obtained with ASAME are within one standard deviation of the mean of those reported for other equlibrium programs. Where it is not, or where the standard deviations are large, it is because the number of programs is small ($n<5$) and the reported thermodynamic data is in significant disagreement. There are no 'correct' answers, since each program is based on tabulated thermodynamic data.

Calculation of Ion Activity Products

The precipitation of a mineral phase from a supersaturated solution is a function of the reaction kinetics of the precipitation and the free energy drive of the reaction. Little information is available concerning the kinetics of precipitation of the trace metal solid phases of interest. Consequently, precipitation kinetics will not be considered. The free energy drive of heterogeneous reactions involving calcium, magnesium, ferrous iron, manganese, zinc, cadmium and lead will be used to determine the saturation state of any solution with respect to a mineral phase. The minerals considered in this study and their respective solubility products are listed in Table 5.

The saturation index, SI, is defined by Troup (1974) as

$$SI = \frac{1}{n} \log \left(\frac{IAP}{K_{sp}}\right) \qquad (8)$$

where IAP is the ion activity product, K_{sp} is the solubility constant, and n is the stoichiometric coefficient of the metal in the solid phase under consideraton. The saturation index is a measure of the free energy drive of a

Species	River Water Test Case	ASAME	Sea Water Test Case	ASAME
Ca^{2+}	3.530 ± .006	3.529	2.057 ± .056	2.058
Mg^{2+}	3.523 ± .007	3.520	1.334 ± .040	1.332
Na^{+}	3.282 ± .001	3.283	.334 ± .024	.332
K^{+}	4.447 ± .002	4.446	1.994 ± .018	1.994
SO_4^{2-}	4.132 ± .014	4.127	1.870 ± .096	2.003
CL^{-}	3.540 ± .046	3.554	.257 ± .021	.256
HCO_3^{-}	2.920 ± .006	2.913	2.940 ± .242	2.854
CO_3^{2-}	5.231 ± .120	5.158	4.597 ± .314	4.580
H^{+}	7.991 ± .008	7.985	8.097 1 .053	8.092
OH^{-}	6.237 ± .288	5.965	5.630 ± .141	5.652
Mn^{2+}	7.256 ± .384	7.137	8.817 ± .330	8.725
Fe^{2+}	8.476 ± 2.527	6.893	-	7.810
Zn^{2+}	8.087 ± .510	9.143	7.596 ± .398	8.076
Cd^{2+}	10.041 ± 1.370	9.427	10.853 ± .309	10.733
Pb^{2+}	11.636 ± 1.688	11.992	11.530 ± 1.354	11.581
PO_4^{3-}	10.133 ± .070	10.036	10.309 ± .204	10.447
HPO_4^{2-}	5.798 ± .018	5.770	6.904 ± .129	6.905
$H_2PO_4^{-}$	6.644 ± .031	6.655	8.412 ± .073	8.308
Ionic Strength	.00251 ±.0002	0.00241	0.653 ± .043	.652

Table 4. Comparison of averaged concentrations (-log molality) and one standard deviaton of major species given in Nordstrom et al. (1979) and those of our model ASAME.

Mineral	Formula	pK_{sp}	Reference
Calcite	$CaCO_3$	8.42	Jacobson and Langmuir, 1974
Aragonite	$CaCO_3$	8.36	Christ et al., 1974
Dolomite	$CaMg(CO_3)_2$	16.70	Sillen, 1971
Siderite	$FeCO_3$	10.68	Smith and Martel, 1976
Rhodochrosite	$MnCO_3$	10.37	Morgan, 1967
Magnesite	$MgCO_3$	7.46	Smith and Martel, 1976
Nesquehonite	$MgCO_3 \ 3H_2O$	5.62	Wagman et al., 1968
Smithsonite	$ZnCO_3$	10.26	Wagman et al., 1968
Otavite	$CdCO_3$	13.74	Smith and Martel, 1976
Cerussite	$PbCO_3$	13.13	Smith and Martel, 1976
Hydroxylapatite	$Ca_5(PO_4)_3OH$	55.6	Stumm and Morgan, 1970
Vivianite	$Fe_3(PO_4)_2 \cdot 8H_2O$	36.00	Nriagu, 1972a
Whitlockite	$Ca_3(PO_4)_2$	28.5	Duff, 1971
Reddingite	$Mn_3(PO_4)_2 \cdot 3H_2O$	34.6	Nriagu and Dell, 1974
α-Hopeite	$Zn_3(PO_4)_2 \cdot 4H_2O$	35.2	Nriagu, 1973
---	$Cd_3(PO_4)_2$	32.6	Sillen and Martell, 1964
Hydroxypyromorphite	$Pb_5(PO_4)_3OH$	76.8	Nriagu, 1972b
Fluorapatite	$Ca_5(PO_4)_3F$	36.08	Roberson, 1969
Chloropyromorphite	$Pb_5(PO_4)_3Cl$	84.43	Nriagu, 1974
Struvite	$MgNH_4PO_4 \cdot 6H_2O$	13.15	Taylor et al., 1963

Table 5. Minerals considered by ASAME and pK_{sp} values used.

metal phase to precipitate or dissolve. For example, a value of SI=2 indicates that the mineral phase is two orders of magnitude supersaturated; a value of SI = 0 indicates that the mineral phase is saturated with the solution; and a negative value indicates that the mineral phase is undersaturated. Using equation (8), the degree of saturation of solutions with respect to several authigenetic metal phases can be compared. Saturation index calculation were performed for calcium, magnesium, ferrous iron, manganese, zinc, cadmium, and lead carbonates and phosphate for the intersititial waters of Lake Erie sediments.

Field Measurements

Saturation index values were calculated for cores collected at the sampling stations located in Fig. 1. The results for station A1 do not differ significantly from those obtained for Station 83. Consequently, they are not presented in this report. The saturation indices for carbonate and phosphate phases from a typical core at Station 83 are presented in Fig. 32 and Fig. 33, respectively.

Smithsonite, otavite and cerrussite, the zinc, cadmium and lead carbonates, respectively, are clearly undersaturated and would not be expected to control the pore water concentrations of zinc, cadmium, or lead. Calcite is undersaturated in the upper portions of the cores, and levels off at a SI=∿0.5 at depth. Slight supersaturation of calcite in hard waters and organic rich waters in not uncommon (Morton and Lee, 1968; Otsuki and Wetzel, 1974; Chave, 1965; Suess, 1970). The interpretation, then, is that the diffusional loss of calcium and bicarbonate from the sediments is balanced by the dissolution of calcite, and that a slight supersaturation is maintained due to organic colloidal interactions. Siderite is at saturation in the top 10 cm of the cores and reaches an SI of ∿0.6 at depth. Rhodochrosite is about one order of mag-

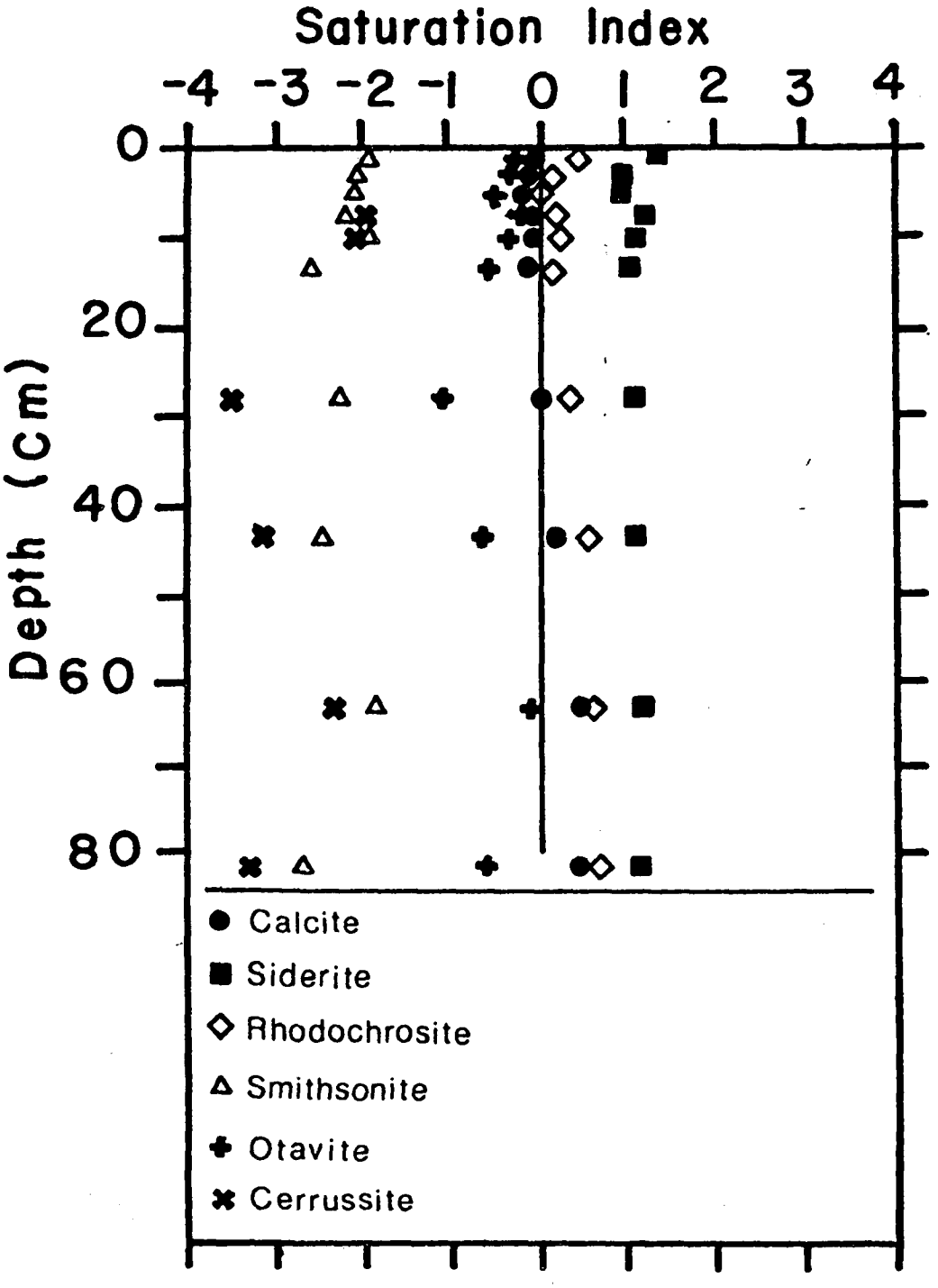

Figure 32. Saturation index versus depth for interstitial water from a typical Station 83 core for calcite ($CaCO_3$), siderite ($FeCO_3$), rhodochrosite ($MnCO_3$), smithsonite ($ZnCO_3$), otavite ($CdCO_3$), and cerrusite ($PbCO_3$).

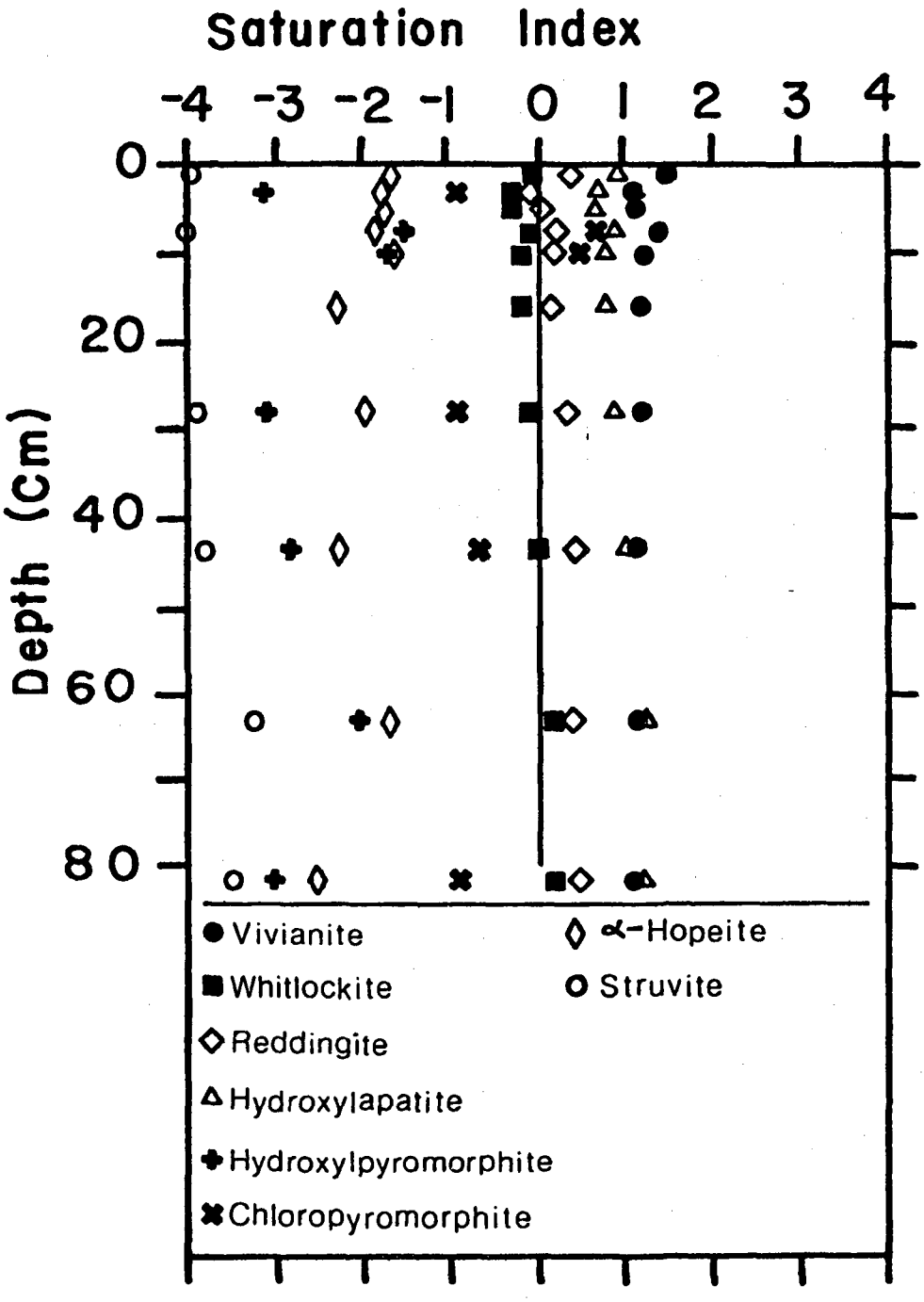

Figure 33. Saturation index versus depth for interstitial waters from a typical Station 83 core for vivianite ($Fe_3(PO_4)_2 \cdot 8H_2O$), whitlockite ($Ca_3(PO_4)_2$), reddingite ($Mn_3(PO_4)_2 \cdot 3H_2O$), hydroxylapatite ($Ca_5(PO_4)_3OH$), hydroxylpyromorphite ($Pb_5(PO_4)_3OH$), chloropyromorphite ($Pb_5(PO_4)_3Cl$), α-hopeite ($Zn_3(PO_4)_2 \cdot 4H_2$)), and struvite ($MgNH_4PO_4 \cdot 6H_2O$).

nitude supersaturated throughout the core. These phases would be expected to precipitate in recent, organic, and metal rich anoxic sediments (Troup, 1974; Robbins and Callender, 1975; Holdren et al., 1975), and should also be precipitating in these sediments.

Other carbonate phases listed in Table 5, but not shown in Fig. 31, include dolomite, aragonite, magnesite, and nesquehonite. The solubility difference between aragonite and calcite is small, and the general observations for calcite may be applied to aragonite. Aragonite is clearly present in many surface sediments as shell fragments, and must be dissolving, as very few shell fragments are found at depth. Dolomite is sourced to the sediments as a detritial particle and behaves like calcite and aragonite. A portion of the sediment diagenesis may be modeled as a dissolution of $CaCO_3$ and dolomite (see 'Stoichiometric Model'). Magnesite and nesquehonite are 1-4 orders of magnitude undersaturated and would not be expected to be present in these sediments.

Table 5 cites 11 known pure end-member phosphate phases that are possible authigenic precipitates. Struvite, hydroxylpyromorphite, and α-hopeite are all clearly undersaturated and should not precipitate in the sediments (Fig. 33). Also undersaturated but not shown for the purpose of clarity in Fig. 33 are fluorapatite (5×10^{-6}M F^-;SI∿-2.5), $Pb_3(PO_4)_2$ (SI∿-10), and $Cd_3(PO_4)_2$ (SI∿-4). Chloropyromorphite shows considerable scatter about the saturation boundary, and may be the controlling mineral for lead concentrations as suggested by Nriagu (1974). The calcium phosphate, whitlockite, is at saturation throughout most cores. The other calcium phosphate, hydroxylapatite, is about an order of magnitude supersaturated. Hydroxylapatite is a common detrital mineral phase in Lake Erie, so that its supersaturation and presence in the sediment does not imply authigenic growth. Furthermore, its

nucleation kinetics are such that several orders of magnitude supersaturation may presist unless large quantities of relatively pure fine grained calcite are present (Martens and Harriss, 1970; Stumm and Morgan, 1970). Stumm and Leckie (1971) demonstrate that hydroxylapatite will form epitaxially on the surface of calcite, but the rate of reaction is very slow under normal sedimentary conditions. Thus, whitlockite and not hydroxylapatite would be expected to be the pure end-member calcium phosphate-controlling mineral phase in these anoxic sediments. Vivianite is a little more than an order of magnitude supersaturated and reddingite has a saturation index of about 0.5. These phases would be expected to precipitate in recent, organic and metal rich anoxic sediments (Nriagu and Dell, 1974; Aller, 1977), and should also be precipitating in these sediments.

Production Experiment

The continued release of alkaline earths, transition metals, and nutrients during the decomposition experiments suggests that a number of mineral phases may reach or exceed saturation during the course of the experiment. The results of mineral equilibria calculations for carbonate phases are given in Fig. 34 and for phosphate phases in Fig. 35.

The data in Figs. 34 and 35 show that the saturation indices of the minerals considered remain roughly constant over the length of the experiment. In general, the variations in the saturation indices are no greater than the spatial variability of the saturation indices from several cores obtained at the same location. Calcite is undersaturated initially, but eventually levels off at an SI$\sim$0.5. This level of supersaturation is also observed in the field cores. The interpretation, then, is that calcium and bicarbonate are released to the pore waters during decomposition by dissolution of calcite,

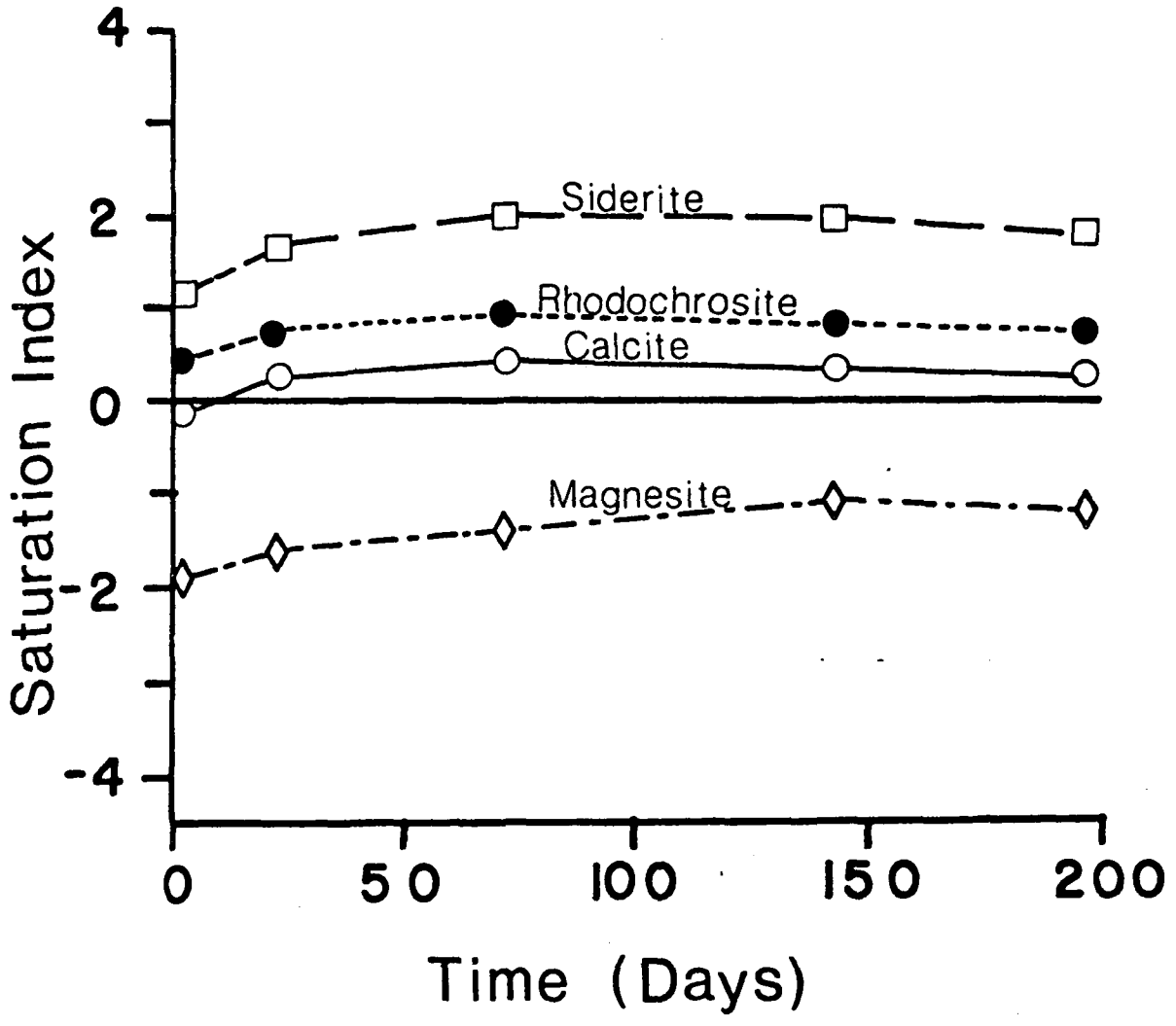

Figure 34. Saturation indices over time for siderite, rhodochrosite, calcite, and magnesite observed in the production experiment.

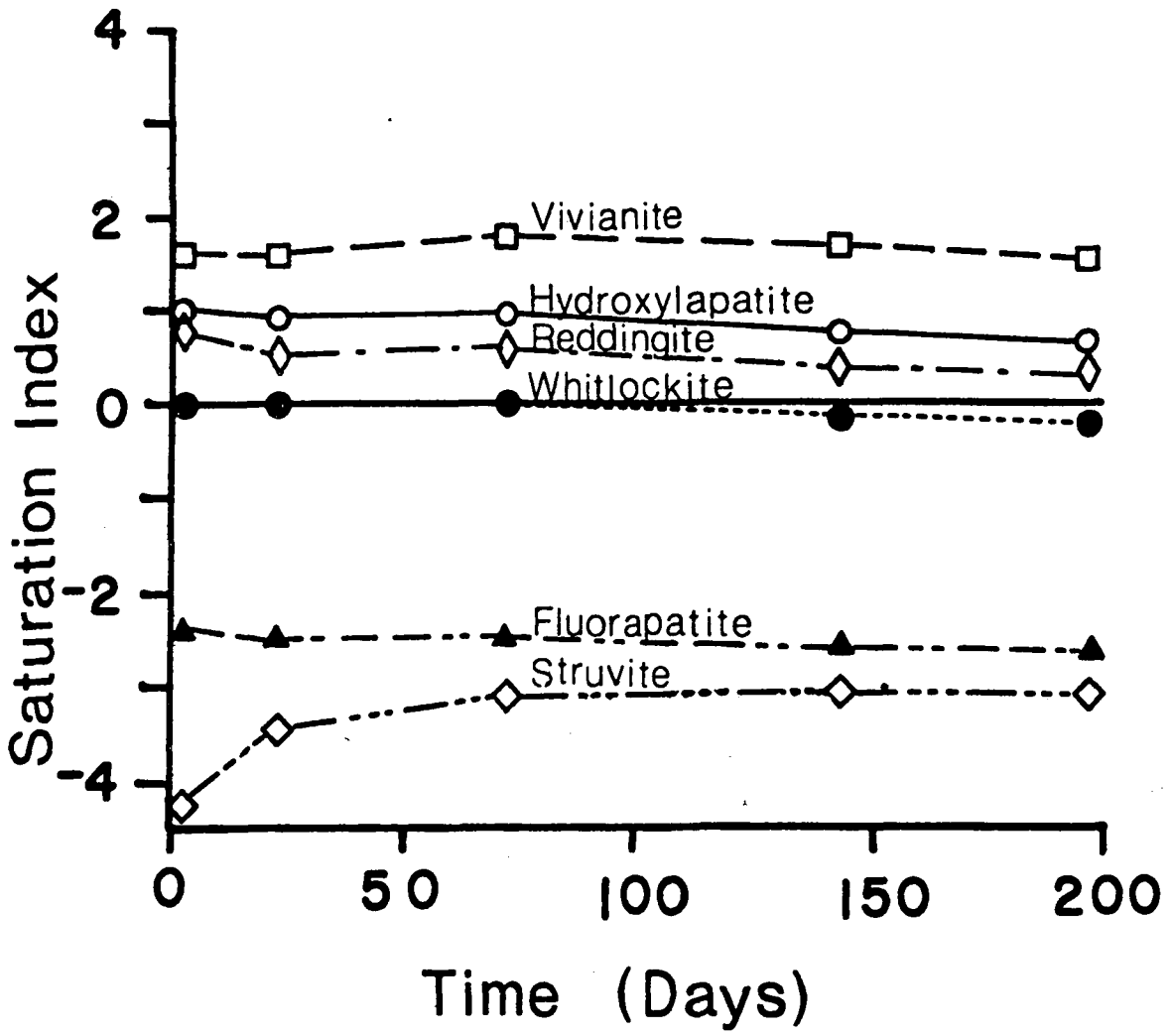

Figure 35. Saturation indices over time for vivianite, hydroxylapatite, reddingite, whitlockite, fluorapatite, and struvite observed in the production experiment.

and that a slight supersaturation is maintained due to organic and collodial interactions. Siderite is one to two orders of magnitude supersaturated and rhodochrosite about one order of magnitude supersaturated.

Fig. 35 includes 6 known pure end-member phosphate phases that are possible authigenic precipitates. The calcium phosphate, whitlockite, is nearly always at saturation. The other calcium phosphate, hydroxylapatite, is about an order of magnitude supersaturated.

As discussed for the field cores, whitlockite and not hydroxylapatite would be expected to be the pure end-member calcium phosphate-controlling mineral phase in these anoxic sediments. Vivianite is a little more than an order of magnitude supersaturated and reddingite has a saturation index of about 0.5. These phases would be expected to precipitate in recent organic and metal rich anoxic sediments, and should also be precipitating in these sediments, but we have been unable to verify their presence.

Flux Experiment

The saturation state of various carbonate and phosphate mineral phases in both the Homogenized Mud and Lake Core experiments was examined by calculating mineral saturation indices using the computer program ASAME (described eariler). Major ion data used in this calculation are given in Tables 6 (Homogenized Mud Core Experiment) and 7 (Lake Core Experiment). For the Homogenized Mud Core Experiment major cations were determined for core H. Sulfate data was estimated from Weiler (1973). For the Lake Core Experiment, major cations were determined for a core taken at Station 83 (GASP XXXII-83). Again, sulfate was estimated from Weiler's (1973) data. Unless major ion data was available for a particular core, the above data was used to estimate major ion concentrations in the Homogenized Mud Core Experiment and Lake Core Experiment, respectively.

Depth cm	Ca µm	Mg µm	Na µm	K µm	Mn µm	SO_4 µm
0	219.9	48.0	90.8	5.86	4.67	29.8
0-1	998.8	239.7	398.0	39.6	34.6	15.4
1-2	1145.5	274.7	401.1	30.1	40.5	14.3
2-3	1275.7	307.1	490.7	44.7	44.1	13.2
3-4	1372.8	332.7	552.4	51.5	47.2	12.3
4-5	1409.7	345.8	563.3	45.5	48.3	11.4
5-6	1420.4	357.3	522.0	46.2	50.5	10.6
6-8	1494.5	379.3	594.2	54.3	53.2	9.5
8-10	1562.1	397.4	649.4	55.8	55.7	8.1
14-18	1673.7	430.2	698.1	60.2	61.0	4.8
22-26	1722.8	450.9	729.5	64.0	62.7	2.6

Table 6 . Major ion data used in thermodynamic calculations. Homogenized mud core experiment data determined for HMC-H. Sulfate data estimated from Weiler (1973).

Depth cm	Ca µm	Mg µm	Na µm	K µm	Mn µm	SO_4 µm
0	884.2	227.7	480.2	44.9	3.1	298.0
0-1	906.2	234.9	527.6	49.8	21.0	154.0
1-2	912.0	234.9	526.5	50.3	21.4	143.0
2-3	918.4	236.2	525.5	50.9	21.9	132.0
3-4	924.4	226.2	524.4	51.4	22.3	123.0
4-5	930.5	226.2	523.4	52.0	22.7	114.0
5-6	936.6	214.3	522.3	52.5	23.1	106.0
6-8	945.7	218.7	520.7	53.3	23.7	95.0
8-10	957.9	219.7	518.6	54.4	24.6	81.0
14-18	997.0	282.5	511.7	57.9	27.3	48.0
22-26	1046.1	304.3	503.2	62.3	30.7	26.0

Table 7 . Major Ion Data used in thermodynamic calculation. Lake core experiment data determined from GASP XXXIII-83 Sulfate data estimated froim Weiler (1973).

Homogenized Mud Core Experiment

The degree of saturation calculated for the various mineral phases did not change over the course of the experiment; between core variations were minimal. The results of the mineral equilibrium calculations for Core H are for both carbonate and phosphate phases are shown in Fig. 36.

Carbonate Phases. Both magnesite and nesquehonite were significantly undersaturated (S.I. = ~-1 to -2 and -3 to -4 respectively). Rhodochrosite and siderite are both supersaturated (S.I. = ~0 to 0.5 and +1 to +1.5 respectively). Calcite was found to be very near saturation (S.I. = ~-0.3 to +0.1) throughout the core. Calcite, siderite, and rhodocrosite all increased their degree of saturation to a depth of 8 to 10 cm. Thereafter, their degrees of saturation were constant.

Phosphate Phases. Flourapatite and struvite were both greatly undersaturated throughout the core (S.I. = ~-2.5 and -4.0 respectively). Vivianite, hydroxylapatite, and reddingite were all supersaturated throughout the core (S.I. = ~+1.5, +1.0, and +0.5 respectively). Whitlockite was very near saturation throughout the core (S.I. = -0.18 to +0.10). Vivianite, hydroxylapatite, reddingite, and whitlockite all showed a higher degree of saturation above a depth of 6 cm. Below this depth, the saturation indices were lower.

The above observations on the degree of saturation of various carbonate and phosphate minerals in the homogenized mud core experiment are comparable both in magnitude and pattern to observations made on cores taken from station 83.

Lake Core Experiment

In the Lake Core Experiment time variation in the degree of saturation for some minerals was observed, but this degree of variation was small (maximum Δ.S.I. = ~1.0). The highest degree of time variation in saturation

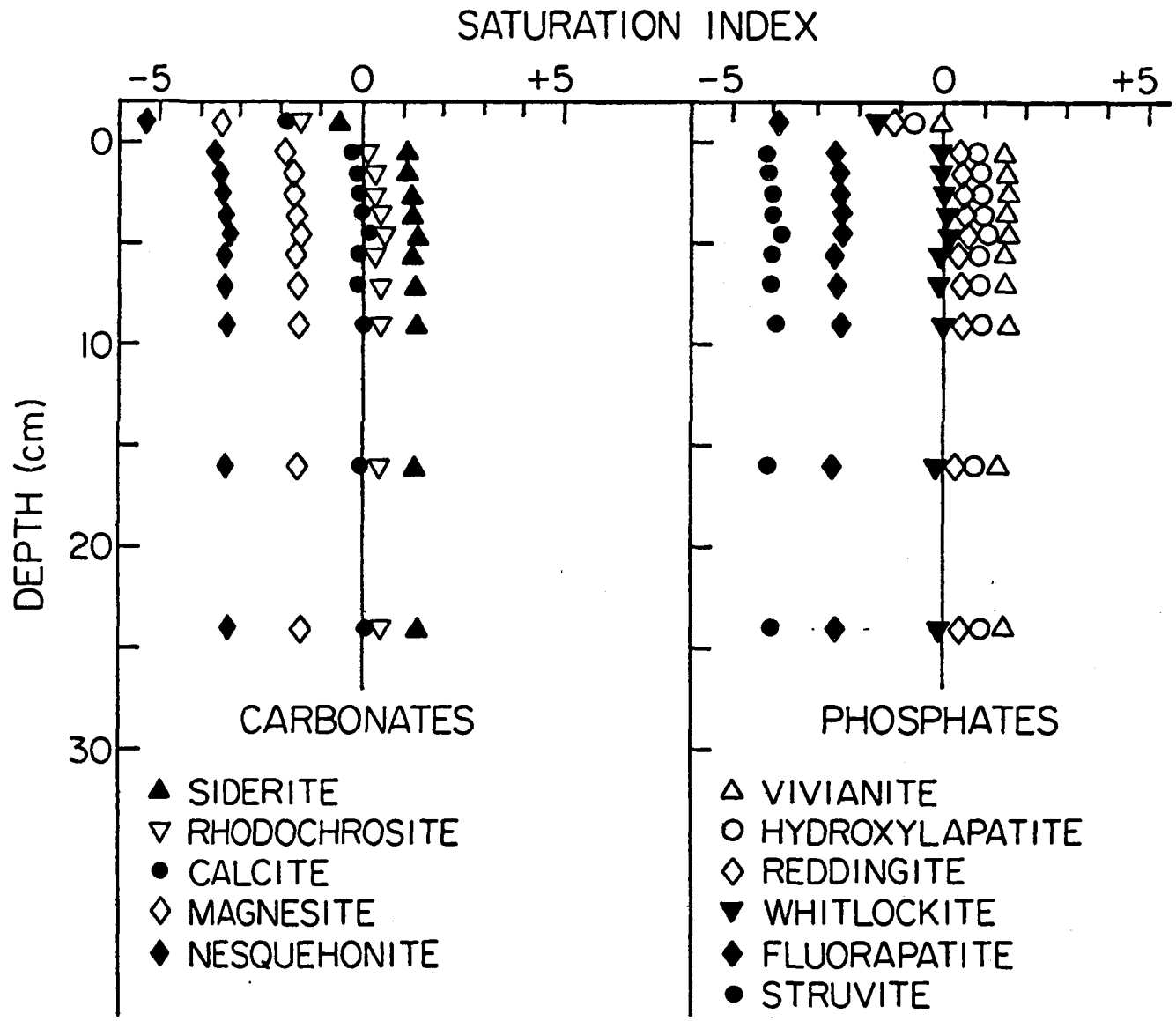

Figure 36. Saturation indices for carbonate and phosphate phases observed in the homogenized mud core experiment.

index was observed for siderite and vivianite. A lesser degree of variation was seen for whitlockite and reddingite. No discernable variation was found for magnesite, hydroxylapatite, rhodocrosite, or calcite. The pattern of variation was the same for all minerals exhibiting variation. For these minerals, the degree of saturation observed between depths of 2 and 6 cm was less in the first core (LCE-6) than all succeeding cores. This probably reflects the temperature increase the cores were subjected to for the experiment (experiment temperature = 16°C; temperature at collection = ~10°C).

Carbonate Phases. Saturation indices observed for the carbonate phasts considered are shown in Fig. 37. Both magnesite and nesquehonite (not shown) were undersaturated at all depths (S.I. ≅ -1.6 and -3.5 respectively). Both rhodochrosite and siderite were found to be supersaturated. Their degree of saturation increased with depth to a maximum at ~4cm then decreased to a more or less constant value by 10 cm (S.I.'s at depth ≅ 0.2 to 0.4 and 0.2 to 0.5 respectively). Calcite was slightly undersaturated at most depths, but tended to be slightly supersaturated between 2 and 4 cm.

Phosphate Phases. Saturation indices for phosphate phases are shown in Fig. 37. Not shown are observations for struvite and flourapatite which were both greatly undersaturated (S.I. ≅ -3.0 to -4.0 and -2.0 to -3.0 respectively). The degree of saturation of all phosphate phases shown increases with depth to a maximum value at ~4cm then decreases to more or less constant value at a depth of ~10cm. Hydroxylapatite, in contrast to all other phosphate phases, was supersaturated at all depths. Further, it was found to be near saturation in overlying water. Vivianite tended to be supersaturated at all depths below 1

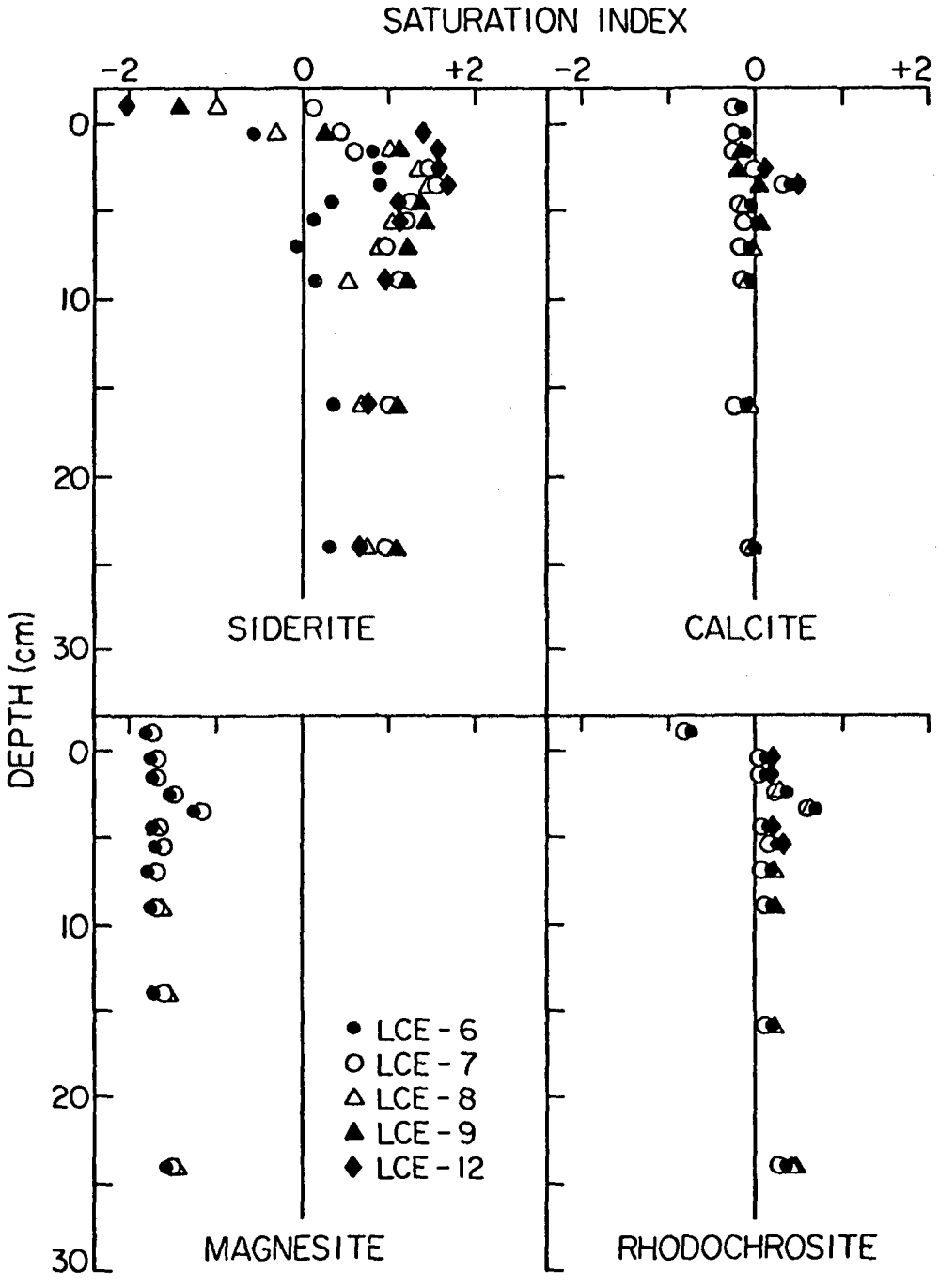

Figure 37. Saturation indices for carbonate phases observed in the lake core experiment.

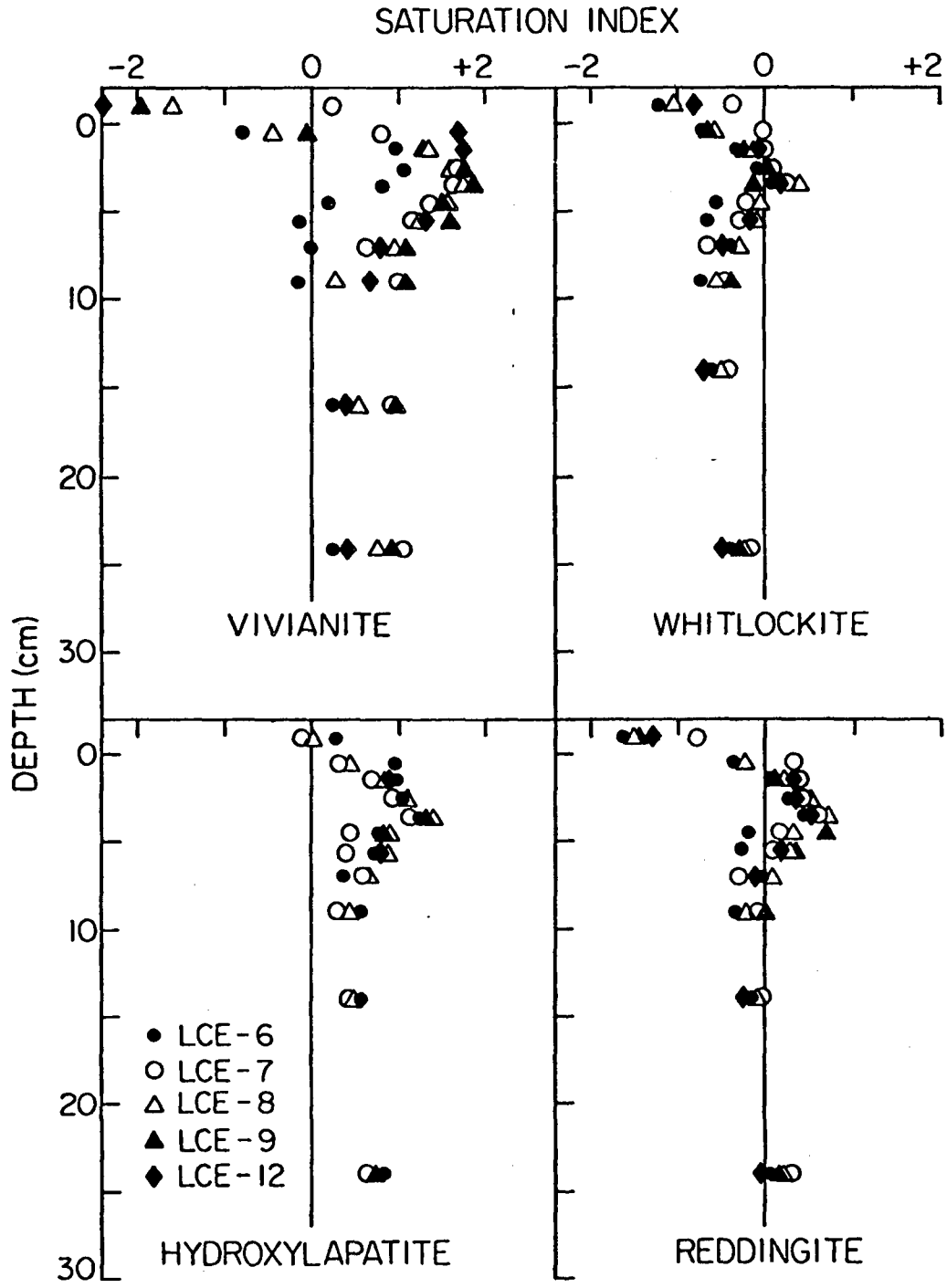

Figure 38. Saturation indices for phosphate phases observed in the lake core experiment.

cm. Both whitlockite and reddingite tended to be undersaturated (S.I. -0.2 to -0.4 and -0.01 to -0.2 respectively) at all depths except a narrow range (2-4 cm and 1-6 cm respectively).

Again, the above observations are entirely consistent with earlier observations (Station 83 cores, Production Experiment, Homogenized Mud Core Experiment). This overall consistency indicates that the precipitation dissolution/chemistry taking place in Lake Erie is adequately replicated in both the production and flux experiments.

Mineral Equilibria in Anoxic Lake Sediments

In a multicomponent solution, such as interstitial water of sediments, precipitated authigenic mineral phases are likely to be chemically mixed. Suess (1979) indentifies a mixed Mn-carbonate $[(Mn_{0.85}Ca_{0.010}Mg_{0.05})CO_3]$ and a mixed Fe-phosphate $[(Fe_{0.86}Ca_{0.14})_3(PO_4)_2]$ in anoxic Baltic Sea sediments. Suess (1979) notes that in the case of the mixed Fe-Ca-phosphate the ion activity product is lower than that of pure $Fe_3(PO_4)_2$. So, for example, it is possible that a mixed Fe-Ca-phosphate might be at saturation while the calculated value for vivianite is about an order of magnitude supersaturated. The slight deviation from calculated saturation in Lake Erie sediments could be due to the precipitation of mixed phases. A similar problem exists for the apatite phases. Atlas and Pytkowitz (1977) show that the solubilities of apatities vary widely, and interpret the results in terms of complex coatings formed on the surface of the apatites. They conclude that apatites cannot be described by the end member phases examined here. They suggest a surface coating of a general form

$$Ca_A(HPO_4)_B(PO_4)_C(OH)_D(F)_E$$

Kramer (1964) suggested that francolite, a carbonate fluorapatite, is the

solid phase which occurs in seawater. He lists the stoichiometry of the mineral as $Na_{0.29}Ca_{9.59}(PO_4)_{5.37}(SO_4)_{0.30}$ $(CO_3)_{0.33}$ F2.04. In anaerobic sediments this phase would probably not crystallize because of the reduction of sulfate to sulfide. Saturation indexes may be calculated, however, from the data in Appendix II. Saturation indices are slightly less than 1 in the top of the cores and slightly greater than 1 at depth. These results indicate that although whitlockite, the pure end member phase, appears to control the interstitial waster concentrations of phosphate, various mixed apatites are probably also forming in the sediments. Reliable thermodynamic data for these mixed phases is non-existent. The indentification of thermodynamic and kinetic data for the phases is essential for further progress in this area.

In addition to carbonate and phosphate mineral phases, sulfide mineral phases are probably forming in the sediments. The free sulfide level is below the detection limit of the sulfide electrode, i.e., less than 10^{-4} $MS^{=}$ at pH 7. Therefore, it was not possible to include sulfide mineral calculations in the thermodynamic model. Tisue (1980) reported that sulfate is reduced to sulfide in Great Lakes sediments. In Lake Erie he found that sulfate did not diffuse into the sediments for more than 5 cm before being reduced. Acid volatile sulfide data (Fig. 5) is as high as 15 μM/gram dry sediment, values comparable to those in marine sediments. Sulfide may precipitate as metal sulfides. Mackinawite, $Fe_{1+x}S$, is thought to be important in controlling the ferrous iron and sulfide levels in some Chesapeake Bay sediment pore waters (Troup, 1974) but does not seem to control ferrous iron concentrations in in Lake Erie pore waters. Since sulfide activities could not be measured directly, they were calculated indirectly from the metal-sulfide solubility equilibria expressions and metal activites. All the sulfide activities fell between $10^{-18.6}$ and $10^{-16.1}$ M but were not equal or consistenly covariant with depth.

Therefore, control of metal concentrations by sulfide is not obvious. By substituting a sulfide activity of 10^{-17} M into the cadmium sulfide equilibrium expression, cadmium equals $10^{-8.9}$M, a realistic value based on data from this study. Mixed metal sulfide mineral phases are common and probably are also forming. Further investigation of the levels of sulfide in the interstitial water is warranted.

Verification of the thermodynamic calculations is difficult. There is sufficient evidence that recent sediments are not in thermodynamic equilibrium, but are driven by kinetic and diffusion mechanisms (Berner, 1974). In addition, some of the thermodynamic constants are not well known and may be very temperature sensitive. Troup (1974) indentified the iron carbonate phase in Chesapeake Bay sediments by x-ray diffraction and Nriagu and Dell (1974) report sand-sized vivianite 'nodules' in Lake Erie sediments at a location not far from station 83. The small grain size and low abundance of the predicted phases makes direct detection difficult. We have been unable to verify any of the predicted phases by optical microscopy, x-ray diffraction, scanning electron microscopy, or x-ray fluourescence.

Neither inorganic complexation nor mineral-solution equilibria with carbonate and phosphate adequately explain the concentration-depth trends exhibited by zinc, cadmium or lead. Organic complexation may be important in solubilizing these trace metals (Rashid and Leonard, 1973). After analyzing the top centimenter of Lake Erie sediments, Kemp (1969) found that humic and fulvic matter comprised 30 percent of the total organic carbon and humin comprised about 60 percent. Nissenbaum et al. (1971) reported that polymerized organic matter accounts for nearly half of the total dissolved organic matter in the interstitial water of Saanich Inlet sediments. Further, he found that this matter was high in trace metals, especially iron, copper and zinc.

Fulvic and humic acid complex metals at carboxyl and phenolic hydroxyl sites and, when present, are probably responsible for the increased solubilities of trace metals (Gamble and Schnitzer, 1973; Rashid and Leonard, 1973).

In sulfide rich water, simple organics, (i.e., amino acids and hydroxycarboxylic acids), do not significantly complex trace metals relative to inorganic complexation (i.e. bisulfide) (Gardner, 1974). In systems containing little sulfide, however, a significant portion of the trace metals are complexed with simple organics. If the same ratio for organic complexation in sulfidic waters is used in the low sulfide system, formation of metal-organic complex follows the reaction

$$K = \frac{(\text{metal})(\text{organic ligand})}{(\text{metal-organic complex})} \qquad (9)$$

Thus, the ratio of free metal-organic complex is independent of sulfide activity. Application of Gardner's (1974) ratio to Lake Erie sediments results in approximately 20% of the zinc being organically complexed. This calculation indicates that if simple organics are present in low sulfide waters in similar concentrations, they may contribute to the solubilities of the trace metals. Complexation with simple organics is insignificant for Pb, which is highly complexed with inorganic ligands and for Cd, which still exists predominantly in the free state, but is significant for Zn, increasing the amount of total complexation by up to 40 percent.

The metals in near surface pore waters may result from (1) release of adsorbed cations from unstable hydrous oxides under reducing conditions, (2) release of the cation from a mineral surface due to a change in adsorbing capacity under low pH and low alkalinity conditions, (3) organic complexation of released metals from hydrous oxides, and (4) release of metals from organic material.

For intersitital water in marine sediments, Brooks et al. (1968) believe that it is not improbable that the increased content of three metals (Cd, Zn and Cu) in the interstitial water can be supplied completely from the marine biosphere. They determined that cadmium and copper concentrations could be accounted for by decomposing biological matter. Since organisms are the source of 90 percent of the organic matter in Lake Erie (Harlow, 1966), biological matter could supply the pore waters with the high levels of metals at the top of the sediment column. Zinc is concentrated in the biota, both on the surfaces of and within algae and other organisms, and is released during biodegradation (O'Connor, 1968). Since up to 66 percent of the total zinc complexed with proteins is loosely bound, it may be leached, transported and become available for mineral deposition (Zajic, 1969).

The ferrous iron concentrations in the Lake Erie pore waters are 2000 time grater than those found in Santa Cruz Basin pore waters; it is not unreasonable to suspect that the release of adsorbed ions from ferric hydroxides under reducing conditions is also an important source of trace metals (Duchart et al., 1973). Lead and zinc often showed surface maxima in Lake Erie cores. This phenomenon may be due to their release from hydrous oxides under reducing conditions. Decaying organic matter, most concentrated in surficial sediments, may then complex metal ions. Upon reduction of hydrous oxides with the addition of plant material, Kee and Bloomfield (1961) found that the metals were present mostly as soluble organic complexes which could not be removed from the fermented extracts by cation exchange resins.

Many of the cores show maximum metal concentrations at the surface and from 5-10 cm below the surface. Walters and Wolery (1974) report a surface minimum of trace metals in the Lake Erie sediments and a maximum at 7-10 cm in the sediments. The interstitial maximum at 7-10 cm may be caused by solution-

mineral equilibria and the surface interstitial maxima may be the result of intense biodegradation and ferric hydroxide reduction. Humic by-products, generated by biodegradation, can complex trace metals and hold them in solution. Cline and Upchurch (1973) explain the surface maxima by the upward transport of metals on bubble surfaces which have been found to concentrate trace metals. They suggest that gases released by bacteria to form bubbles in sediments could act as a transport mechanism for heavy metals released by the same bacteria from chelation sites on the organics. Upon reaching the biologically active surface sediments, the metals are immobilized as they form new complexes or inorganic precipitates. In Lake Erie, most organics, such as lipids, proteins and carbohydrates, decrease in an exponential manner with depth as chemi-specific bacteria metabolize functional groups capable of complexing cations (Cline and Upchurch, 1973). Contact of the adsorbed metals with the complexing organic matter may cause the metals to become immobilized in the sediment rather than passing out of the sediments on the bubble surfaces. Since many of the cores collected contain pockets of gas, the upward movement of gas bubbles (e.g., CO_2, NH_3, CH_4) carrying adsorbed metals may be another mechanism of upward metal transport.

Stoichiometric Model

A stoichiometric model may be constructed utilizing the observed release rates and assumed chemical reactions to predict the stoichiometry of the decomposing organic matter and the nature of the hydrogen buffer. The model is presented in Table 8. The principal driving reaction is anaerobic fermentation. Reduction of CO_2 is also a driving reaction, but it is quantitatively half as important as fermentation (Wetzel, 1975). These two reactions release nutrients, methane, and dissolved CO_2 to the interstitial water which is buffered by ammonium equilibria and the dissolution of solid carbonate and sulfide phases. In this scenario for anoxic sediments, ammonium and phosphate are produced only by the decomposition of organics, while bicarbonate is produced by both organic decompositon and metal carbonate dissolution. Since quantitative data regarding their authigenesis is lacking, precipitating phases predicted by the thermodynamic model are not included in the stoichiometric model. This exclusion will not quantitatively affect the results for the major species (carbon, nitrogen, magnesium, calcium) but could underestimate the release rates of the minor species (phosphate, iron, manganese).

A solution for this set of equations can be obtained from the relative rates of release of the nutrients and metals. A typical relationship is given in Fig. 39, where the apparent rates of release of calcium + iron + manganese are plotted versus the producton rate of bicarbonate. The slope of the regression line gives the relative rate of release. Strictly speaking, the data from the different temperatures should not necessarily fall on a single line. The above treatment assumes that the thermal kinetics of all the reactions are the same -- an assumption which is obviously incorrect. There is, however, sufficient scatter in the data to warrant the use of this simplifying assump-

EQUATIONS:

(1)	$A(CH_2O)_X(NH_3)_Y(H_3PO_4)_Z$	$\rightarrow$	$\frac{A}{2}X\ CO_2 + \frac{A}{2}X\ CH_4 + AY\ NH_3 + AZ\ H_3PO_4$	Anaerobic Fermentation
(2)	$\frac{A}{2}X\ CO_2 + 2AX\ H$	$\rightarrow$	$\frac{A}{4}X\ CH_4 + \frac{A}{2}X\ H_2O$	CO_2 Reduction
(3)	$AY\ NH_3 + AY\ H^+$	=	$AY\ NH_4^+$	Ammonia Equilibria
(4)	$AZ\ H_3PO_4$	=	$AZ\ HPO_4^= + 2AZ\ H^+$	Phosphate Equilibria
(5)	$\frac{A}{4}X\ CO_2 + \frac{A}{4}X\ H_2O$	=	$\frac{A}{4}X\ HCO_3^- + \frac{A}{4}X\ H^+$	CO_2 Hydration
(6)	$B\ CaCO_3 + B\ H^+$	=	$B\ Ca^{++} + B\ HCO_3^-$	Calcite/Aragonite Dissolution
(7)	$C\ CaMg(C)_3)_2 + 2C\ H^+$	=	$C\ Ca^{++} + C\ Mg^{++} + 2C\ HCO_3^-$	Dolomite Dissolution
(8)	$D\ FeS + D\ H^+$	=	$D\ Fe^{++} + D\ HS^-$	Machinawite Dissolution
(9)	$E\ MnS + E\ H^+$	=	$D\ Fe^{++} + D\ HS^-$	Alabandite Dissolution

NET REACTION:

$$A(CH_2O)_X\ (NH_3)_Y\ (H_3PO_4)_Z + 2AX\ H + B\ CaCO_3 + C\ CaMg\ (CO_3)_2 + D\ FeS + E\ MnS$$

$$+ (AY + B + 2C + D + E - 2AZ - \frac{A}{4}X)\ H^+$$

$$\frac{3}{4}AX\ CH_4 + AY\ NH_4^+ + AZ\ HPO_4^= + \frac{A}{4}X\ H_2O + (B + C)\ Ca^{++} + C\ Mg^{++} + D\ Fe^{++} + E\ Mn^{++}$$

$$+(\frac{A}{4}X + B + 2C)\ HCO_3^- + (D + E)\ HS^-$$

STOICHIOMETRIC CONSTRAINTS:

(1)	$(\frac{A}{4}X + B + 2C)$	=	$R_{HCO_3^-}$	Bicarbonate Production
(2)	$4.77\ AY$	=	$(\frac{A}{4}X + B + 2C)$	Ammonium vs. Bicarbonate
(3)	$5.24\ (B + C)$	=	$(\frac{A}{4}X + B + 2C)$	Calcium vs. Bicarbonate
(4)	$3.08\ C$	=	$(B + C)$	Magnesium vs. Calcium
(5)	$3.74\ (B + C + D + E)$	=	$(\frac{A}{4}X + B + 2C)$	Calcium + Iron + Maganese vs. Bicarbonate
(6)	$7.78\ E$	=	D	Manganese vs. Iron
(7)	$38.9\ AZ$	=	$(\frac{A}{4}X + B + 2C)$	Phosphate vs. Bicarbonate

SOLUTION:

AX	=	29.9
AY	=	2.10
AZ	=	0.257
B	=	1.29
C	=	0.620
D	=	0.679
E	=	0.087

Table 8. Stoichiometric model for decomposing Lake Erie sediments.

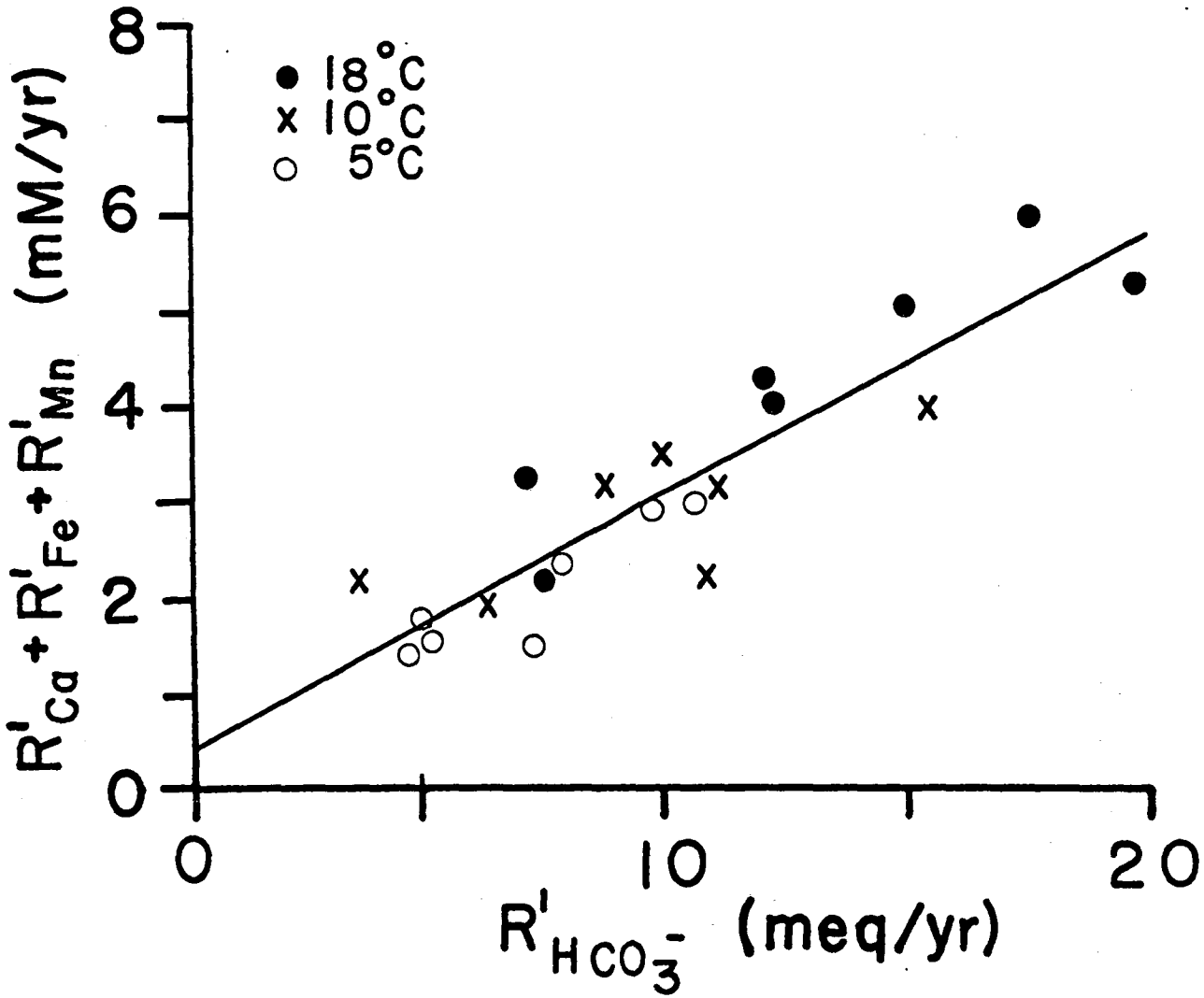

Figure 39. Rate of carbonate production ($R'_{HCO_3^-}$) versus the sum of the rates of calcium (R'_{Ca}), iron (R'_{Fe}) and manganese (R'_{Mn}) production for three temperatures.

tion. Of course, the validity of the assumption is greatest for reactions having similar thermal kinetics.

This system of equations does not permit an independent evaluation of the parameter 'A'. Consequently the results are expressed as per mole of decomposing organic matter. The solution is given in Table 8 .

One test of the model is the determination of the effectiveness of the hydrogen buffer in the net reaction. The hydrogen buffer is given by the expression (written as a reactant):

$$(AY + B + 2C + D + E - 2AZ - \frac{A}{4} X). \qquad (10)$$

If the value of this expression is zero, there is no net consumption or production of hydrogen ions; pH remains fixed. Substitution of the results of the stoichiometric model gives a value for equation (9) of -2.59. This value is significantly different from zero and indicates a net production of hydrogen ions equivalent to that of ammonium or calcium. Pore waters in Lake Erie and in the jar experiments, however, appear to be well buffered at pH $\cong$ 7.2. Consequently, an additional hydrogen consuming reaction must be taking place. The most likely possibility is that more ammonia is released than is measured (Rosenfeld, 1979). If all of the excess hydrogen ion were consumed by liberated ammonia, the total release rate of ammonium would be (2.10 + 2.59)/2.10 = 2.2 times the observed rate. This corresponds to an adsorption coefficient of 1.2, a reasonable value for recent sediments (Rosenfeld, 1979).

The proportion of the observed bicarbonate increase that is the direct result of organic decomposition, $\frac{A}{4} X$, is given by:

$$\frac{\frac{A}{4} X}{\frac{A}{4} X + B + 2C} \qquad (11)$$

where the denominator of equation (10) represents the total release rate. Substituting values obtained from the stoichiometric model indicates that ∿75% of the observed release of bicarbonate is from organic decomposition and ∿25% of the release is from the dissolution of carbonate mineral phases.

Another test of the model examines the rate of release of methane in the net reaction. Unfortunately, we were unable to measure methane in the jar experiment throughout the course of this study. However, D. Adams (pers. comm.) has made available interstitial water methane data from Station 83 and Station A-1. Since the relative diffusivities of methane and ammonium are approximately equal, and since transport of methane by diffusion and by bubbles deep in the cores is small, the molar concentration ratio of methane to ammonium deep in the cores is given in the net reaction:

$$CH_4 : NH_4^+ = \frac{3}{4} AX : AY. \qquad (12)$$

Substituting values shows that the molar ratio of methane to ammonium at depth in the sediment should be about 10:1. The concentration ratios are 500μm:100μm = 5:1 at Station 83 and 2000μm:200μm = 10:1 at Station A-1. These results are in good agreement with the stoichiometric model.

Solid Phase Prediction

The release of nutrients and metals to the pore water is necessarily accompanied by a decrease of these materials in the sediment solids. The depth dependent formulations of the rates may be used to calculate the vertical distributions of these materials in the sediments. The amount of a substance, i converted from the solid phase to the solution phase over a depth interval z_1 to z_2 was calculated assuming steady loading and constant porosity:

$$\Sigma i \text{ lost from solids} = \frac{MFW}{MFS} \times \frac{1 \text{ liter}}{1000g\ H_2O} \times \frac{1}{\omega} \int_{Z_1}^{Z_2} R(Z)\ dz \qquad (13)$$

where ω is the sedimentation rate, MFW is the mass fraction of water, and MFS is the mass fraction of sediment, and all other terms are as previously described. Since most of the variation in the production rates, bacterial abundance, and sediment solids data occur over the top 7 centimeters, equation (13) was integrated over the depth interval 0-7 cm. The results of the calculations are given in Table 9. The data from 0 and 7 cm is based on single samples (except carbon, obtained from Fig. 3). The C:N:P ratio of lost material is ∿135:9:1 while that of the calculated lost material is ∿84:11:1. The ratios are in reasonable agreement. Further, predictions of nutrient loss derived from the apparent rate data are in accord with measurements of nutrient regeneration in Lake Erie (Burns, 1976; Burns et al., 1976; Burns and Ross, 1972). The ratio of C:N:P of the decomposing organic matter calculated from the stoichiometric model is given by the AX:AY:AZ ratio and is 103:8:1. The C:N:P of the sediment solids can be determined from the data in Table 9. At the sediment-water interface, C:N:P is ∿100:7:1 and at 7 cm is ∿72:5:1. These results indicate that carbon is recycled as fast or faster than nitrogen and that both are recycled faster than phosphorous. This can also be seen in the organic carbon to organic nitrogen and organic nitrogen to organic phosphorous ratios with depth in the sediment where the C:N ratio is approximately constant and the N:P ratio decreases with depth.

In general, the model predicts that metals should be lost from the sediment in far greater quantities than is observed. This means that the release of the metals by the dissolution of carbonate and sulfide phases must be accompanied by the precipitation of other metal phases. The relative rates of

Parameter, i	[i], Z=0 $x10^{-6}$Moles/g dry sed	[i] Z=7 $x10^{-6}$Moles/g dry sed	Σ [i] Lost $x10^{-6}$Moles/g dry sed	
			Obs.	Calc.
Carbon	2914	1166	1749	1482
Nitrogen	200	85.7	114	192
Phosphorous	29.1	16.1	12.9	17.7
Calcium	145	97.3	47.4	317
Magnesium				129
Iron	598	555	43.0	91.6
Manganese	5.46	5.46	0	13.1

Table 9. Results of the solid phase prediction calculation compared to the observed solid phase.

release by decomposition and of removal by precipitation are such that release has dominated over the course of this experiment. This single mass balance, however, requires that most of the metals be retained by the sediments in natural conditions. Presumably, some or all of the thermodynamically predicted authigenic phases are forming.

Prediction of Pore Water Concentration

The concentrations of materials in sediment pore waters may be also be predicted from the decomposition rates. For example, the vertical distribution of ammonia dissolved in interstitial waters can be determined by solving the equation (Rosenfeld, 1979)

$$\frac{\partial C}{\partial t} = D \frac{\partial^2 C}{\partial Z^2} - (1 + K)\, \omega \frac{\partial C}{\partial Z} - R'_{ot}(T)\, e^{-\alpha(T)Z} \qquad (14)$$

where C is concentration, t is time, D is the coefficient of diffusivity (adjusted for porosity and tortuosity), Z is depth is the sediment (measured positively downwards), K is the coefficient of adsorption, ω is the sedimentation rate, $R'_{ot}(T)$ is the true rate of ammonia production at temperature T and z = 0, and $\alpha(T)$ is the decay constant for the exponential at temperature T as defined earlier. Assuming steady state (i.e. $\partial C/\partial t = 0$), and the boundary conditions

1) $C(z=0) = C_0$

2) $\left.\frac{dc}{dZ}\right|_{Z\to\infty} = 0;\ C(z=\infty) = C_\infty$

the following solution is obtained:

$$C(Z) = C_o + \frac{R'_{ot}(T)}{D\alpha(T)^2 + \omega\alpha(T)(1+K)} \left(1 - e^{-\alpha(T)Z}\right) \qquad (15)$$

As $Z \rightarrow \infty$, and substituting typical values for the parameters, eq. (15) reduces to

$$C_{\infty} = \frac{R_o'(T)}{D\alpha(T)^2} \tag{16}$$

For ammonium, the calculated concentration profile is in reasonable agreement with observed ammonium concentrations for depths less than ∿5-7 cm, but the calculated concentrations are a factor of 2-5 too high as $Z \rightarrow \infty$. Since the rates were used successfully in the previous section to calculate the loss of material from the solid phases by decomposition, there is every reason to believe the reported rate data. Thus, the assumptions underlying the pore water calculation are suspect. In particular, the assumption of steady state must be evaluated.

One factor which regulates the supply of oxidizable organic matter to the sediment-water interface is biological productivity in the overlying water. In turn, biological productivity is regulated by nutrient supply. In Lake Erie, nutrient loading has increased over time as has biological productivity (Sly, 1976). Nutrient loading to Lake Erie exhibits a sharp increase beginning around 1947. This data corresponds to a depth of ∿5 cm (ω = .168 cm/yr) for station 83. This evidence suggests that the system is not at steady state; that is, $R_{ot}'(T)$ is not constant in time. Eq. (16) shows that by applying a present-day value of $R_{ot}'(T)$ which is substantially larger than the value when the sediment at depth was deposited, the calculated value of C_{∞} will also be too high. Hence, application of the rate data reported in this study to the prediction of pore water concentration profiles and fluxes requires additional information on the historical record of $R_{ot}'(T, \text{time})$. The fact that the observed decreases in concentration of the nutrients were accurately predicted

by the rate formulations implies that decomposition and not loading quantitatively accounts for the majority of the changes in concentration of sediment solids in the near surface sediments. Calculation of the pore water profile for depths larger than 5-7 cm requires the determination of a loading curve at the sediment surface, from which R'_{ot}(T, time) may be determined.

Direct and Indirect Flux Estimates

The flux of an material across the sediment water interface may be estimated directly by observing concentration changes in a known volume of water overlying a known area of sediment surface or indirectly by applying Fick's first law to concentration gradients observed in the sediment column.

$$F_i = D_i \left.\frac{dc}{dz}\right|_{z=0} \tag{17}$$

F_i is the flux of component i across the sediment-water interface (moles/unit area/ unit time). D_i is the effective coefficient of diffusivity for component i (length^2/unit time; adjusted for porosity, tortrosity, and temperature). The concentration gradient (moles/length^3/length), dc/dz is that at the sediment-water interface (i.e. z = 0) and is generally approximated as the concentration difference between the overlying water and the pore water concentration in the first sampling interval (0-1 or 0-2 cm depth) divided by the mean depth of the sampling interval. Under field conditions, it is generally inconvenient to attempt direct estimates of chemical fluxes, consequently the indirect means described above is used. Unfortunately, few comparisons between direct and indirect estimates of chemical fluxes have been made. One goal of the flux experiments was to do just this.

Laboratory Flux Experiments

In the flux experiments, direct flux estimates were based on observed concentration changes in the overlying water. Estimates of flux were made for ammonia, ferrous iron, SRP, bicarbonate, and SRS. For redox insensitive materials (SRS and bicarbonate) all of the data collected following the closure of the microcosms was used. For redox sensitive materials (ammonia, ferrous iron, and SRP) only data taken during the initial concentration increase observed for those paramenters was used. Since crashes in concentration of redox sensitive materials following the initial rise in concentration were probably due to the inadvertant admission of small quantites of oxygen during sampling operations, it was felt that the most reliable estimates of direct flux could only be made from initial rise data.

Indirect flux extimates were made using observed concentration profiles at the time of core sacrifice. For purposes of the flux calculations, concentration gradients were assumed to be linear at the sediment water interface. The concentration in the 0-1 cm sampling interval was taken to be the concentration at 0.5 cm and the concentration in the overlying water was taken to be the concentration at the sediment-water interface. Indirect flux extimates were made using Fick's law. Diffusion coefficients used in these calculations are given in Table 10. The results of the direct and indirect flux calculations are given in Table 11.

Ideally, if the process controlling the movement of a material across the sediment water interface is simple diffusion, and the concentration gradient at the interface is well approximated by the difference in concentration between overlying water and the 0-1 cm sampling interval, direct flux estimates should equal indirect flux estimates. Indirect flux extimates for all parameters except ferrous iron are greater than the direct flux estimates. In the case of ferrous iron, the data show no clear pattern. Further, between

COEFFICIENT OF DIFFUSIVITY (Cm^2/sec)

ION	T=8°C	T=16°C
NH_4^+	10.15	12.02
Fe^{++}	3.53	4.16
HCO_3^-	5.58	7.12
Cl^-	10.46	13.34
$SO_4^=$	5.18	6.61
$HPO_4^=$	3.47	4.42
$H_2PO_4^-$	4.00	5.09
Ca^{++}	3.86	4.93
Mg^{++}	3.69	4.70
Na^+	6.50	8.29
K^+	10.21	13.03
Mn^{++}	3.16	4.03
H_4SiO_4	3.99	4.73
Zn^{+2}	3.47	4.11
Cd^{+2}	3.53	4.18
Pb^{+2}	4.72	5.60
Cu^{+2}	3.53	4.18

Table 10. Effective diffusion coefficients used in indirect flux calculations. (Field estimates=8°C; flux experiment estimates = 16°C). Data from Li and Gregory (1974) and Wollast and Garrels (1972). Coefficients listed above are adjusted for a porosity to tortuosity squared ratio (ϕ/θ^2) = 0.75.

Core	NH_4^+ Direct	NH_4^+ Indirect	Fe^{+2} Direct	Fe^{+2} Indirect	SRP Direct	SRP Indirect	HCO_3 Direct	HCO_3 Indirect	H_4SiO_4 Direct	H_4SiO_4 Indirect
	$x10^{-6}$ $M/m^2/day$		$x10^{-6}$ $M/m^2/day$		$X10^{-6}$ $M/m^2/day$		$x10^{-3}$ $M/m^2/day$		$x10^{-6}$ $M/m^2/day$	
LCE-6	n.d	561	n.d	22	n.d	30	n.d	4	n.d	1414
LCE-7	1050	2306	581	79	597	343	8	9	3868	2752
LCE-8	883	1807	342	30	86	51	4	2	4286	748
LCE-9	1050	1371	51	126	169	30	9	5	3520	1076
LCE-12	1276	3552	71	685	160	509	6	14	2265	5597
Mean	1065	1919	261	188	253	193	7	7	3485	2317
Variance	161	1115	251	281	232	221	2	5	871	1985
C.V.	15.1	58.1	96.2	149.5	91.7	114.5	28.6	71.4	25.0	85.7
HMC-R	n.d	6085	n.d	462	0**	71	23	20	2362	3342
HMC-N	341	1788	836	766	581	690	11	23	1097	3697
HMC-B	564	1797	1336	514	1710	707	24	16	1232	5007
HMC-H	677	2349	592	805	388	537	6	36	588	3473
HMC-J	741	1044	371	437	192	165	6	24	1168	3123
HMC-T	684	1410	769	464	96	194	5	14	847	2151
Mean	601	2412	781	575	593	394	13	22	1216	3466
Variance	159	1851	359	166	651	284	9	8	610	926
C.V.	26.5	76.7	46.0	28.9	109.8	72.1	69.2	36.4	50.2	26.7
HMC-G*	n.d	3713	n.d	292	0**	670	22	16	814	2053
HMC-A*	1200	3933	0	712	54	447	24	18	1042	2659
HMC-Q*	180	5020	79	661	68	914	8	20	1072	3446
HMC-O*	1402	5630	736	875	204	433	7	29	1129	3145
HMC-C*	1128	347	293	70	120	10	13	7	958	1332
HMC-E*	410	2751	280	1356	70	221	5	33	932	2566
Mean	864	3566	347	661	103	449	13	21	825	2534
Variance	535	1874	277	451	62	319	8	9	384	761
C.V.	61.9	52.6	79.8	68.2	60.2	71.0	61.5	42.9	46.5	30.0

Table 11 Direct and indirect flux estimates obtained from the lake core experiment and the homogenized mud core experiment. SRP flux is reported as moles $P/m^2/day$. * = tubificid population present. ** zero values not considered in calculation of mean and variance (before anoxia). n.d = not determined

core variability is higher in both the homogenized mud core experiment and the lake core experiment. On the whole, direct flux estimates tend to be less variable (overall mean C.V.~58%) than the indirect flux estimates (overall mean C.V. ~70%). The paramenter showing the least overall variability in estimated direct flux was NH_4^+ (C.V.=34.5%) followed by SRS = (C.V.=40.6%), HCO_3^- (C.V.=53.1%), Fe^{+2} (C.V.=74%), and SRP (C.V.=87.2%). The parameter exhibiting the least overall variation in estimated indirect flux was SRS (C.V. = 47.5%) followed by HCO_3^- (C.V.=50.2%), NH_4^+ (C.V. = 62.4%), Fe^{+2} (C.V.=82.2%) and SRP (C.V.=85.9%).

Homogenized Mud Core Experiment

Because of the high degree of variation in estimated flux between cores, no statistically significant difference in flux (either direct or indirect) between with and without worm cases was found. If, however, only the means are considered the following pattern emerges: The presence of tubificids appears to have no effect on bicarbonate flux. Ammonia flux (both direct and indirect estimates) is higher by a factor of ~1.44 (direct) to 1.48 (indirect) in the presence of tubificids. Silica flux (both direct and indirect estimates) is higher in the absence of tubificids by a factor of 1.47 (direct) to 1.37 indirect. Direct flux estimates for ferrous iron (x 2.25) and SRP (x 5.76) are higher in the absence of worms while indirect flux estimates for these paramenters are elevated in the presence of worms (x 1.15 for Fe^{+2}; x 1.14 for SRP). From this information, we can reach the following tentative conclusions: The presence of tubificid oligochaetes (at least at higher population densities) appears to enhance ammonia flux by a factor of ~1.4 and suppress silica flux by approximately the same factor. Examination of the ammonia concentration profiles shows that this is probably the result of enhanced near-surface ammonia production in the presence of worms. The sup-

pression of silica flux in the presence of worms appears to be the result of their reduction of the silica concentration gradient at the sediment-water interface. No reason for this phenomenon is immediately apparent. The presence of tubificids has no effect on bicarbonate flux. Tubificid inhabited sediments exhibited suppressed ferrous iron flux (factor of ~ 2) and SRP flux (factor of ~ 6) even though indirect flux estimates based on the same cores suggest that the presence of worms weakly enhances the flux of these two materials (factors of 1.15 and 1.14 respectively). This result indicates that the movement of Fe^{+2} and SRP from sediments to overlying water is controlled by processes at the sediment-water interface that are modified by the presence of worms. Tubificid activities have little effect on pore water gradients of either SRP or Fe^{+2}, but clearly affect the flux of both materials. The most likely reason for this is as follows: In the absence of tubificids both SRP and Fe^{+2} diffuse toward the sediment-water interface. Ferrous iron precipitates there as ferric exyhydroxide which adsorbs SRP. This process results in the formation of a surface layer rich in both iron and phosphorous. In the presence of worms such a layer is prevented from forming by the worms' particle reworking activities (see Fisher et al., 1980).

Lake Core Experiments

Comparison of flux estimates for silica, ammonia, ferrous iron, and SRP between the lake core and homogenized mud experiments can be made since these materials were either not present or present at very low levels in the filtered lake water overlying sediments in the lake core experiment. Lake cores exhibited a higher direct ammonia flux estimate than either the with or without worm homogenized sediments, but indirect flux estimates place the lake core sediments midway between the homogenized sediments with worms (highest) and the without worm homogenized sediments (lowest). Ferrous iron flux (both direct and indirect estimates) was lower in the lake core experiments than in

either of the homogenized mud core experiments. This may reflect mobilization of iron by the homogenization process (e.g. oxidation of stoichiometric iron sulfides). The flux estimates show the lake core sediments to be roughly comparable to the homogenized sediments with worms, but the latter case showed the greatest difference between the direct and indirect flux estimate. With respect to silica flux, the lake core experiment sediment possessed the highest direct flux, but estimates of indirect silica flux place the lake core sediments midway between the with and without work homogenized mud sediments. This result is not surprising since the lake cores have diatom-rich surface layer that is lacking in the homogenized mud cores.

Iron and Phosphorous. Examining flux data from all experiments, it was found that direct flux estimates of ferrous iron were modestly correlated (r=.794) with direct SRP flux estimates. A regression line calculated for this data had a slope .962. A very weak correlation, however, was found to exist between the indirect flux estimates for ferrous iron and SRP (r=.36). Flux estimates (direct and indirect) of ferrous iron and SRP are compared in Fig. 40.

Field Cores

Indirect flux estimates from field measurements at stations 83 and A1 are given in Tables 12 and 13 (temperature assumed to be equal to 10°C).

Load and Loss Calculations

Metals

Industrialization has increased the loading of toxic metals to the environment. Most toxic metals do not occur in high concentrations in soils and groundwater, and do not form colloids that are easily transported. Instead, they form soluble complexes that remain dissolved or adsorbed to surfaces. These metals are specifically adsorbed to ferric hydroxides which have a positive surface charge at the pH of natural waters (Stumm and Morgan, 1970), or adsorb to negatively charged surfaces such as the surfaces of clay platelets. Iron forms a highly insoluble ferric hydroxide in oxygenated waters and

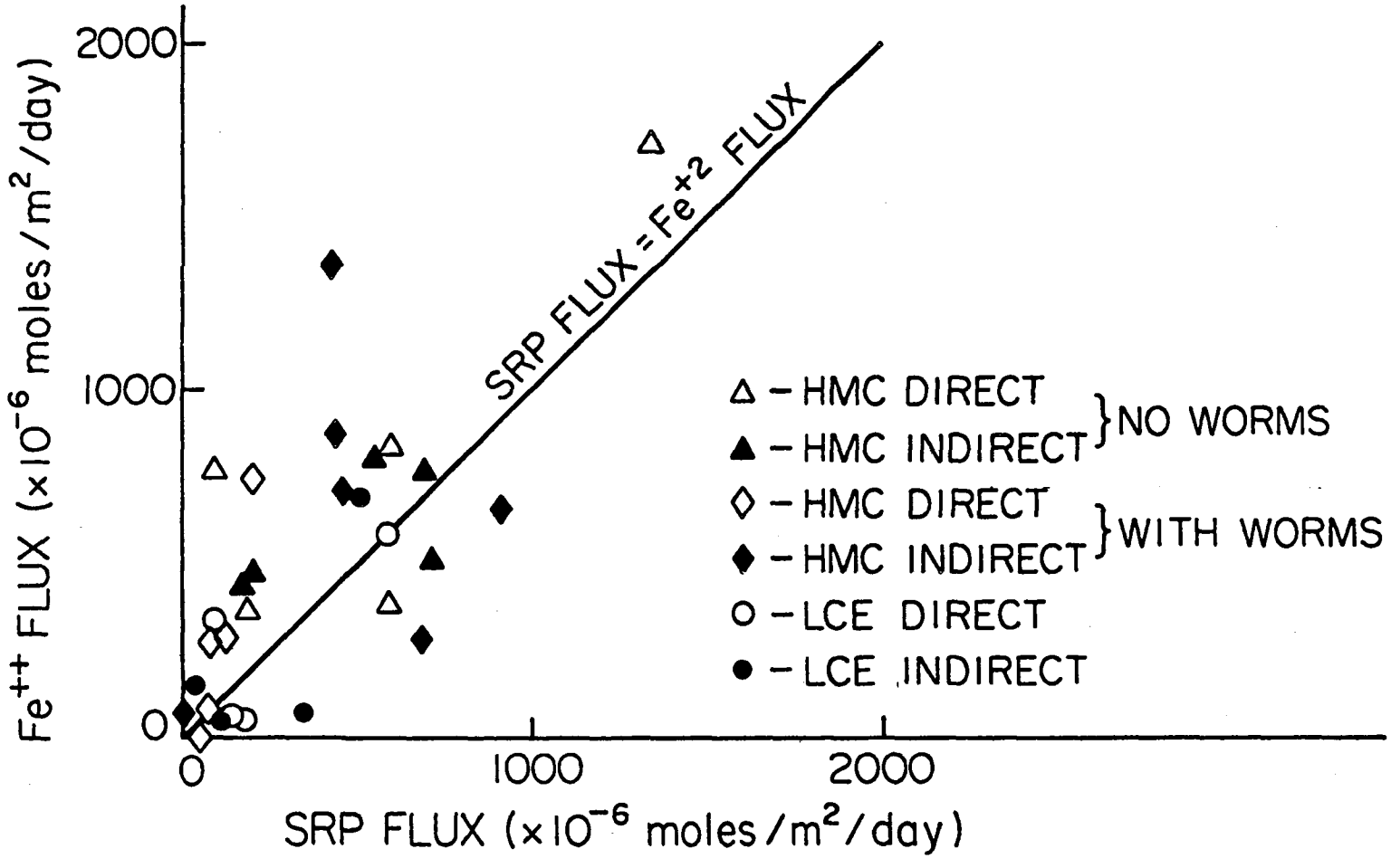

Figure 40. Phosphorous flux estimates versus iron flux estimates (direct and indirect) for the homogenized mud core experiment (with and without worms) and the lake core experiment.

SPECIES	STATION 83 31-V-78	17-V1-78	21-V11-79	16-V111-78	MEAN ± SD	STATION A1 CORE	PEEPER	MEAN ± SD
HCO_3	-1109	1061	1109	-675	97±1001	867	410	639±229
Cl^-	371	578		1536	829±508	-741	-56	-399±342
$HPO_4^=$ $H_2PO_4^-$	175	6	5.5	18.2	51.1±71.5	25	10.2	17.6±7.4
H_4SiO_4		801	785	973	853±85	976	200	588±389
Ca^{++}	500	834	417	168	479±238			
Mg^{++}	-481		76.6	22.3	-128±291			
Na^+			351	130	240±111			
K^+			187	20.3	104±84			
Fe^{++}	54.9	0	1.8	37.8	23.7±23.5	387	179	283±105
NH_4^+	403	649	719	602	594±118	1228	49	638±589
Mn^{++}			58.4	49.4	54.1±4.2			

Table 12. Indirect flux estimates determined from field measurements at Station 83 and Station A1. Units are $x10^{-6}$ Moles/m^2/day.

Species	Flux (10^{-6} moles/m^2/day)	
	Station 83	Station A1
HCO_3^-	97±1000	639±229
Cl^-	829±508	-399±342
SRP	51±72	18±7
SRS	853±85	588±389
Ca^{+2}	480±239	-
Mg^{+2}	128±251	-
Na^+	240±111	-
K^+	140±84	-
Fe^{+2}	24±24	283±105
NH_4^+	594±118	639±589
Mn^{+2}	54±4	-
Zn^{+2}	0.634±3	-
Cd^{+2}	0.024±0.028	-
Pb^{+2}	0.046±0.205	-
Cu^{+2}	0.208±0.188	-

Table 13. Summary of the flux calculations for Stations 83 and A1. Negative fluxes indicate a flux to the sediments.

under low oxygen conditions reduces to ferrous iron. Iron occurs in high concentrations in terrigenous soils and groundwater, and is carried to lakes as a colloid or adsorbed to mineral surfaces (Carrol, 1957).

Ferric hydroxide coatings are unstable under anoxic conditions (e.g. buried lake sediments); they dissolve and release their adsorbed and coprecipitated trace metals. Further, sorption equilibria may change under different alkalinities and pH's in the interstitial water system to release metals. The released metals would be free to diffuse and react to form authigenic mineral phases, and like phosphorous, would be expected to be concentrated in the oxidized surface layer of sediments whch is rich in iron hydroxides. If the hypolimnion becomes anoxic, the adsorbed metals might be expected to be released into the water column when the ferric hydroxides dissolve.

Factors governing the selectivity of clays for different cations are valance, hydrated ionic radius, electronegatively, and free energy of formation (Leland et al., 1974). Based on the frequently used tool for predicting adsorption behavior, ionic potential, the order of ionic displacement on clays is approximately:

Cu>Pb>Ni>Co>Zn>Ba>Rb>Sr>Ca>Mg>Na>Li

(Mitchell, 1964) where copper is the strongest displacer. The order is only approximate and depends on relative concentrations in solution and the type of adsorption surface: clays, hydroxides, oxides, or quartz grains. In his study of limonitic concretions, Hirst (1962) found higher concentrations of lead associated with the ferric hydroxides than with the clay fraction, and recent literature has stressed the importance of trace metal association with organic matter and ferric hydroxides rather than with clays (Lerman and Childs, 1973). This would suggest that burial by sedimentation of toxic metal containing sediment would remove metals from the system (i.e. overlying water) and lessen their potential pollution hazard.

Metals can be incorporated into the crystal lattice of clays and other minerals. For example, due to its similar ionic radius, lead replaces potassium in its structural position in clays (Pinta and Ollat, 1961). Once the metal ion is incorporated into the inner structure of a particle, it is no longer available to water systems (Matson, 1968).

Organic complexing may tie up significant amounts of trace metals in both particulate and soluble phases. Due to their similarities in chemical properties, heavy metals can substitute for other trace and alkali metals. The degree of complexation is dependent on concentrations available in the environment, properties of each ion, organic ligands available for chelation and complexation, and stability of the organic-metal complexes formed. No generalizations concerning relative affinities can be made, since the order of stability is different for each metal-organic complex and depends on the specific conditions of pH, Eh and metal and ligand concentration at the time of formation. Algae show an affinity for trace metals according to the following order:

Zn>(Br), Cu>As>Cr>Co (Leland _et al._, 1974)

and considering that most organic matter in Lake Michigan sediments is of autochthonous origin, a relationship between Lake Michigan trace element concentrations in phytoplankton and organic carbon in the surficial sediments is expected (Leland _et al._, 1974). Leland found that surficial sediments showed an affinity for trace metals according to the following order:

Zn>Rb>Cr>(Br)>Cu>As>Ni>Co.

With the exception of chromium, organic affinity for cations is the same in Lake Michigan phytoplankton and surficial sediments.

The above result suggests that a large percentage of the metal delivered to the lake can be expected to end up in the sediments. Several investigators

have determined metal contents in surficial sediments in order to identify the anthropogenic and natural inputs of metals to sediments (Walters, et al., 1974; Kemp et al., 1976; Nriagu et al., 1979). Knowledge of sedimentation rate, water content, and metals concentrations is used to calculate the flux of metals to sediments. The age of the sediment at depth, z, may be calculated as (Berner, 1980):

$$\tau = \frac{1}{(1 - \phi_\infty)\omega_\infty} \int_0^z (1 - \phi_z)dz \qquad (18)$$

where ϕ_∞ is porosity at depth in the sediment, and

$$\omega_\infty = \frac{R}{\rho_s (1 - \phi_\infty)}, \qquad (19)$$

the sedimentation rate at depth in the sediment where R is the mass flux of sediment to the sediment-water interface ($g/cm^2/yr$) (usually determined by radioisotope dating tecniques) and ρ_s is the density of the sediment solids. For Station 83, this relationship is approximately:

$$\tau(\text{years}) = 14.857 * z(\text{cm}) + 139.14 * (e^{-0.08615 * z(\text{cm})} - 1) \qquad (20)$$

The flux of metals to the sediment is calculated as:

$$F(ug/cm^2/yr) = R(mg/cm^2/yr) * C(ug/g) * \frac{1}{1000} (g/mg) \qquad (21)$$

where C is the concentration of metal in the sediment (ug/g dry sediment).

Metal concentration data obtained from stations 83 and A1 sediment solids is given in Appendix II. In general, this data agrees with the findings of Nriagu et al. (1979) from their stations 5 and 6 (near our stations 83 and A1, respectively).

At station 83, toxic metal concentrations typically decreased rapidly immediately below the sediment-water interface and reach approximately constant values below 5-10 cm. From equation 17 it can be determined that the material at 10 cm represents the year ~1910. This supports the interpretation of Nriagu et al. (1979) that the constant concentration at depth reflects 'natural' or background flux of metal and the increased concentration near the surface is the result of anthropogenic metal input to the lake. It should be noted, however, that the alternative interpretation that the metals are undergoing vertical transport (via molecular diffusion of dissolved metals) and are deposited in the surficial oxidized sediment cannot be ruled out on the basis of the above findings. Pore water concentration gradients indicate that diffusive transport is not occurring and these data lend further support to the anthropogenic loading interpretation.

We have adopted the mass balance of Nriagu et al. (1979), with the exception that we have included a flux of dissolved metal from the sediments to the lake water as indicated by the interstitial water concentration data. The amount of metal retained in the sediments was calculated from the difference between total inputs and total outputs and not from indirect flux calculations. The calculated mass balance does not include a component for the accumulation of metal within the lake water (dissolved + particulate). Our simplified two compartment model is given in Fig. 41. F_1 represents the natural flux of metal into the lake. F_{12} represents the flux of metal from compartment 1, the lake water (dissolved + particulate) to the sediments. F_{21} is the flux of metal in the opposite direction. F_{12} is predominantly particulate while F_{21} is transport in the dissolved state. F_3 represents export from the lake to the Niagara River and the Welland Canal. F_2 is the anthropogenic flux, and is considered to be zero before 1850 and to increase exponentially with time since then (i.e. mirror population growth in the drainage basin).

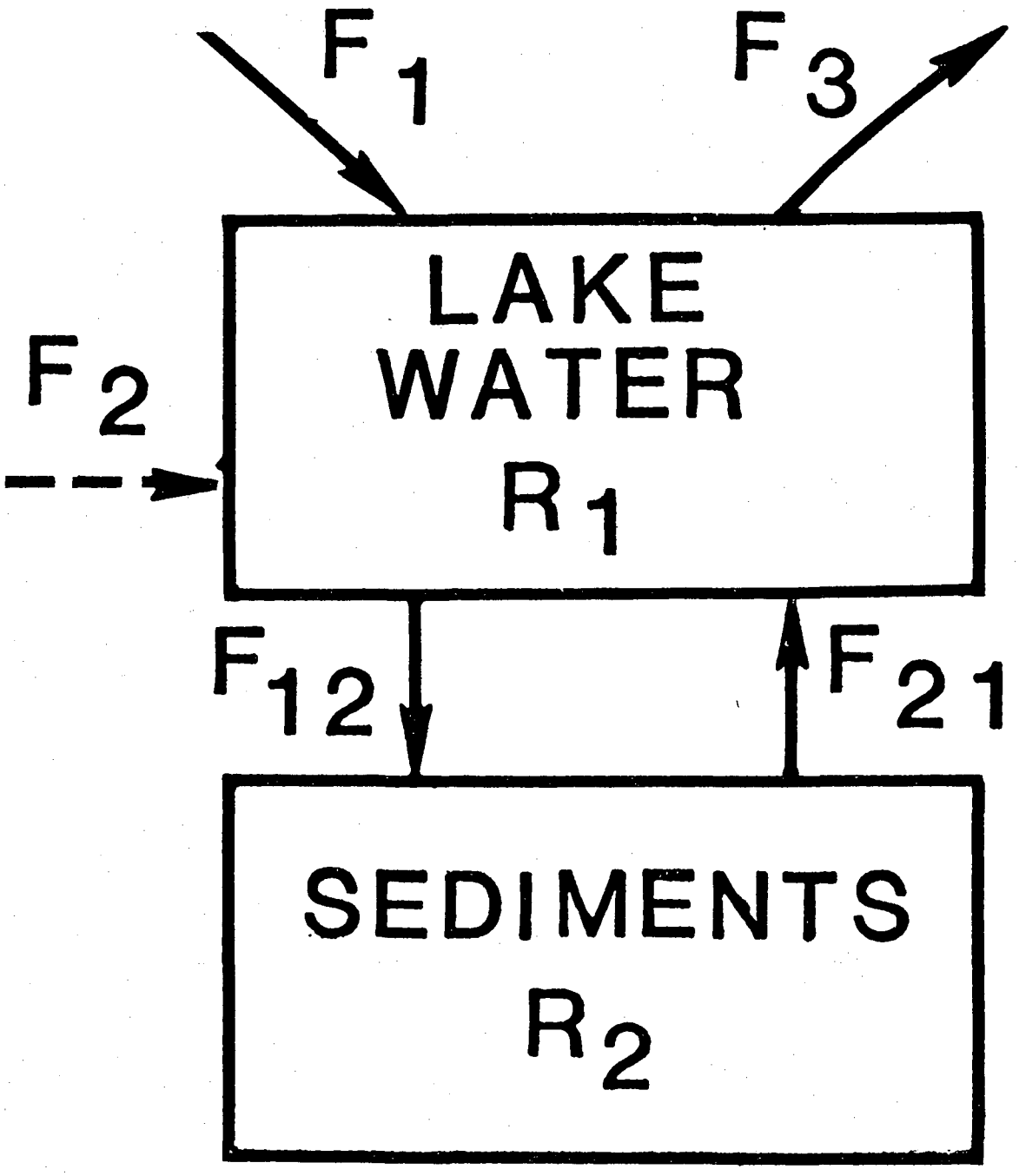

Figure 41. Schematic diagram of the simplified two compartment model. F_1 represents natural flux to the lake. F_{12} represents the flux of metal from compartment 1, the lake water (dissolved and particulate) to the sediments. F_{21} is the flux of metal in the opposite direction. F_3 represents export from the lake to the Niagara River and the Welland Canal. F_2 is the anthropogenic flux to the lake.

The modified mass balance is given in Table 14. The basic difference between the mass balances in Table 14 and Nriagu et al. (1979) is the inclusion of a flux from the sediments in our balance. Fluxes were calculated from Fick's first law,

$$F_i = D_i \left.\frac{dc_i}{dz}\right|_{z=0} \tag{22}$$

Values of D_i were calculated from data given in Li and Gregory (1974) and are presented in Table 10. Concentration gradients at the sediment-water interface (z = 0) were taken as the linear change between the overlying water and the first sediment sample. Results of the flux calculations are given in Table 12. Data from all cores at a single station were averaged and are reported as the average ± the standard deviation (Table 13).

The toxic metals data display a large variability, but like iron and manganese they are fluxed from the sediment to the water column. The mean values were used in determining F_{21} in Fig. 41. Table 14 is incomplete for Cd. Consequently, only fluxes for Cu, Pb, and Zn were determined.

The molar ratio of Cu:Pb:Zn in the metals fluxing from the sediment is 4.5:1:13.8, and the molar ratio for the same metals in the accumulating sediments is 4.0:1:8.6. Thus, the flux of these metals from the sediment, F_{21}, is proportional to the flux to the sediment, F_{12}; $F_{21} = \alpha F_{12}$. Values for α can be estimated from data in the mass balance and can be assumed to be constant in time and independent of metal loading:

Cu: $F_{21} = 1.19 \times 10^6$ M/yr

$F_{12} - F_{21} = 22.23 \times 10^6$ M/yr

$F_{12} = 23.42 \times 10^6$ M/yr

$\alpha = .0508$

	Flux (10^6 moles/yr)			
Input:	Cd	Cu	Pb	Zn
Detroit River		25.81	3.04	79.85
Tributaries, USA		1.57	0.251	4.15
Tributaries, Ontario		0.488	0.092	2.14
Sewage	0.049	7.05	1.37	11.61
Dredge Spoils	0.037	0.661	0.270	2.68
Atomosphere	0.347	3.24	3.11	13.81
Shoreline Erosion	0.070	2.99	1.07	4.71
Flux from Sediment*	0.138	1.19	0.261	3.62
Total*		43.00	9.46	122.57
OUTPUT:				
Niagra River and Welland Canal		20.77	3.19	67.31
Retained by Sediment (mass balance)*		22.34	6.27	55.26

Table 14. Inventory of sources and sinks of heavy metals in Lake Erie.

* All data except "Flux from sediment' 'Total' and 'Retained by Sediment' from Nriagu et al. (1979).

Pb: $F_{21} = .261 \times 10^6$ M/yr

$F_{12} - F_{21} = 6.27 \times 10^6$ M/yr

$F_{12} = 6.531 \times 10^6$ M/yr

$\alpha = .0400$

Zn: $F_{21} = 3.62 \times 10^6$ M/yr

$F_{12} - F_{21} = 55.26 \times 10^6$ M/yr

$F_{12} = 58.88 \times 10^6$ M/yr

$\alpha = .0615$

From Table 3 of Nriagu et al. (1979), the fraction of the total flux of metals to the sediments that can be assumed to be the "natural" or "pre-cultural" component is as follows:

Cu: 0.527 ± 0.153

Pb: 0.339 ± 0.194

Zn: 0.327 ± 0.117

Calculation of F_1:

Assume the amount of metal accumulating in the sediment is proportional to the total metal input to the lake. The current amount accumulating is $F_{12} - F_{21}$ and the total input to the lake is $F_1 + F_2 + F_{21}$. The ratios are:

Cu: $\frac{22.23}{43.00} = .5170$

Pb: $\frac{6.27}{9.46} = .6628$

Zn: $\frac{55.26}{122.57} = .4508$

The natural accumulation in the sediment is $F_{12(Natural)} - F_{21(Natural)}$ and is

calculated as the product of the fraction that is natural times the current total flux to the sediment:

Cu: $.527 \times 22.23 \times 10^6 = 11.72 \times 10^6$ M/yr

Pb: $.339 \times 6.27 \times 10^6 = 2.13 \times 10^6$ M/yr

Zn: $.327 \times 55.26 \times 10^6 = 18.07 \times 10^6$ M/yr

The total natural metal input is $F_1 + F_{21}$, and may be calculated as

$$\frac{F_{12(Natural)} - F_{21(Natural)}}{\dfrac{F_{12} - F_{21}}{F_1 + F_2 + F_{21}}}$$

Cu: $11.72 \times 10^6/.5170 = 22.67 \times 10^6$ M/yr

Pb: $2.13 \times 10^6/.6628 = 3.21 \times 10^6$ M/yr

Zn: $18.07 \times 10^6/.4508 = 40.08 \times 10^6$ M/yr

From the previous proportionality factors, $F_{21(Natural)}$ and $F_{12(Natural)}$ are related.

Cu: $F_{21(Natural)} = 0.0508\ F_{12(Natural)}$

Pb: $F_{21(Natural)} = 0.0400\ F_{12(Natural)}$

Zn: $F_{21(Natural)} = 0.0615\ F_{12(Natural)}$

Accumulation in the sediment is $F_{12} - F_{21}$

Cu: Accumulation $= 11.72 \times 10^6$ M/yr $= (1 - 0.508)F_{12}$

$F_{12(Natural)} = 12.35 \times 10^6$ M/yr

$F_{21(Natural)} = 0.627 \times 10^6$ M/yr

Pb: Accumulation $= 2.13 \times 10^6$ M/yr $= (1 - .0400)F_{12}$

$F_{12(Natural)} = 2.22 \times 10^6$ M/yr

$F_{21(Natural)} = 0.088 \times 10^6$ M/yr

Zn: Accumulation = 18.07×10^6 M/yr = $(1 - .0615)F_{12}$

$F_{12(Natural)} = 19.25 \times 10^6$ M/yr

$F_{21(Natural)} = 1.184 \times 10^6$ M/yr

Therefore, F_1 = Total natural influx - $F_{21(Natural)}$

Cu: 22.67×10^6 M/yr - $.627 \times 10^6$ M/yr = 22.04×10^6 M/yr

Pb: 3.21×10^6 M/yr - $.0888 \times 10^6$ M/yr = 3.12×10^6 M/yr

Zn: 40.08×10^6 M/yr - 1.184×10^6 M/yr = 38.90×10^6 M/yr

Calculation of F_2, the anthropogenic input:

This flux is set equal to zero for times prior to 1850, and is assumed to increase exponentially until present (1975, Nriagu et al. (1979) mass balance year). Further, for the purposes of demonstration, the exponential rate of increase in the anthropogenic loading is assumed to continue for the next 100 years (2075). At any time t > 1850, $F_2(t) = F_{Total\ input} - F_1 - F_{21}(t)$ $F_2 = 0$ in 1850 and may be calculated for t = 125 yr from the mass balance data.

Cu: $F_2(125) = 43.00 - 22.04 - 1.19 = 19.77 \times 10^6$ M/yr

Pb: $F_2(125) = 9.46 - 3.12 - .261 = 6.079 \times 10^6$ M/yr

Zn: $F_2(125) = 122.57 - 38.90 - 3.62 = 80.05 \times 10^6$ M/yr

Assuming exponential growth between t = 0 (1850) and t = 125 (1975), $F_2(t)$ may be formulated as $F_2(t) = A(e^{Kt} - 1)$

Cu: $F_2(t) = 22.04\ (e^{.0051t} - 1) \times 10^6$ M/yr

Pb: $F_2(t) = 3.12\ (e^{.00865t} - 1) \times 10^6$ M/yr

Zn: $F_2(t) = 38.90\ (e^{.0089t} - 1) \times 10^6$ M/yr

Calculation of F_{12} and F_{21}:

Because F_2 is time dependent, F_{12}, F_{21}, and F_3 are also time dependent. The time dependencies of F_{12} and F_{21} may be determined using the previous assumption that the amount of metal accumulating in the sediment ($F_{12} - F_{21}$) is proportional to the total input to the lake ($F_1 + F_2 + F_{21}$); $F_{12} - F_{21} = F_{12}(t)(1 - \alpha)$.

Therefore,

$$F_{12}(t)(1 - \alpha) = \beta(F_1 + F_2(t) + F_{12}(t)\alpha)$$

where β has also been previously determined. Thus,

$$F_{12}(t) = \frac{\beta\ (F_1 + F_2(t))}{(1 - \alpha - \alpha\beta)} \qquad = \gamma(F_1 + F_2(t))$$

.. Cu: $F_{12}(t) = 12.35\ e^{.0051t} \quad x\ 10^6$ M/yr

$F_{21}(t) = .627\ e^{.0051t} \quad x\ 10^6$ M/yr

Pb: $F_{12}(t) = 2.22\ e^{.00865t} \quad x\ 10^6$ M/yr

$F_{21}(t) = 0.088\ e^{.00865t} \quad x\ 10^6$ M/yr

Zn: $F_{12}(t) = 19.25\ e^{.0089t} \quad x\ 10^6$ M/yr

$F_{21}(t) = 1.184\ e^{.0089t} \quad x\ 10^6$ M/yr

Calculation of $F_3(t)$:

F_3 is assumed to be proportion to the mass of metal contained in reservoir 1:

$$F_3(t) = K_3\ R_1(t)$$

$$K_3 = \frac{F_3(125)}{R_1(125)}$$ from the present mass balance.

Cu: $K_3 = \dfrac{20.77 \times 10^6 \text{ M/yr}}{11.07 \times 10^6 \text{ Moles}} = 1.876\ \text{yr}^{-1}$

Pb: $K_3 = \dfrac{3.19 \times 10^6 \text{ M/yr}}{4.53 \times 10^6 \text{ Moles}} = 0.704\ \text{yr}^{-1}$

Zn: $K_3 = \dfrac{67.31 \times 10^6 \text{ M/yr}}{43.05 \times 10^6 \text{ Moles}} = 1.564\ \text{yr}^{-1}$

where $R_1(125)$ is the present reservoir size = concentration of the metal in the lake water (dissolved plus particulate) times the volume of the lake (469 Km^3).

Calculation Procedure:

Because of the set-up of the problem, the knowns are for the present time. The accumulation of the metal in the sediment represents deposition at previous times. $R_1(t)$ and $F_3(t)$ do not have explicit formulations and must be solved simultaneously in terms of the other parameters. Thus, the calculation was run backwards in time from t = 125 yrs (1975) until t = 0 (1850). Then the future was extrapolated by extending the calculations for 100 yrs to 5 = 225. The calculations were performed step-wise with small Δt increments. This resulted in a small discontinuity at ~1975 (not shown). The two relationships are:

Backward:

$$R_1(t_2) = \frac{[R_1(t_1) + (F_1 + F_2(t_2) + F_{21}(t_2) - F_{12}(t_2))\Delta t]}{(1 + K_3\ \Delta t)} \qquad (22)$$

Forward:

$$R_1(t_2) = R_1(t_1) + [F_1 + F_2(t_1) + F_{21}(t_1) - F_{12}(t_1) - K_3R_1\ (t_1)]\ \Delta t \qquad (23)$$

The results of the calculations are shown in Figures 42 and 43. The effect of the exponential loading is seen clearly in Fig. 42 where the concentrations of the toxic metals in the lake water (dissolved plus particulate) also increases exponentially. However, even with an exponential increase in toxic metal loading in Lake Erie for the next 100 years, the concentration of these metals in the lake water increase by about a factor of 3-5. Most of this increase would be

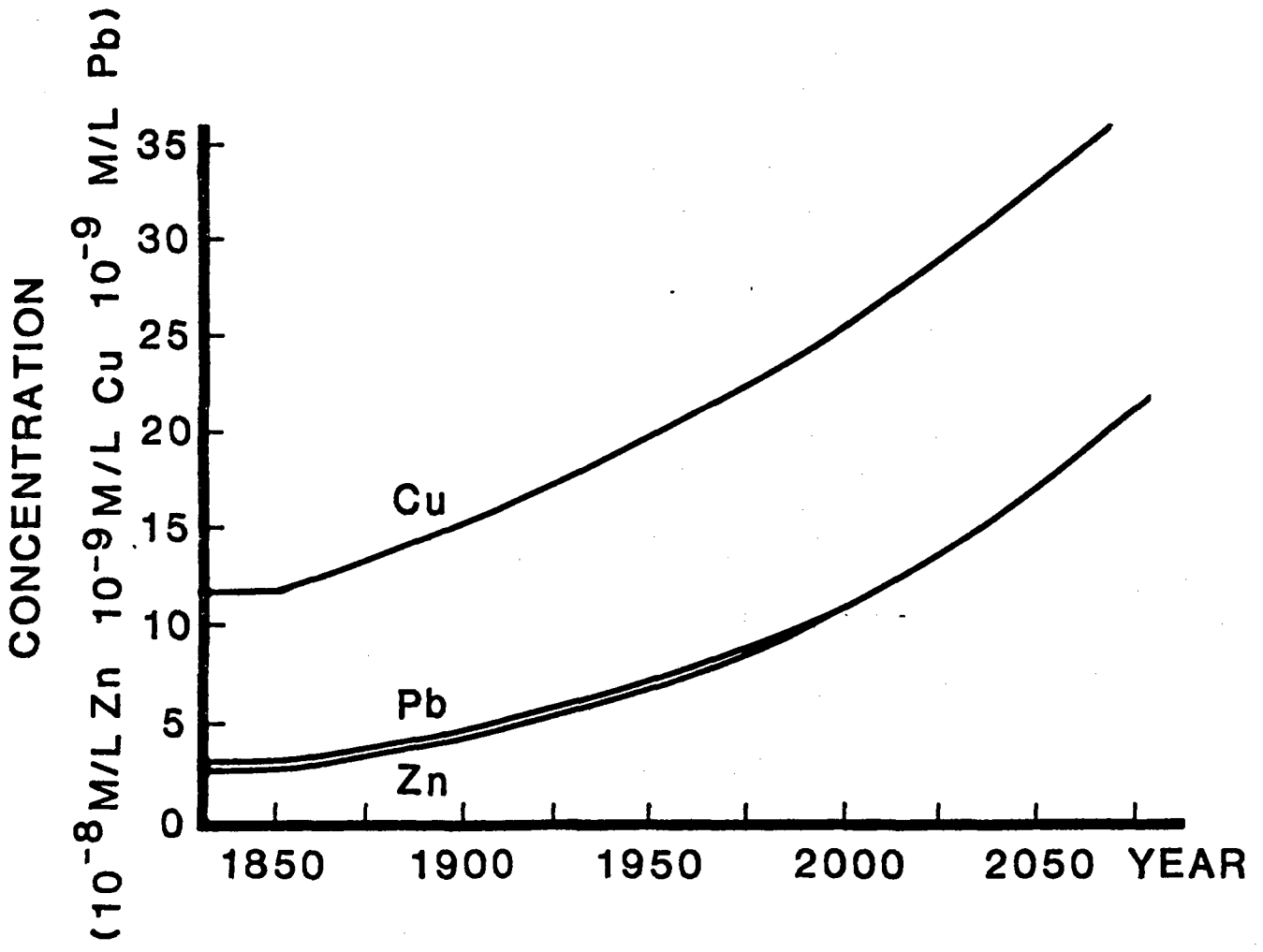

Figure 42. Model predictions of Zn, Pb, and Cu concentrations in Lake Erie water to the year 2075.

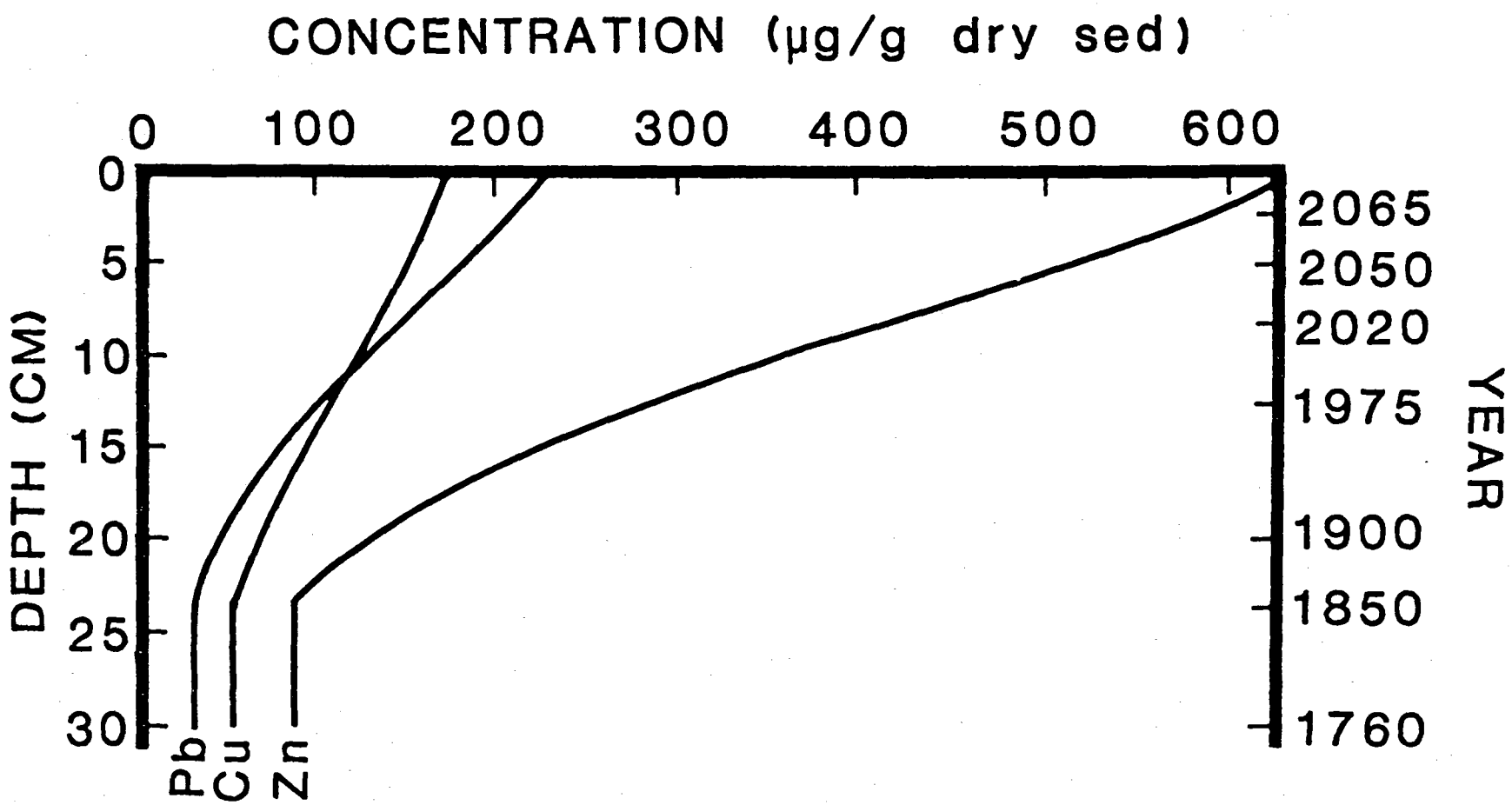

Figure 43. Model predictions of Zn, Pb, and Cu concentrations in Lake Erie sediments (Station 83) to the year 2075.

in the particulate component, but there is insufficient data to partition the concentraton between dissolved and particulate. The effect of the exponentially increasing load to the lake is recorded in the hypothetical sediment profile in the year 2075 seen in Fig. 43. The accumulation of metal in the sediment since 1850 is apparent, but an exponentially increasing load is not. If loading rates continue to incease exponentially, the concentration of lead in the sediments will surpass that of copper in about the year 2000. The extent of mans influence on the toxic metals is Zn >>Pb >Cu, while the natural abundances is Zn > Cu > Pb.

Nutrients

The cultural eutrophication of Lake Erie and its effects on the lake's environment and biota has been will documented (e.g. Beeton, 1965; 1969; I.J.C., 1969). Even so, evidence for changes in Lake Erie over the past century has depended mainly on the water quality data (from municipal water intakes) and records of commercial fish catches. Few scientific studies (Beeton, 1969) are available, and the detailed limnologic history of man's effects on Lake Erie is not known. Studies of sediment cores have revealed much about man's influence on toxic metal's budget (e.g. Nriagu, et al. 1979), but knowledge of historic nutrient budgets for Lake Erie is scant. Historic phosphorous loadings have been estimated from population growth data for the basin (I.J.C., 1969), and attempts have been made to reconstruct nutrient loadings from sediment stratigraphic data (Kemp et al., 1967). As noted by Sly (1976), however, the use of sediment stratigraphy to reconstruct nutrient loading must be carefully assesed with respect to the effects of in situ degradation, bioturbation, and physical reworking. Lake Erie's sediments do contain a record of the chemical, physical, and biological history of the

lake. The question is whether or not we can interpret the record. This section represents a first attempt to provide an answer to this question. Here an attempt will be made to deconvolve the history of nitrogen loading to Lake Erie using data on the present day concentration (solid phase) of organic nitrogen in a core from Lake Erie (Station 83) and the present day rate of organic nitrogen destruction (i.e. ammonia production) at the same locale. Bioturbation and physical reworking are not considered.

In anoxic lake sediments, particulate organic nitrogen is transformed to ammonia via bacterial action. The change in ammonia concentration with time is assumed to be dependent on the amount of particulate organic nitrogen present. At any depth, z,

$$\frac{dA}{dt}(z) = K_1(z)\, N_p(z) \tag{24}$$

where dA/dt is the time rate of change in ammonia concentration, N_p is the concentration of particulate nitrogen, and K_1 is the rate constant. The change in particulate organic nitrogen can be related to the change in ammonia concentration by:

$$\frac{dA}{dt}(z) = K_2 \frac{dN_p}{dt}(z) \tag{25}$$

where K_2 is a constant used to convert units. Combining equations 24 and 25 results in

$$\frac{dN_p}{dt}(z) = \frac{K_1(z)}{K_2} N_p(z) \tag{26}$$

A solution for this equation is

$$N_p(z) = N_{po}\ (t_o - \frac{z}{\omega})e^b \tag{27}$$

where

$$b = -\frac{1}{\omega} \int_o^z \frac{K_1(z)}{K_2}\, dz \tag{28}$$

N_{po} is the concentration of particulate organic nitrogen at the time of deposition, $(t_o - z/\omega)$, ω is the sedimentation rate, and t_o is the present time. Compaction is accounted for by considering ω as a mass flux (mass of dry sediment /length^2/unit time) and z as overlying dry sediment mass (mass/ length^2).

Equation 27 was used to calculate the history of particulate nitrogen flux to the sediment-water interface at Station 83. Empirical determinations of the rate of ammonia production as a function of depth (10°C data, Production Experiment), particulate organic nitrogen (measured as total kjeldhal nitrogen) as a function of depth, sediment porosity (ratio of pore water volume to total volume) as a function of depth, and sedimentation rate (by Pb-210, J.A. Robbins, pers. comm). were used in the calculation. (see Figs. 7, 17, and 44). The dependence of K_1 on depth (i.e. time, taken here as comulative mass of dry sediment) was determined from the empirical data using equation 27. The form of K_1 (z) is well approximated as an exponential (r = .997) (see Fig. 45). If dA/dt and dN_p/dt are expressed in equivalent units (e.g. moles/volume wet sediment/time) K_2 is dimensionless and has a numerical value one. Once K_1 and K_2 are known, N_{po} $(t_o - z/\omega)$ is calculated using

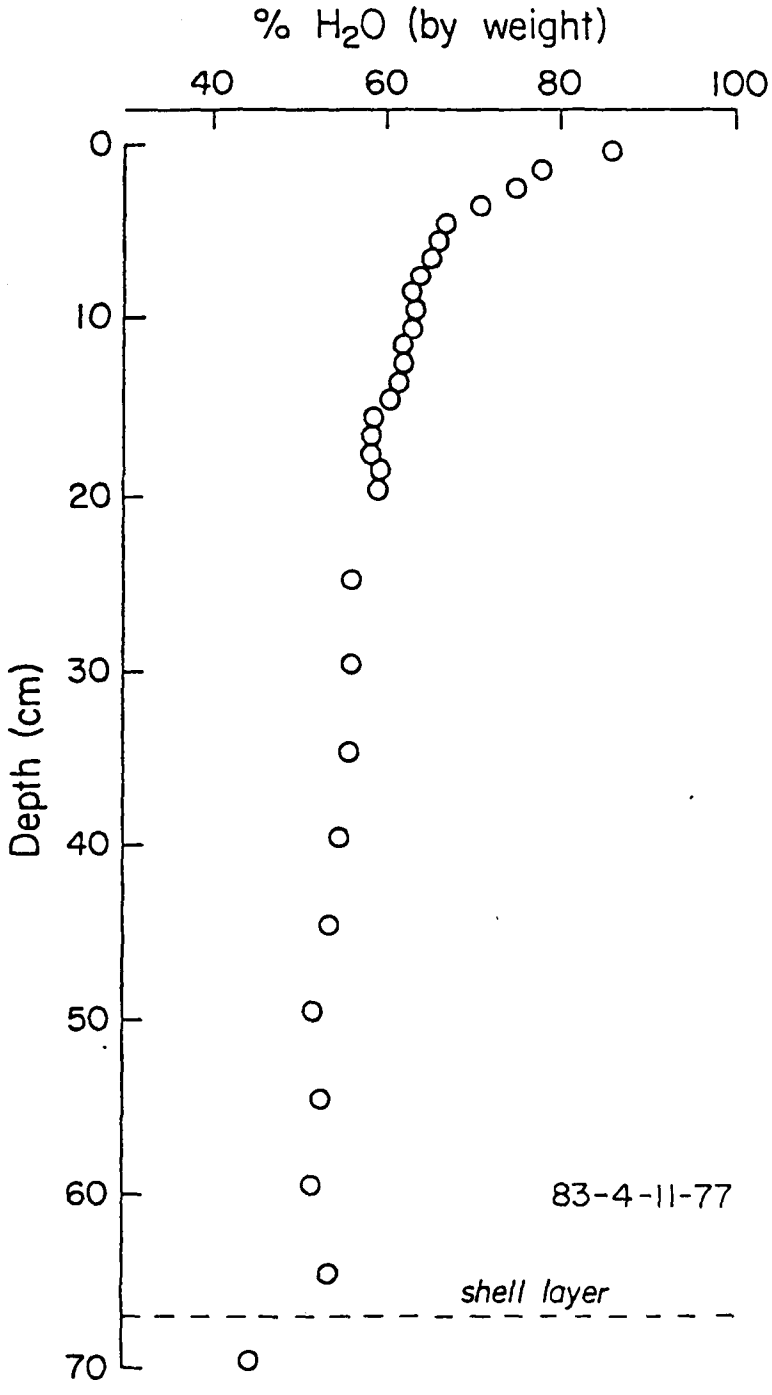

Figure 44. Water content (%H_2O) versus depth at Station 83.

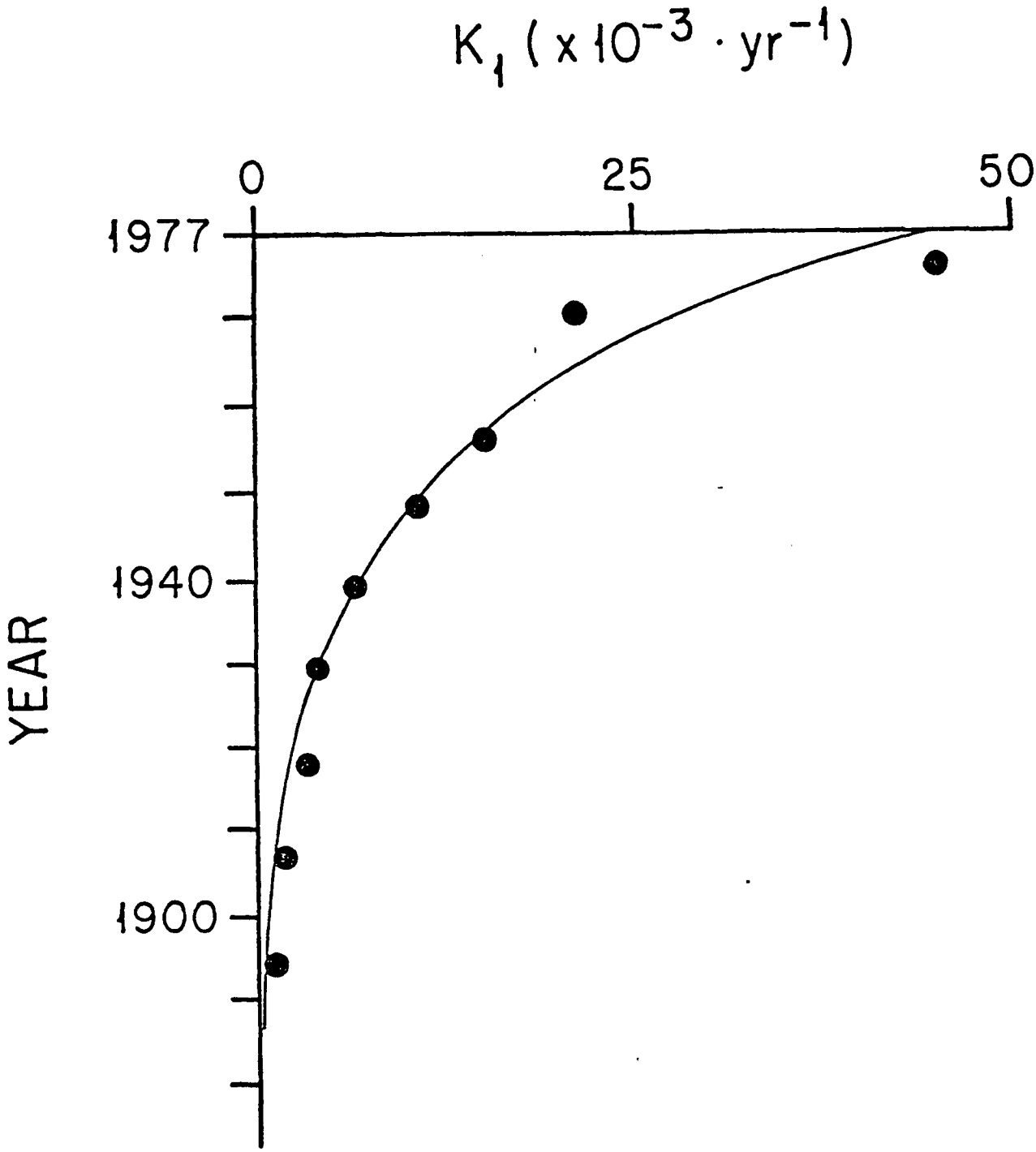

Figure 45. K_1 as a function of time of sediment deposition at Station 83.

equation 27. The results of this calculation are shown in Fig. 46. which illustrates the calculated history of particulate organic nitrogen loading, N_{po}, and the amount of particulate organic nitrogen remaining at present, N_p. Examination of Fig 46 reveals that the loading of particulate organic nitrogen to sediments at station 83 has increased since ~1950. Scatter in the data, preclude a detailed examination of particulate organic nitrogen flux increase prior to this date. The above result agrees well with phosphorous loading for Lake Erie's drainage basin (Sly, 1976). In the early nineteenth century, the flux of particulate organic nitrogen to the sediment water interface, $\omega * N_{po}$ (1820, 1860), was ~ .165 moles/M^2/year, while $\omega * N_{po}$ (1974, 1977) was ~ .285 moles/m^2/year. This result indicates that the present ratio of anthropogenic to natural nitrogen loadings at station 83 is ~ 0.73. This result is substantially lower than the estimates of this ratio made by Kemp et al. (1976). These workers calculated the average ratio of anthropogenic to natural nitrogen loading to Lake Erie sediments to be ~ 1.79±0.78. Kemp et al. (1976) did not consider decomposition of nitrogen containing organic matter. This omission will increase the apparent ratio of anthropogenic to natural nitrogen loading. For example, application of the methodology of Kemp et al. (1976) to our organic nitrogen data for station 83 results in a anthropogenic to natural nitrogen loading ratio of 1.99 for the present day. The neglect of organic decompositon in estimates of man's effects on the flux of decomposable materials to lake sediments results in a significant overestimate of anthropogenic inputs. The method outlined above for taking decomposition into account should be tested at other locales and in other environments.

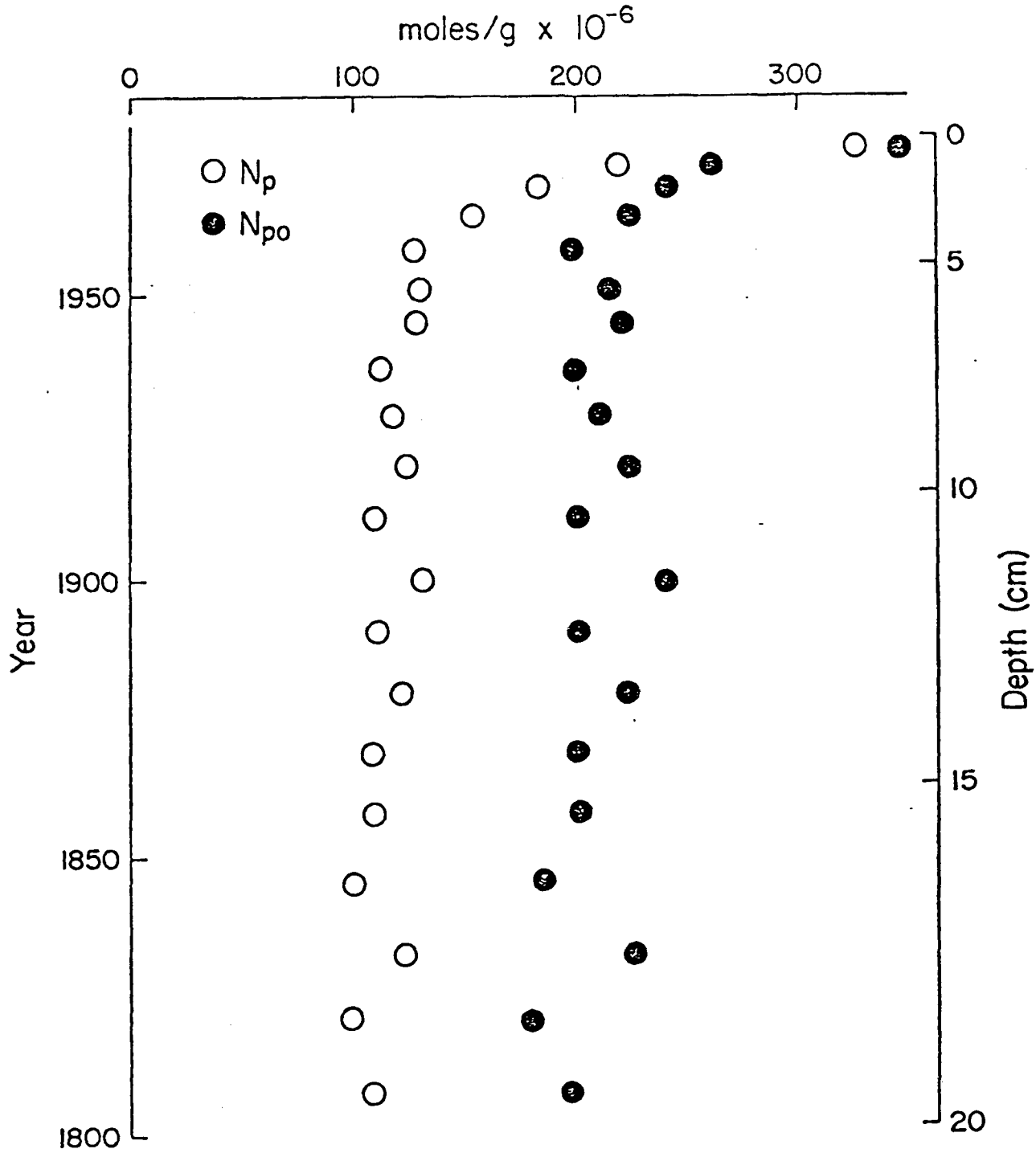

Figure 46. Present day particulate organic nitrogen concentration (N_p) and calculated organic nitrogen concentrations at the time of deposition (N_{po}) plotted versus depth and time of deposition at Station 83.

Prediction of Pore Water Chemistry

Equlibrium modeling of sediment pore water chemistry provides useful informtion concerning potential solid phase sinks for materials of interest (nutrients, toxic metals, etc). Further, such modeling can be used to check consistency in understanding and interpretation of diagenetic processes in sediments (Aller, 1977). Equlibrium modeling, however, cannot predict pore water chemistry. Predictive modeling of pore water chemistry requires a transport-reaction approach.

In Lake Erie reactive materials fall onto the sediment surface, move into the sediments at the net rate of sedimentation, ω, and react. Solutes derived from these reactions either move across the sediment-water interface via molecular diffusion or precipitate as anthigenic minerals. Using this scenario (which ignores bioturbation and physical mixing), changes in the chemistry of interstitial water can be described by one-dimensional transport-reaction models. Formally, such a model can be written (ignoring compaction) (Aller, 1977);

$$\frac{\partial c}{\partial t} = \frac{1}{1+K} \frac{\partial}{\partial z} \left(D \frac{\partial c}{\partial z}\right) - \omega \frac{\partial c}{\partial z} + \frac{R}{1+K} \qquad (29)$$

where:

C = concentration of pore water constituent being considered

z = vertical dimension, origin (z=0) at sediment-water interface; postive downwards

ω = sedimentation rate

D = effective diffusion coefficient modified for porostiy and tortuosity

R = reaction; function of z, and temperature

K = Langmuir adsorption coefficient

t = time

Using data from the production and flux experiments, we have attempted transport-reaction models for the time evolution of ammonia and bicarbonate profiles for the simplest case - the homogenized mud core experiment without worms. In these experiments there is no sedimentation, temperature is constant, there is no depth variation in the vertical distribution of reactive material, and K is constant in both depth and time. In this situation, the transport-reaction model is

$$\frac{\partial c}{\partial t} = \frac{D}{(1+K)} \frac{\partial^2 c}{\partial z^2} + R, \qquad (30)$$

and appropriate boundary and initial conditions are

$$C(Z > 0, 0) = C_i$$

and

$$C(0, t) = C_o$$

Where C_i is the initial concentration at all depths and C_o is the concentration at z=0. The solution of equation (30) under these conditions for the semi-infinite case is given by Carslaw and Jaeger (1959):

$$C(z,t) = [\Delta C + \frac{Rt}{(1+K)} + \frac{Rz^2}{2D}] \operatorname{erf} [\frac{z}{2\sqrt{(\frac{Dt}{1+K})}}]$$

$$+ \frac{Rz}{D} [\frac{Dt}{\pi(1+K)}]^{\frac{1}{2}} \exp [\frac{-Z^2(1+K)}{2Dt}] - \frac{RZ^2}{2D} + C_o$$

Where $\Delta C = C_i - C_o$

This equation was used to predict the evolution of ammonia and bicarbonate profiles in the homogenized mud core experiment without worms. Values for R were obtained from the production experiment data by fitting regression lines to R vs TKN and R vs organic carbon data. For the ammonia calculation, K was taken as 1.2 (the value obtained in the production experiment). Values for D were obtained by fitting the models calculations to the observed profiles of ammonia and bicarbonate. Values for C_i and C_o were obtained fromt the flux experiment data. The numerical values for D,R,K, C_o, and C_i, used for the calculations are given in Table 15.

The results of these calculations are compared with the experimental data in Fig. 47. The agreement between the model results and the observed pore water profiles is good for both ammonia and bicarbonate. The ammonia profiles do not vary strongly with time while the bicarbonate profiles show strong time variation. The model results track these trends well. For this case, homogenized sediment with no worms, a one-dimensional transport-reaction model provides an adequate representation of the behavior of ammonia and bicarbonate. Even for this simple case, however, more complex models which consider mineral equlibria and reactions near the sediment- water interface are required to describe the behavior of iron and phosphorous. The addition of tubificids to homogenized sediments confounds the model presented above since ammonia is sourced near the sediment-water interface. The situation presented by the real lake cores in even more complex as the distribution of decomposable organic matter is not constant with depth and animals are present.

	Ammonia Model	Bicarbonate Model
D (cm^2/yr)	3.8×10^2	2.25×10^2
K	1.2	0
R (mM/yr)	0.315	7.60
C_o (mM)	.100	2.5
C_i (mM)	.160	2.5

Table 15. Values for D,K, R, C_o, and C_i used in the time dependent ammonia and bicarbonate transport-reaction calculations.

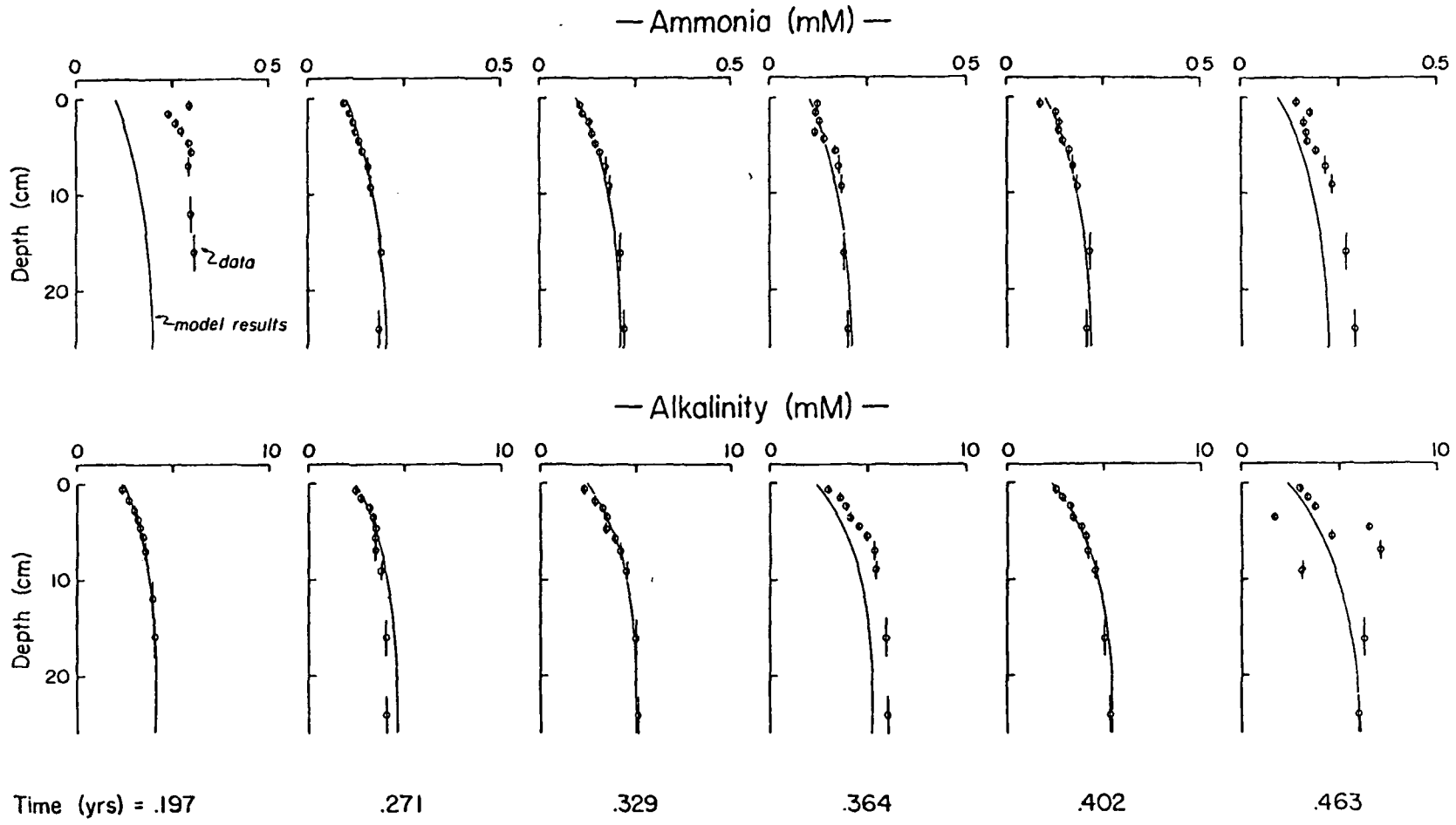

Figure 47. Observed and calculated concentration profiles of ammonia and alkalinity (HCO_3^-) for the homogenized mud core experiment (without worms).

References

1. Agemian, H. and Chau, A.S.Y., 1975, An atomic adsorption method for the determination of 20 elements in lake sediments after acid digestion. Anal Chim. Acta 80: 61-66.

2. Aller, R.C., 1977, The influence of macrobenthos on chemical diagenesis in marine sediments. Unpublished Ph.D. Dissertation, Yale University New Haven.

3. Atlas, E. and Pytkowicz, R.M., 1977, Solubility behavior of apatites in seawater. Limnol. Oceanogr. 22: 290-300.

4. Bachmann, R.W., 1963, Zinc-65 in studies of the freshwater cycle. In Radioecology (eds. V. Schultz and A.W. Klement), pp. 485-496, Rheinhold.

5. Bancroft, K., Paul, E.A., And Wiebe, W.J., 1976, The extraction and measurement of adenosine triphosphate from marine sediments. Limnol. Oceanogr. 21: 473-479.

6. Beeton, A.M., 1965, Eutrophication of the St. Lawrence Great Lakes Limnol. Oceanogr. 10: 240-254.

7. Beeton, A.M., 1969, Changes in the environment and biota of the Great Lakes. In Eutrophication: Causes, Consequences, Correctives, Nat. Acad. Sci.

8. Berner, R.A., 1970, Sedimentary pyrite formation. Amer. J. Sci. 268: 1-23.

9. Berner, R.A., 1971, Principles of Chemical Sedimentology. McGraw HIll, 240pp.

10. Berner, R.A., 1974, Kinetic models for the early diagenesis of nitrogen, sulfur, phosphorous, and silicon in anoxic marine sediments. In: The Sea, Vol. 5, Marine Chemistry (ed. E.D. Goldberg) pp. 427-450, John Wiley and Sons.

11. Berner, R.A., 1976, The inclusion of adsorption in the modeling of early diagenesis. Earth Planet. Sci. Lett. 29: 333-340.

12. Berner, R.A., 1980, Early Diagenesis: A Theoretical Approach. Princeton University Press, 241pp.

13. Bradford, W.L., 1972, A study of the chemical behavior of zinc in Chesapeake Bay waters using anodic stripping voltammetry. Chesapeake Bay institute Technical Report, 76, Ref. 72-7.

14. Bray, J.T., 1973, The behavior of phosphate in the interstitial waters of Chesapeake Bay sediments. Unpublished Ph.D. Dissertation, The Johns Hopkins University, Baltimore.

15. Bremner, J.M, 1965, Total nitrogen. In Methods of Soil Analysis, Part 2. Agronomy (ed. C.A. Black), pp. 1149-1178, Amer. Soc. Agron.

16. Bricker, O.P., and Troup, B.N., 1975, Sediment-Water exchange in Chesapeake Bay. In Estuarine Research (ed L.E. Cronin), Vol. 1, pp 3-27, Academic Press.

17. Bricker, O.P., Matisoff, G., and Holdren, G.R. Jr., 1977, Interstitial water chemistry of Chesapeake Bay sediments. Basic Data Report No. 9, Maryland Geological Survey, 67 pp.

18. Brooks, R.R., Presley, B.J., And Kaplan, I.R., 1968, Trace elements in the interstitial waters of marine sediments. Geochim Cosmochim. Acta 32: 397-414.

19. Burns, N.M., 1976, Nutrient budgets for Lake Erie, 1970, J. Fish. Res. Bd. Can. 33: 520-536.

20. Burns, N.M. and Ross, C., 1972, Oxygen-nutrient relationships within the central basin of Lake Erie. In Project Hypo (eds. N.M. Burns and C. Ross), Can. Cent. Inland Waters Pap. No. 6, pp. 85-119.

21. Burns, N.M., Williams, J.D. H., Jaquet, J.-M., Kemp, A. L. W., and Lam, D.C.L., 1976, A phosphorous budget for Lake Erie. J. Fish Res. Bd. Can. 33: 564-573.

22. Carroll, D., 1957, Role of clay minerals in the transportation of iron. Geochim. Cosmochim. Acta 14: 1-27.

23. Carslaw, H.S. and Jaeger, J.C., 1959, Conduction of Heat in Solids. Glarendon Press, 510 pp.

24. Chave, K.E., 1965, Carbonates: Association with organic matter in surface seawater. Science 148: 1723-1724.

25. Chawla, V.K. and Chau, Y.K., 1969, Trace elements in Lake Erie. Proc. 12th Conf. Great Lakes Res: 175-184.

26. Christ, C.L., Hostetler, P.B., and Siebert, R.M., 1974, Stability of calcite and aragonite. J. of Res., U.S. Geol. Surv. 2: 175-184.

27. Cline, J.T. and Upchurch, S.B., 1973, Mode of heavy metal migration in the upper strata of lake sediments. Proc. 16th Conf. Great Lakes Res: 349-356.

28. Duchart, P., Calvert, S.E., and Price, N.B., 1973, Distribution of trace metals in the pore waters of shallow marine sediments. Limnol. Oceanogr. 18: 605-610.

29. Duff, E.J., 1971, Orthophosphates. Part IV. J. Chem Soc. A. 1971: 921-926.

30. Emerson, S., 1976, Early diagenesis in anaerobic lake sediments: chemical equlibria in interstitial waters. Geochim. Cosmochim Acta 42: 925-934.

31. Emerson, S., and Widmar, G., 1978, Early diagenesis in anaerobic lake sediments - II. Thermodynamic and kinetic factors controlling the formation of iron phosphate. Geochim Cosmochim Acta 42: 1307-1316.

32. Fisher, J.B., and Matisoff, G., in press, High resolution vertical profiles of pH in recent sediments. Hydrobiol.

33. Fisher, J.B., and Lick, W.J., McCall, P.L., and Robbins, J.A., 1980. Vertical mixing of lake sediments by tubificid oligocheates. J. Geophys. Res. 85: 3997-4006.

34. Gamble, D.S. and Schnitzer, M., 1973, The chemistry of fluvic acids and its reactions with metal ions. In Trace Metals and Metal-Organic Interactions in Natural Waters (ed. P.C. Singer) pp. 265-302, Ann Arbor Science.

35. Gardiner, J., 1974a, the chemistry of cadmium in natural water - I. A study of cadmium complex formaton using the cadmium specific electrode. Wat. Res. 8: 23-30.

36. Gardiner, J., 1974b, The chemistry of cadmium in natural water - II. The adsorption of cadmium on river muds and naturally occurring solids Wat. Res. 8: 157-164.

37. Gardner, L.R., 1974, Organic versus inorganic trace metal complexes in sulfidic marine waters. Geochim. Cosmochim. Acta 38: 1297-1302.

38. Garrels, R.M. and Thompson, M.E., 1962, A chemical model for sea water at 25°C and one atmosphere total pressure. Amer. J. Sci. 260: 57-66.

39. Goldhaber, M.B., Aller, R.C., Cochran, J.K., Rosenfeld, J.K., Martens, C.S., and Berner, R.A., 1977, Sulfate reduction, diffusion, and bioturbation in Long Island Sound sediments: Report of the FOAM group. Am. J. Sci . 277: 193-237.

40. Gunkel, W. And Oppenheimer, C.H., 1963, Experiments regarding the sulfide formation in sediments of the Texas Gulf Coast. In Symposium on Marine Microbiology (eds. C.H. Oppenheimer and C. Thomas) pp. 674-683.

41. Harlow, G. L., 1966, Major sources of nutrients for algal growths in western Lake Erie. St. Johns Rev. Div., Univ. of Mich., Pub. No. 15, 389 pp.

42. Hem, J. D., 1972, Chemistry and occurrence of cadiumm and zinc in surface water and ground water. Wat. Resourc. Res. 8: 661-679.

43. Hesslein, R.H., 1976, The fluxes of CH_4, ΣCO_2, and NH_3-N from sediments and their consequent distribution in a small lake. Unpublished Ph.D. Dissertation, Columbia University, New York.

44. Hirst, D.M., 1962, Geochemistry of modern sediments from the Gulf of Paria II. The location and distribution of trace elements. Geochem. Cosmochim. Acta 26: 1147-1187.

45. Holdren, G.R., Jr., Bricker, O.P., and Matisoff, G., 1975, A model for the control of dissolved manganese in the interstitial waters of Chesapeake Bay. In Marine Chemistry in the Coastal Environment (ACS Symposium Series 18), (ed. T.M. Church), pp. 364-381, American Chemical Society.

46. International Joint Commission, 1969, Pollution of Lake Erie, Lake Ontario, and the international section of the St. Lawrence River. Vol. 2 -- Lake Erie. Int. Joint Comm. Rept. : 316 pp.

47. Jacobson, R.L. and Langmuir, D., 1974, Dissociation constants of calcite and CaHCO from 0 to 50 C. Geochim. Cosmochim. Acta 38: 301-318.

48. Jenne, E.A., 1968, Controls on Mn, Fe, Co, Cu, Zn concentrations in soils and water: The significant role of hydrous Mn and Fe oxides. In Trace Inorganics in Water, Advances in Chemistry Series 73, pp. 337-387.

49. Kee, N.S. and Bloomfield, C., 1961, the solution of some minor element oxides by decomposing plant materials. Geochim. Cosmochim. Acta 24: 206-226.

50. Kemp, A. L., 1969 Organic matter in sediments of Lake Ontario and Erie. Proc. 12th Conf. Great Lakes Res. : pp. 237-249.

51. Kemp, A.L. W., Thomas, R.L., Dell, C. I., and Jaquet, J.-M, 1976, Cultural impact on the geochemistry of sediments in Lake Erie J. Fish Res. Bd Can. 33: 440-462.

52. Leland, H.V., Shulka, S.S., and Shimp, N.F., 1973, Factors affecting the distribution of lead and other trace metals in sediments of southern Lake Michigan. In Trace Metals and Metal-Organic Interactions in Natural Waters (ed. P.C. Singer) pp. 89-130, Ann Arbor Science.

53. Lerman, A., 1975, Maintenance of steady state in ocean sediments. Amer. J. Sci. 275: 609-635.

54. Lerman, A. and Childs, C.W., 1973, Metal-organic complexes in natural waters: Control of distribution by thermodynamic, kinetic, and physical factors. In Trace Metals and Metal-Organic Interactions in Natural Waters (ed. P.C. Singer) pp. 201-236, Ann Arbor Science.

55. Li, Y-H. and Gregory, S., 1974, Diffusion of ions in seawater and in deep sea sediments. Geochim. Cosmoshim. Acta 38: 703-714.

56. Lu, J.C.S. and Chen, K. Y., 1977, Migration of trace metals in interfaces of seawater and polluted surficial sediments. Environ. Sci. Technol. 11: 174-182.

57. Martens, C.S., and Berner, R.A., 1974, Methane production in the interstitial waters of sulfate depleted marine sediments. Science 185: 1167-1169.

58. Martens, C.S. and Harriss, R.C., 1970, Inhibition of apatite precipitation in the marine environment by magnesium ions. Geochim Cosmoshim Acta 34: 621-629.

59. Matisoff, G., Harris, A., Matis, S., and Soster, F., in press, Trace metals mineral equlibria in Lake Erie sediments. J. Great Lakes Res.

60. Matson, W.R., 1968, Trace metals, equlibrium and kinetics of trace metal complexes in natural media. Unpublished Ph.D. Dissertation, Massachuesetts Institute of Technology, Cambridge.

61. McCall, P.L. and Fisher, J.B., 1980, Effects of tubificid oligochaetes on physical and chemical properties of Lake Erie sediments. In Aquatic Oligochaete Biology (eds. R.O. Brinkhurst, And D.G. Cook), pp. 253-317, Plenum.

62. Mitchell, R.L., 1964, Trace elements in soils. In Chemistry of the Soil (ed. E.F. Bear) pp. 57-78, Reinhold.

63. Morgan, J.J. 1967, Chemical equlibria and kinetic properties of manganese in natural waters. In Principles and Applications of Water Chemistry (eds. S.D. Faust and J.V. Hunter) pp. 561-624, John Wiley and Sons.

63. Mortimer, C.H., 1941, The exchange of dissolved substances between mud and water in lakes J. Ecol. 30: 280-329.

64. Mortimer, C.H., 1942, The exchange of dissolved substances between mud and water in lakes. J. Ecol. 30: 147-201

65. Morton, S.D. and Lee, G.F., 1968, Calcium carbonate equlibria in lakes. J. Chem Educ. 45: 511-513.

66. Muller, G., 1969, Diagenetic changes in interstitial waters of Holocene Lake Constance sediments. Nature 224: 258-259.

67. Murphy, J. and Riley, J.P., 1962, A modified single solution method for the determination of phosphate in natural waters. Anal Chim. Acta 27: 31-36.

68. Murry, J.W., Grundmanis, V., and Smethie, W. M. Jr., 1978, Interstitial water chemistry in sediments of Saanich Inlet. Geochim. Cosmoshim. Acta. 42: 1011-1026.

69. Nelson, D.W. and Sommers, L.E., 1972, A simple digestion procedure for the estimation of total nitrogen in soils and sediments. J.Environ. Qual. 1: 423-425.

70. Nissenhaum, A., Baebecker, M.S., and Kaplan, I.R., 1971, Studies on dissolved organic matter from interstitial water of a reducing marine fjord. In Advances in Organic Geochemistry (eds. H.R. Von Gaertner and H. Wehner) pp. 427-440, Pergamon.

71. Nordstorm, D.K., Plummer, L.N., Wigley, T.M.L., Wolrey, T.J., Ball, J.W., Jenne, E.A., Bassett, R.L., Crerar, D.A., Florence, T.M., Fritz, B., Hoffman, M., Holdren, G.R. Jr., Lafon, G.M., Mattigod, S.V., McDuff, R.E., Morel, F., Reddy, M.M., Sposito, G., and Thrailkill, J., 1979, A comparison of computerized chemical models for equlibrium calculations in aqueous systems. In Chemical Modeling in Aqueous Systems (ed. E.A. Jenne) pp. 857-892, Amer. Chem. Soc. Symp. Ser. No. 93.

72. Nriagu, J.O., 1972a, Stability of vivianite and ion-pair formation in the system $Fe_3(PO_4)_2$-H_3PO_4-H_2O. Geochim. Cosmochim. Acta 35: 459-479.

73. Nriagu, J.O., 1972b, Lead orthophosphates I. Solubility and hydrolysis of secondary lead orthophosphate. Inorg. Chem. 11: 2499-2503.

74. Nriagu, J.O., 1973, Solubility equlibrium constant of α-hopeite. Geochim. Cosmochim. Acta 37: 2357-2362.

75. Nriagu, J.O., 1974, Lead orthophosphates - IV. Formation and stability in the environment. Geochim. Cosmochim. Acta 38: 887-898.

76. Nriagu, J.O., 1975, Sulfur isotopic variations in relation to sulfur pollution of Lake Erie. In Isotope Ratios as Pollutant Source and Behavior Indicators. pp. 77-93, IAEA.

77. Nriagu, J.O., and Dell, C.I., 1974, Diagenetic formation of iron phosphates in recent lake sediments. Am. Miner. 59: 934-946.

78. Nriagu, J.O., Kemp, A.L.W., Wong, H.K.T., and Harper, N. 1979, Sedimentary record of heavy metal pollution in Lake Erie. Geochim. Cosmochim. Acta 43: 247-258.

79. O'Connor, T.T. and Renn, C.E., 1964, Soluble-desorbed zinc equlibrium in natural waters. J. Am. Waterworks Assoc. 56: 1055-1061.

80. Otsuki, A. and Wetzel, R.G., 1974, Calcium and total alkalinity budgets and calcium carbonate precipitation in a small hard-water lake. Arch. Hydrobiol. 73: 14-30.

81. Pankow, J.F., and Morgan, J.J., 1980, Dissolution and tetragonal ferrous sulfide (mackinawite) in anoxic aqueous systems. 2. Implications for the cycling of iron, sulfur, and trace metals. Environ. Sci. Technol. 14: 183-186.

82. Pinta, M. and Ollat, C., 1961, Recherches physico-chemiques des elements -traces dans les sols tropicaux - I. Etude de quelques du Dahomey Geochim Cosmochim. Acta 25: 14-23.

83. Presley, B.J., Koloday, Y., Nissembaum, A., and Kaplan, I.R., 1972, Early diagenesis in a reducing fjord, Sannich Inlet, British Columbia - II, Trace element distribution in interstitial water and sediment. Geochim. Cosmochim. Acta 36: 1073-1090.

84. Rashid, M.A. and Leonard, J.D., 1973, Modification in the solubility and precipitation behavior for various metals as a result of their interaction with sedimentary humic acid. Chem. Geol. 11: 89-97.

85. Reeburgh, W. S., 1967, An improved interstitial water sampler Limnol. Oceanogr. 12: 163-165.

86. Reeburgh, W.S., and Heggie, D.T., 1977, Microbial methane consumption reactions and their effect on methane distribution in freshwater and marine environments. Limnol. Oceanogr. 22: 1-9.

87. Richards, R.A., 1965, Anoxic basins and fjords. In Chemical Oceanography (eds. J.P. Riley and G. Skirrow), Vol. 1., pp. 611-645, Academic Press.

88. Riley, J.P., and Taylor, D., 1972, The concentrations of Cd, Cu, Fe, Mn, Mo, Ni, V, and Zn in part of the tropical north-east Atlantic Ocean. Deep Sea Res. 19: 207-318.

89. Robbins, J.A., and Callender, E., 1975, Diagenesis of manganese in Lake Michigan sediments. Amer. J. Sci. 275: 512-533.

90. Roberson, C.E., 1969, Solubility implication of apatite in seawater. U.S. Geol. Sur. Prof. Pap. 550-D, pp. D178-D185.

91. Rosenfeld, J.K., 1977, Nitrogen diagenesis in nearshore anoxic sediments. Unpublished Ph.D. Dissertation, Yale University, New Haven.

92. Sandell, E.B., 1959, Colorimetric Determination of Traces of Metals, Interscience, 1032 pp.

93. Semkin, R.G. and Kramer, J.R., 1976, Sediment geochemistry of Sudbury-area lakes. Can. Miner. 14: 73-90.

94. Sholkovitz, E., 1973, Interstitial water chemistry of Santa Barbara Basin sediments. Geochim. Cosmochim. Acta 37: 2043-2073

95. Siever, R., Beck, K.C., and Berner, R.A., 1965, Composition of interstitial waters of modern sediments. J. Geol. 73: 39-73.

96. Sillen, L.G., 1971, Stability constants of metal-ion complexes. Suppl. 1. Spec. Pub. 25. The Chem Soc., London, 865 pp.

97. Sillen, L.G. and Martell, A.E., 1964, Stability constants of metal-ion complexes. Spec. Pub. 17. The Chem. Soc., London, 754 pp.

98. Sly, P. G., 1976, Lake Erie and its basin. J. Fish Res. Bd. Can. 33: 355-370.

99. Smith, R.M. and Martell, A.E., 1976, Critical Stability Constants. Vol. 4: Inorganic Complexes. Plenum, 257 pp.

100. Solorzano, L., 1969, Determination of ammonia in natural waters by the phenol hypochlorite method. Limnol. Oceanogr. 14: 799-801.

101. Sommers, L.E., and Nelson, D.W., 1972, Determination of total phosphorous in soils: A rapid perchloric acid digestion procedure. Soil Sci.Soc. Amer. Proc. 36: 902-904.

102. Standard Methods For the Examination of Water and Wastewaters, 1975, 14th Edition, American Public Health Association, 1193 pp.

103. Strickland, J.D.H. and Parsons, T.R., 1969, A practical handbook of seawater analysis. Can. Fish Res. Bd. Bull. 167: 311 pp.

105. Stumm, W. and Leckie, J.O., 1971, Phosphate exchange with sediments; its role in the productivity of surface waters. In Proc. of the 5th Int. Conf. of Water Pollution Res. 1970 (ed. S.H. Jenkins), Paper III-26 pp. 1-16, Pergamon.

106. Stumm, W., and Morgan J.J., 1970, Aquatic Chemistry, John Wiley and Sons, 583 pp.

107. Suess, E., 1970, Interaction of organic compounds with calcuim carbonate. I. Association phenomena and geochemical implications. Geochim. Cosmochim. Acta 34: 157-168.

108. Suess, E., 1979, Mineral phases formed in anoxic sediments by microbial decomposition of organic matter. Geochim Cosmochim. Acta. 43: 339-352.

109. Taylor, A.W., Frazier, A.W., and Gurney, E.L., 1963, Solubility products of magnesium ammonium and magnesium potassium phosphates. Trans. Faraday Soc. 59: 1580-1584.

110. Tisue, T., 1980, Sulfate reduction in the interstitial fluids of Great Lakes sediments. 23rd Conference on Great Lakes Research, Abs., Kingston, Ontario, May 19-22, 1980.

111. Tobin, R.S. and Anthony, D.H.J., 1978, Tritiated thymidine incorporation as a measure of microbial activity in lake sediments. Limnol. Oceanogr. 23: 161-165.

112. Troup, B.N., 1974, The interaction of iron with phosphate, carbonate, and sulfide in Chesapeake Bay interstitial waters: a thermodynamic interpretation. Unpublished Ph.D. Dissertation, the Johns Hopkins University, Baltimore.

113. Vosjan, J.H., 1974, Sulfate in water and sediment of the Dutch Wadden Sea. Neth. J. Sea Res.. 8: 208-213.

114. Wagman, D.D., Evans, W.H. Parker, V.B, Halow, I., Bailey, S.M. and Schumm, R.H., 1968, Selected values of chemical thermodynamic properties. National Bureau of Standards Technical Note 270-3.

115. Walters, L.J. and Wolrey, T.J., 1974, Transfer of heavy metal pollutants from Lake Erie bottom sediments to the overlying water. Water Resources Center, Engineering Experiment Station. Ohio State University.

116. Walters, L.T., Wolrey, T.J., and Myser, R.D., 1974, Occurrence of As, Cd, Co, Cr, Cu, Fe, Hg, Ni, Sb, and Zn in Lake Erie sediments. Proc. 17th Conf. Great Lakes Res.: pp. 219-234.

117. Watson, S.W., Novitsky, T.J., Quinby, H.L., and Valois, F.W., 1977, Determination of bacterial number and biomass in the marine environment. Appl. and Environ. Microbio. 34: 940-946.

118. Weiler, R.R., 1973, The interstitial water composition in the sediments of the Great Lakes - I, Western Lake Ontario. Limnol. Oceanogr. 18: 918-931.

118. Weiler, R.R., And Chawla, V.K., 1968, The chemical composition of Lake Erie. Proc. 11th Conf. Great Lakes Res. : 583-608.

119. Wetzel, R.G., 1975, Limnology. W.B. Saunders Company, 743 pp.

120. Wheeler, R., and Duriming, C., 1976, Trace element geochemistry of piston cores from western Michigan coastal lakes. The Can. Miner. 14: 23-31.

121. Wollast, R. and Garrels, 1971, Diffusion coefficient of silica in seawater. Nature, Physical Science 229: 94.

122. Zajic, J.E., 1969, Microbial Biogeochemistry, Academic Press, 345 pp.

123. Zirino, H. and Healy, M.L., 1970, Inorganic zinc complexes in seawater. Limnol. Oceanogr. 15: 956-958.

APPENDICES

I. CHEMICAL METHODS

Aqueous Samples

Interstititial water samples were apportioned for several analyses:

1. First 8 mls were collected in an electrode cell or a vial to measure pH and sulfide.
2. 3 mls of sample were drained into graduated test tubes containing reagents for complexing Fe(II).
3. The remainder was collected in acid-washed sample bottles to be apportioned as below:
   a. 1 ml for analyses of NH_4^+, NO_2^- - NO_3, soluble reactive phosphate (SRP), and soluble reactive silica (SRS).
   b. 1 ml for alkalinity titration.
   c. 1 ml for a chlorinity titration.
   d. The remainder was saved for later trace metal and major cation analyses.

NH_4^+, NO_2^--NO_3^-, SRP, SRS, carbonate alkalinity, pH and sulfide analyses were all performed within six hours of sample collection.

Sulfide and pH

These measurements were made on the interstitial water samples in a glove box under a nitrogen atmosphere since (1) oxygen affects the sulfide concentrations in the pore water, and (2) equilibration of dissolved CO_2 with CO_2 in the atmosphere affects the pH of the sample. Samples were drained from a squeezer directly into small vials. A Fisher miniature glass universal electrode, a calomel or silver/silver chloride double junction reference electrode and an Orion Ag+/AgS sulfide electrode were used for these measurements. All sulfide values were found to be below the detection limit of the electrode ($\sim 10^{-7}$M at pH 7) and are not recorded in this report.

pH was measured with a Fisher miniature microprobe micro combination electrode on a Fisher Accumet 420 pH/ion meter.

Chlorinity

Chlorinity was determined in one of two ways. The shipboard method is described in Standard Methods (1975). One milliliter of sample was placed in a vial and titrated with standard mercuric nitrate delivered via microburet. An acidified mixed indicator composed of diphenylcarbazone, xylene cyanol FF, and nitric acid gives a purple endpoint at a pH of about 2.5. For some labor-

atory work, chlorinity was determined on a Technicon Auto Analyzer II. Mercuric thiocyanate and ferric nitrate are mixed with the sample where chloride can displace the thiocyanate ion which then reacts with ferric ion to form a highly colored complex whose absorbance, read colorimetrically at 480 nm, is proportional to the original chloride concentration.

Alkalinity

Total carbonate alkalinity was determined as described in Standard Methods (1975). One milliliter of sample was placed in a vial and titrated with standard (0.02N) hydrochloric acid delivered via microburet to a mixed bromcresol green - methyl red endpoint (pH = 4.7.)

Ammonia

The method of Solorzano (1969) was used for the determination of ammonia. An appropriate aliquot of the pore water was diluted to five milliliters. To this were added sequentially ethanolic phenol, sodium nitroprusside and a mixture of alkaline sodium citrate and sodium hypochlorite. The amount of the blue indophenol formed was determined spectrophotometrically at 640 nm after one hour. Shipboard analyses for ammonia utilized the same reaction, however, the analysis was performed with the aid of a techncion Auto Analyzer II.

Nitrate-Nitrite

Nitrate plus nitrite nitrogen was determined with a Technicon Auto Analyzer II on a suitably diluted aliquot of the pore water sample. Nitrate is reduced to nitrite by a copper-cadmium reduction column. The nitrite ion then reacts with sulfanilamide under acidic conditions to form a diazo compound. This compound then couples with N-1 naphthylethylene-diamine dihydrochloride to form a reddish-purple azo dye whose color is read at 550 nm.

Soluble Reactive Phosphate (SRP).

SRP was determined with a Technicon Auto Analyzer II on a suitably diluted aliquot of the pore water sample. A single reagent solution, when added to the sample, forms a phosphomolybdenum complex which is reduced by ascorbic acid to a blue compound. The intensity of absorbance, measured colorimetrically at 880 nm, is proportional to the original phosphate concentration.

Soluble Reactive Silicate (SRS)

The procedure for SRS given by Strickland and Parsons (1969) was modified for small water volumes. The sample is reacted in a test tube with acidified ammonium molybdate for fifteen minutes. A combined reagent containing p-methylaminophenol sulfate reduces the silicomolybdate to a blue compound while oxalic acid removes phosphorus interference. The absorbance was read spectrophotometrically at 810 nm between three and six hours after reagent addition. A Technicon Auto-Analyzer II provided an alternate method of analysis. The chemistry involved is similar to the manual determination described above except that ascorbic acid is used as the reducing agent. Absorbance is read 660 nm.

Ferrous Iron

Fe(II) concentrations were determined using 1, 10-o-phenathroline as the colorimetric complexing reagent, as descrived by Sandell (1959). In a glove box under a nitrogen atmosphere, 3 mls of pore water sample were drained directly into graduate test tubes containing phenanthroline reagent buffered at pH 3.6 (Troup, 1974). After 30 minutes, the Fe(II) complex is stable with respect to oxygen and can be removed from the glove box and read spetrophotometrically at 510 nm.

Calcium, Magnesium, and Mananese

Calcium, magnesium and manganese were determined using a Perkin Elmer 360 atomic absorption spectrophotomater in an air-acetylene flame for pore water samples which had been acidified upon collection with Ultrex nitric acid to pH 1 and refrigerated in polyethylene bottles. All samples were diluted before being run (calcium and magnesium with 5% HCL - 0.2% LaO; manganese with deionized water).

Zinc, cadmium and lead

Zinc, cadmium and lead present in trace amounts in pore waters were determined by differential pulse anodic stripping voltammetry using a Princeton Applied Research Model 174 polarographic analyzer. Pore waters were squeezed directly into polyethylene bottles, acidified with Ultrex nitric acid to pH 1, and refrigerated until analyzed. Prior to analysis, an aliquot was pipetted into a beaker and acidified at the rate of one milliliter of Ultrex Nitric acid per ten milliliters of sample. The sample was covered by a watchglass and taken to dryness in an 80°C oven. The sample was reconstituted by adding ten millilters of 0.1N Ultrex nitric acid and 100µl of 10% hydroxylamine hydrochloride and warming at 80°C for fifteen minutes. Addition of 15 milliliters of 0.2N ammonium citrate buffer of pH 3.5 brought the sample pH to 3.1 ± 0.2.

An aliquot of the diluted sample was pipetted into a polarographic cell. Electrodes were inserted into the cell, and the cell was purged with oxygen -free nitrogen. Following purging, a fresh mercury droplet was dialed on the hanging mercury drop electrode. Metals were concentrated onto the mercury drop from the stirred solution for two minutes at -1.2 volts vs. S.C.E. Deposition was continued for an additional fifteen seconds with no stirring. A voltage ramp was then applied at a rate of five millivolts per second in a positive direction for approximately 1.4 volts. Superimposed on this ramp are voltage pulses. Low detection limits were achieved by measuring current flow differentially immediately before and immediately after pulse application. The resulting polarogram records differential current per change in voltage vs. voltage. As a result of increased current flow at the metals' characteristic oxidation potentials, a peak-shaped waveform results whose height is proportional to the amount of metal originally present. Zinc produced a peak at about -1 volt, cadmium, at -0.6 volts and lead near -0.4 volts. After the polarogram was run on the diluted sample, a known quantity of zinc, cadmium and lead was added to the cell, and the cell was nitrogen purged. The previous mercury drop was dislodged, a new one was dialed, and another polarogram was obtained with increased peak heights. Usually, three standard additions were made for a total of four polarograms. The original metal concentrations were determined from the change in peak height based on the known additions. Blanks comprised of diluent nitric acid, hydroxylamine and citrate buffer were run daily. The contamination measured was subtracted from the sample values.

Several tests were performed to evaluate the precision and accuracy of the entire procedure. The concentrations of 37 sample blanks over a period of several months yielded Zn = 1.27 ± .57 ppb; Cd = .03 ± .06 ppb; Pb = .59 ± .22 ppb. A similar study on a synthetic sample was conducted. A sample con-

sisting of (approximately) 30 ppb Zn, 3 ppb Cd, and 4 ppb Pb, was made. Twelve aliquots of this sample were withdrawn over a period of about 7 months and analyzed. The results were Zn = 24.64 ± 2.95 ppb; Cd = 3.93 ± 2.39 ppb; and Pb = 4.33 ± 2.80 ppb.

This test gives a realistic estimate of the accuracy and precision of the entire procedure. The precision is good, considering the concentration levels of these particular metals. It might be improved somewhat by using a higher purity nitric acid in the digesting procedure and even stricter controls against contamination (using a laminar flow hood, for example). The accuracy is difficult to evaluate. The difference between the measured concentrations and the 'true' concentrations in the sample could have resulted from 1) a small error in the 'true' concentrations magnified by successive dilutions involved in making the standards, 2) loss (or gain) of metal by adsorption (or desorption) on the sides of the volumetric and storage bottles during the sample preparation and storage, and/or 3) a statistically significant inaccuracy in the analytical procedure and method. Even so, the data are reliable enough to permit their interpretation and use in models of the system, because the errors associated with these models are often larger than the analytical errors.

Sediment Solids

Sediments that had previously been squeezed for pore waters and then frozen, were removed from their polyethylene bags, placed in polystyrene weighing boats, and dried under heat lamps at ~60°C. The station 83 core collected on 4/11/77 was carefully sectioned, weighed wet and weighed dried for water content determination. The dried sediment was ground in a Spex Mixer Mill for ten minutes using a hardened steel container and tungsten carbide balls. Glass vials were used for storage of the sediment until it was needed for analysis.

Carbon

Total carbon was determined with a LECO induction furnace connected to a hydroxide absorption pipette determinator. Ground sediment was oven-dried at 65°C and dessicated prior to weighing 0.05-0.15 grams into a LECO crucible. Iron and copper chip accelerations were added to the crucible and gently mixed with the sample. The prepared sample was combusted in a stream of oxygen at >1600°C. Liberated gases were collected in a gas burette. When combusion was complete, the gases were passed to a potassium hydroxide absorption pipette where they were allowed to react for one minute. The remaining gases were returned to the gas buret. Percent carbon was determined by noting the volume change after CO_2 adsorption.

Organic carbon was determined as total carbon remaining after acid pre-treatment. The sample containing crucible was placed under heat lamps at ~60°C. The sample was wetted with a few drops of deionized water and then 1 N HCl was added dropwise to drive off inorganic carbon. The crucible was swirled and acid was added as needed until fizzing stopped. Then, a few more drops of acid were added. The sample was left under the heat lamps overnight to dry. These samples were covered with aluminum foil and stored in air until run. Inorganic carbon was determined by difference between total carbon and organic carbon.

Sulfur

Total sulfur was determined with a LECO induction furnace connected to an automatic buret. Ground sediment was oven-dried at 65°C and dessicated prior to weighing 0.2 to 0.5 grams into a LECO cruicble. Copper chip accelerator was added to the crucible and gently mixed with the sample. The prepared sample was combusted in a stream of oxygen. Combustion gases were passed to the automatic buret where sulfur was determined idiometrically.

Acid volatile sulfur was determined idiometricially. Freshly collected sections of wet sediment (10 to 20 g wet weight) were placed in 300 ml erlenmeyer flasks and kept under N_2. So that the content of acid volatile sulfur could be expressed in moles/mass dry sediment, an aliquot of each section was analyzed for water content. The wet sediment sections were reacted with concentrated HCl (10 ml, slow addition) in the presence of $SnCl_2$ (0.1 g $SnCl_2$/ g wet sediment). The acid-sediment mixture gently stirred.

Evolved gases were passed to a trap containing a saturated zinc acetate solution where H_2S contained in the reaction gases was precipitated as ZnS. The reaction was allowed to proceed for 30 min. A flow of N_2 was maintained at all times. At the end of the reaction period, the zinc acetate trap was removed for analysis. The amount of ZnS precipitated was determined idiometrically.

Phosphorous

The perchloric acid digestion of Sommers and Nelson (1972) was used for the determination of total phosphorus. Aliquots of 0.1-0.3 ground dessicated sediments were placed 50-ml graduated Folin-Wu N.P.N tubes. Perchloric acid was added and the digestion was effected by heating the tubes for 75 minutes at 205°C in an aluminum heating block. The tubes were cooled, diluted, vortex mixed, and left to stand while the particles settled out. An aliquot of the supernatant liquid was withdrawn, neutralized with 5N NaOH to a p-nitrophenol endpoint, and partially diulted in a volumetric flask. The single solution reagent of Murphy and Riley (1962) was added and the contents of the flask were brought to volume. Absorbance of the phosphomolybdenum blue complex was read with a Beckman DU spectrophotometer at 880 nm after one hour.

Total Kjeldahl Nitrogen

A modified digestion procedure proposed by Nelson and Sommers (1972) based on the work of Bremner (1965) was employed for the determination of total Kjeldahl nitrogen. Ground sediments were oven-dried at 65°C and dessicated before weighing 0.05-0.25 grams into 50-ml graduated Folin-Wu N.P.N. tubes. The tubes were placed into an aluminum heating block and the sediment was digested at >350°C by a mixture of sulfuric acid and potassium sulfate. Copper sulfate and selenium acted as catalysts. Heating was continued for three hours after clearing. The samples were cooled and neutralized with 50% NaOH to a phenolphthalein endpoint. Sulfuric acid (5N) was then added dropwise to just clear the pink color. The tubes were diluted to volume, vortex mixed, and particulates allowed to settle. An aliquot was withdrawn and diluted to five ml. Nitrogen was determined as ammonia using the method of Solorzano (1969).

Metals

Approximately 0.1 g of dessicated ground sediment was weighed into the Teflon cup of a PARR 4745 acid digestion bomb. The hydrofluoric, nitric and perchloric acid digestion mixture used was that suggested by Agemian and Chau, (1975). The liquid resulting after heating the bomb at 140°C for 3.5 hours was mixed with boric acid and made to volume in a volumetric flask. Samples thus prepared were stored in polyethylene bottles until needed for analysis. Metals were determined on a Perkin Elmer model 360 atomic adsorption spectrophotometer.

Bacterial Abundance

Bacterial numbers were determined after the methods of Watson et. al (1977). Approximately one gram aliquots of wet sediment were placed in preweighed bottles containing 10 ml of 2% gluteraldehyde and shaken. A seperate determination of sediment water content was also made. The gluteraldehyde

treated samples may be stored or counted immediately. The sample was diluted by a factor of 1,000 to 10,000 (2,000 x was found to be the optimum dilution). A 10 ml aliquot of diluted sample was stained with acridine orange (three minute contact time). A 2ml aliquot of stained sample was drawn through a 0.2μm Nucleopore filter (previously stained with Irgalan black) using a maximum pressure differential of 0.5 atm. the filter was then placed on a microscope slide with a drop of immersion oil and covered with a coverslip. The slides were examined with a Leitz orthoplan microscope fitted with a Ploemopak 2.2 fluorescence vertical illuminator and 150 W high pressure xenon lamp. Fluorescing bacteria in twenty fields were counted and the data averaged. Bacterial abundance was reported as number of bacteria per gram dry weight of sediment.

II. FIELD CORE DATA

STATION: GASP XXX1-83
DATE: 4-1X-77

Sampling Interval (cm)	Water Content %	Total C %	Organic C %	Kjeldahl N µM/g	Total P µM/g	Total S µM/g	Acid Volatile S µM/g	Ca µM/g	Mg µM/g	Fe µM/g	Mn µM/g	Zn µM/g	Cd µM/g	Pb µM/g	Cu µM/g
0-1	86.0	3.58	3.83	326	30.1	47.32	14.88	228	612	650	9.80	5.13			1.10
1-2	77.8	2.42	2.27	220	22.6		9.62	300	708	580	6.01	1.56			0.43
2-3	75.1	1.68	1.74	182	21.2	29.42	10.11	150	602	580	7.00	2.68			0.54
3-4	71.1	1.14	1.52	155	22.8		10.49	687	1011	550	8.36	1.78			0.42
4-5	67.0	1.47	1.41	127	23.0	22.60	5.65	166	560	640	6.23	2.20			0.37
5-6	65.8	1.50	1.18	130	22.6		1.73	3.06	731	620	7.71	2.03			0.39
6-7	64.6	1.20	1.32	128	22.2	17.15	2.27	159	565	640	5.55	1.88			0.42
7-8		1.35	1.29	112	22.9		1.27	225	653	550	6.93	1.97			0.36
8-9	63.3			118	21.8	31.19	1.06	180	542	640	7.56	1.62			0.63
9-10	63.5	1.34	1.29	124	22.6		0.58	142	553	620	4.95	1.98			0.55
10-11	63.4			110	22.0	55.41	0.29	137	559	630	6.03	1.81			0.36
11-12	62.4	1.28	1.19	132	21.0		0.27	132	578	640	7.41	1.87			0.45
12-13	62.4			112	21.8		0.29	167	556	610	6.71	2.01			0.42
13-14	61.5	1.35	1.13	122	22.4		0.28	141	604	620	7.51	1.37			0.36
14-5	60.5			109	21.6		0.26	129	584	640	4.75	1.83			0.54
15-16	58.8	1.34	1.36	111	21.0	53.95	0.25	176	601	620	6.82	1.49			0.53
16-17	58.6			101	20.9		0.23	223	586	580	6.12	1.48			0.57
17-18	58.8	1.28	1.21	124	21.2		0.27	208	619	640	6.00	1.90			0.51
18-19	59.3			99	19.8	40.23	0.34	200	609	600	7.34	1.54			0.53
19-20	59.3	1.36	1.29	108	22.2		0.25	162	556	570	6.95	1.78			0.42
24-25	56.2	1.51	1.05	106	20.8	15.28	1.20	305	682	590	6.78	1.23			0.60
29-30	56.2	1.49	1.13	102	21.6	14.66	0.79	167	545	580	7.09	1.57			0.37
34-35	56.1	1.47	0.92	103	20.3		0.85	311	730	630	6.81	1.41			0.61
39-40	55.3	1.57	1.23	97	21.4	32.44	1.70	173	622	640	7.05	2.18			0.63
44-45	54.0	1.14	1.06	91	21.4	29.00	2.99	430	876	580	8.08	1.64			0.62
49-50	52.0	2.32	1.03	76	20.1	13.09	1.65	178	572	540	5.92	2.89			0.54
54-55	52.7	2.12	0.86	88	19.4		0.38	575	940	580	7.20	1.54			0.54
59-60	52.1	1.91	1.12	91	18.6	8.42	1.57	747	900	550	7.34	1.46			0.46
64-65	53.7	1.98	0.80	72	20.6	16.21	0.62	599	780	620	6.92	1.86			0.54
69-70	44.8														

Table 2. Field Core Data.

STATION: GASP XXX1-83
DATE: 17-V1-78

Sampling Interval (cm)	Water Content %	Total C %	Organic C %	Kjeldahl N µM/g	Total P µM/g	Total S µM/g	Acid Volatile S µM/g	Ca µM/g	Mg µM/g	Fe µM/g	Mn µM/g	Zn µM/g	Cd µM/g	Pb µM/g	Cu µM/g
0-2		3.14	2.11	1.70	26.6			513	725	510	6.87	2.61			0.69
2-3		2.19	1.32	1.04	21.7			494	670	480	6.59	1.71			0.54
3-5		1.80	1.00	0.80	10.0			531	672	500	4.39	1.28			0.43
5-6.5		1.68	0.84	0.59	18.4			548	649	450	5.14	0.85			0.12
6.5-8.5		1.82	0.76	0.55	19.8			658	744	470	5.10	1.24			0.26
8.5-11.5		1.89	1.09	0.50	20.2			697	822	470	7.04	1.07			0.26
11.5-16		2.32	0.75	0.46	19.2			763	900	460	6.79	0.83			0.10
16-21		2.44	0.81	0.46	18.7			1002	1003	460	7.14	1.22			0.25
21-25		2.64	0.94	0.41	18.9			1218	1031	430	7.30	1.10			0.00
25-29.5		2.78	0.79	0.48	18.0			1364	921	450	7.27	0.98			0.13

STATION A-1
DATE: 6-1X-79

0-2															
2-4		4.21	3.68	3.71	42.2			367	594	810	9.73	8.21			0.84
4-6		4.42	3.89	4.17	46.0			245	582	600	7.48	7.30			0.78
6-8		4.65	3.79	4.50	36.0			185	595	640	7.76	5.15			0.92
8-10		3.68	3.48	3.16	40.6			236	589	650	9.47	6.85			1.04
10-13		4.00	3.43	3.38	36.2			294	607	670	10.5	6.30			0.96
17-21		3.56	3.17	2.94	38.7			247	619	660	7.82	5.62			1.01
29.33		3.03	2.71	2.28	30.8			178	632	640	9.15	4.49			1.01
37-41		1.39	1.41	1.39	23.7			127	599	610	9.14	2.16			0.56
45-49		1.43	1.11	1.36	22.2			143	591	660	8.58	1.95			0.52

Table 2. Field Core Data (cont'd).

STATION: GASP XXXI-83
DATE: 31-V-78

Sample No.	I.W. Depth (cm)	pH	Carb. Alk. meq/l	Cl^- meq/l	Fe(II) µg-at/l	SRP µg-at/l	NO_2-NO_3 µg-at/l	NH_4^+ µg-at/l	SiO_2 µg-at/l	Zn ng-at/l	Cd ng-at/l	Pb ng-at/l	Cu ng-at/l	Mn µg-at/l	Ca µg-at/l	Mg µg-at/l	Na µg-at/l	K µg-at/l
0	(.W		1.87	.544		0.1	67	13		629	16	14	78		900	518		
1	0-2	8.05	1.64	.585	18.0	54	47	59	243	1874	22	20	253		1050	367		
2	2-3.5	7.61	2.13	.605	50.6	12	43	90	462	272	4	6	161		1300	377		
3	3.5-5.5	7.68	2.30	.599	28.2	17	47	104	525	414	0	16	92		1250	467		
4	5.5-7	7.68	2.68	.597	60.9	22	62	124	545	292	-4	8	47		-	356		
5	7-9.5	7.89	2.80	.603	55.9	25	28	102	603	1536	-1	72	72		-	-		
6	9.5-12	8.01	2.85	.605	61.5	20	92	179	603	186	-5	4	17		1400	509		
7	12-17	7.95	3.01	.612	52.7	17	21	97	507	143	-10	6	-4		1150	567		
8	17-21	7.82	3.08	.625	49.9	25	100	246	482	11835	4	125	270		1800	464		
9	21-26	7.87	3.11	.630	48.5	26	107	185	518	507	-4	74	57		1200	493		
10	32-36.5	7.97	3.08	.632	33.6	10	85	151	462	230	56	5	42		1150	-		

STATION: GASP XXXII-83
DATE: 17-VI-78

0	O.W.		1.74	.586		0.03	67	40	61.5	1957	2	103	37		950			
1	0-2	7.69	1.96	.650	0	1.9	21	114	257	548	13	6	60		1200			
2	2-3	7.74	1.99	.679	0.7	1.9	54	57	287	927	232	25	107		-			
3	3-5	-	2.29	.614	18.8	4.3	10	132	658	365	19	17	113		-			
4	5-6.5	7.80	2.47	.530	48.5	14	68	123	695	631	25	39	115		-			
5	6.5-8.5	7.72	2.54	.645	32.8	30	50	125	710	386	26	12	16		-			
6	8.5-11.5	7.84	2.73	.601	87.1	16	97	154	712	164	2	38	45		-			
7	11.5-16	7.86	3.00	.628	43.4	12	64	127	582	325	9	7	-25		1100			
8	16-21	7.94	3.00	.614	32.0	13	50	107	545	825	3	3	24		1250			
9	21-25	7.97	3.07	.650	32.6	15	54	111	535	186	8	-11	71		1250			
10	25-29.5	8.01	3.05	.613	22.5	13	61	126	503	588	3	3	13		1100			

Table 2. Field Core Data (Cont'd)

STATION: GASP XXXIII-83
DATE: 21-VII-78

Sample No.	I.W. Depth (cm)	pH	Carb. Alk. meq/l	Cl^- meq/l	Fe(II) µg-at/l	SRP µg-at/l	NO_2-NO_3 µg-at/l	NH_4^+ µg-at/l	SiO_2 µg-at/l	Zn ng-at/l	Cd ng-at/l	Pb ng-at/l	Cu ng-at/l	Mn µg-at/l	Ca µg-at/l	Mg µg-at/l	Na µg-at/l	K µg-at/l
0	O.W.		1.87			0.18	52	9.1	27.5	285	16	7	106	0.2	900	206	489	14.7
1	0-4		2.33		1.2	3.6	290	173	412	815	11	22	74	43.0	1150	254	614	57.2
2	4-7		2.20		37.6	21.7	13	135	688	373	11	8	-28					
3	7-10		2.42		42.5	28.1	191	252	728	801	21	24	13					
4	10-12		2.56		36.7	31.9	9	186	680	996	55	19	93					
5	12-14		2.51		24.5	29.9	161	146	610	1158	20	35	349					
6	14-16		2.62		24.1	13.7	2	145	578	749	10	19	36					
7	16-19		2.78		46.8	19.7	151	187	615	466	10	28	-7	33.1	1150	302	508	34.9
8	19-23		2.93		33.8	15.7	0	125	592	461	3	3	-39	28.2	1050	262	498	30.5
9	23-26		2.76		7.0	8.9	151	138	588	326	3	3	-54	25.9	1050	260	469	19.2
10	26-30		2.91		29.9	16.1	0	142	565	293	4	5	-44	25.7	1050	266	470	23.7

STATION: GASP XXXIV-83
DATE: 16-VIII-78

0	O.W		1.82	.485		0.85	30.7	5.3	31.8	197	2	5	11	3.1	950	228	480	46.7
1	0-2	7.24	1.68	.655	12.4	6.5	18.8	74	270	678	22	36	40	21.4	1000	235	503	49.0
2	2-5	7.24	1.73	.611	41.6	21.9	0	61	490	767	18	3	-7	21.7	1100	226	541	51.3
3	5-7	7.30	2.10	.580	43.4	7.0	47.8	109	393	692	17	8	10	22.3	1050	214	540	55.1
4	7-9	7.25	2.28	.598	-	12.9	0	71	569	592	10	5	2	25.8	1000	223	608	55.8
5	9-11	7.25	2.32	.593	41.4	9.9	0	110	604	566	15	10	9	25.5	1000	219	560	55.8
6	11-13	7.29	2.44	.581	58.1	11.8	2.6	130	613	748	15	12	-32	25.1	1000	216	511	55.8
7	19-25	7.28	2.66	.859	58.4	18.0	141.4	191	718	33344	15	52	122	43.2	1500	349	501	75.2
8	32.5-38	7.39	3.01	.593	25.0	9.8	0	121	661	562	10	11	22	31.9	1100	293	491	59.6
9	41.5-47	7.48	3.06	.575	10.7	6.0	0	94	639	70	0	4	20	29.3	1050	304	511	41.5
10	47-52	7.56	2.97	.657	30.2	11.8	25.2	166	600	1020	8	5	13		-			

Table 2. Field Core Data. (cont'd)

STATION: GASP XL1-A1
DATE: 6-IX-79

Sample No.	I.W. Depth (cm)	pH	Carb. Alk. meq/l	Cl^- meq/l	Fe(II) µg-at/l	SRP µg-at/l	NO_2-NO_3 µg-at/l	NH_4^+ µg-at/l	SiO_2 µg-at/l	Zn ng-at/l	Cd ng-at/l	Pb ng-at/l	Cu ng-at/l	Mn µg-at/l	Ca µg-at/l	Mg µg-at/l	Na µg-at/l	K µg-at/l
0	O.W.		1.95	.796		.36		5.4	52.4									
1	0-2				127	8.1		145	291									
2	2-4		2.31	.632	156	31.6		145	333									
3	4-6		2.76	.581	197	47.8		207	466									
4	6-8		2.92	.556	226	59.4		145	541									
5	8-10		2.49	.594	189	41.6		187	707									
6	10-13		2.92	.606	190	44.4		232	749									
7	17-21		3.01	.568	195	39.2		235	841									
8	29-33		3.28	.606	228	44.1		250	915									
9	37-41		3.67	.606	164	30.8		281	874									
10	45-49		3.44	.581	124	29.7		276	832									

Table 2. Field Core Data (cont'd).

STATION: GASP-XL1-A1
Peeper
DATE: 6-IX-79

Sample No.	I.W. Depth (cm)	pH	Carb. Alk. meq/l	Cl^- meq/l	Fe(II) µg-at/l	SRP µg-at/l	NO_2-NO_3 µg-at/l	NH_4^+ µg-at/l	SiO_2 µg-at/l	Zn ng-at/l	Cd ng-at/l	Pb ng-at/l	Cu ng-at/l	Mn µg-at/l	Ca µg-at/l	Mg µg-at/l	Na µg-at/l	K µg-at/l
1	-10		2.08	606		1.9		55	91.5									
2	-5		2.60	581		30.5		79	358									
3	-2		2.90	556		30.7		91	566									
4	0		2.94	556	58.7	49.2		110	599									
5	1		3.01	530	48.0	29.2		119	599									
6	2		2.98	543	52.8	44.2		118	599									
7	3		2.99		38.3	42.8		115	599									
8	4		2.88	467		40.4		122	599									
9	5				52.1													
10	6				54.0													
11	7		2.90	518	52.0	37.5		130	583									
12	8				55.9													
13	9				63.1													
14	10		2.94	505		37.8		157	649									
15	12				62.2													
18	18		3.08	556		33.4		289	674									
19	20				58.5													
22	32		3.19	518	58.7	24.9		118	658									
24	40				75.7													
25	50		3.51	505	101	36.8		250	583									
26	60		3.58	480		33.9		221	574									
27	70		3.58		82.7	35.5		146	558									
28	80		3.24	430		30.7		198	458									
29	90		3.67		89.2	52.9		206	541									

Table 2. Field Core Data (cont'd).

III. PRODUCTION EXPERIMENT DATA

JARS t = 2 days
DATE: 20-IX-78

Sample No.	I.W. Depth (cm)	pH	Carb. Alk. meq/l	Cl^- meq/l	Fe(II) µg-at/l	SRP µg-at/l	NO_2-NO_3 µg-at/l	NH_4^+ µg-at/l	SiO_2 µg-at/l	Zn ng-at/l	Cd ng-at/l	Pb ng-at/l	Cu ng-at/l	Mn µg-at/l	Ca µg-at/l	Mg µg-at/l	Na µg-at/l	K µg-at/l
1	0-2		3.84	0.566	179.8	120.4		39.0	980	107	10	6	-113	69	1400	529		
2	2-4		3.22	0.567	85.0	≈120		0	1025	174	19	8	-2	41	1300	461		
3	4-6		2.74	0.574	19.2	15.5		0	846	312	13	-1	15	25	1050	446		
4	6-10		2.89	0.583	34.4	5.1		0	655	751	11	8	17	24	1100	431		
5	10-14		2.36	0.599	39.4	7.7		0	733	188	5	-3	-42	20	900	348		
6	14-18		2.16	0.610	40.8	15.5		117.0	733	158	1	6	0	21	800	328		
7	35-39		2.47	0.630	-1.6	1.7		0	756	423	17	9	47	19	850	407		

Table 3. Jar Experiment Data.

JARS t = 22 days
Low Temp.
DATE: 10-X-78

Sample No.	I.W. Depth (cm)	pH	Carb. Alk. meq/l	Cl^- meq/l	Fe(II) µg-at/l	SRP µg-at/l	NO_2-NO_3 µg-at/l	NH_4^+ µg-at/l	SiO_2 µg-at/l	Zn ng-at/l	Cd ng-at/l	Pb ng-at/l	Cu ng-at/l	Mn µg-at/l	Ca µg-at/l	Mg µg-at/l	Na µg-at/l	K µg-at/l
1	0-2		4.89	0.555	154.1	46.5		204	163	211	7	1	-74	71	1700	608		
2	2-4		4.55	0.560	137.2	138.9		154	637	54	10	3	-15	56	1600	609		
3	4-6		3.75	0.557	54.3	12.0		213	452	316	9	9	44	39	1500	593		
4	6-10		5.20	0.599	131.6	38.5		196	494	199	4	3	-23	47	1650	656		
5	10-14		3.98	0.657	114.1	29.8		217	502	177	4	-2	-7	37	1400	546		
6	14-18		2.60	0.644	61.5	21.3		131	534	231	-1	0	-24	26	950	352		
7	35-39		2.57	0.746	38.0	11.5		171	540	1170	0	7	-2	30	1000	502		

JARS t = 24 days
Medium Temp.
DATE: 12-X-78

1	0-2		3.14	0.348	265.5	35.9		307	810	46	5	4	-46	79	1900	701		
2	2-4		5.19	0.363	190.0	55.1		352	759	-3	2	0	-27	59	1850	719		
3	4-6		4.54	0.412	102.0	66.8		248	680	10	2	0	-37	47	1750	679		
4	6-10		3.82	0.384	86.3	26.0		243	582	18	2	3	-22	36	1600	596		
5	10-14		3.40	0.427	85.3	24.9		142	584	46	2	1	-19	30	1250	487		
6	14-18		2.88	0.420	64.6	23.7		167	647	47	1	3	-11	28	950	382		
7	35-39		2.92	0.448	28.6	15.3		444	584	26	3	3	7	26	950	454		

JARS t = 23 days
High Temp.
DATE: 11-X-78

Sample No.	I.W. Depth (cm)	pH	Carb. Alk. meq/l	Cl^- meq/l	Fe(II) µg-at/l	SRP µg-at/l	NO_2-NO_3* µg-at.l	NH_4^+ µg-at/l	SiO_2 µg-at/l	Zn ng-at/l	Cd ng-at/l	Pb ng-at/l	Cu ng-at/l	Mn µg-at/l	Ca µg-at/l	Mg µg-at/l	Na µg-at/l	K µg-at/l
1	0-2		6.60	0.345	360.1	54.1		506	894	105	2	4	-127	99	2250	838		
2	2-4		6.16	0.368	217.8	54.9		378	835	72	3	0	-87	66	2050	782		
3	4-6		5.48	0.384	165.9	69.9		249	825	150	2	9	-26	57	2100	857		
4	6-10		4.25	0.376	87.0	25.1		250	601	70	3	5	4	43	1700	707		
5	10-14		3.82	0.507	77.6	28.9		323	553	93	3	15	-11	34	1350	545		
6	14-18		2.97	0.453	54.3	23.4		192	639	95	4	12	9	26	1000	396		
7	35-39		2.83	0.484	3.1	8.5		212	528	167	4	19	15	23	950	448		

Table 3. Jar Experiment Data (cont'd)

JARS t = 71 days
Low Temp.
DATE: 28-XI-78

Sample No.	I.W. Depth (cm)	pH	Carb. Alk. meq/l	Cl^- meq/l	Fe(II) µg-at/l	SRP µg-at/l	NO_2-NO_3* µg-at/l	NH_4^+ µg-at/l	SiO_2 µg-at/l	Zn ng-at/l	Cd ng-at/l	Pb ng-at/l	Cu ng-at/l	Mn µg-at/l	Ca µg-at/l	Mg µg-at/l	Na µg-at/l	K µg-at/l
1	0-2		6.03	0.509	377.1	37.4	14.4	424	698	66	5	5	-18	98	2250	872		
2	2-4		5.67	0.548	235.9	39.7	13.0	461	678	3	5	4	5	63	2100	809		
3	4-6		5.12	0.576	153.2	88.9	21.2	347	570	15	6	6	-5	49	1850	781		
4	6-10		4.13	0.576	122.0	21.8	17.5	273	451	174	5	3	12	33	1750	742		
5	10-14		3.73	0.597	97.7	26.2	20.8	243	480	172	12	5	33	30	1400	572		
6	14-18		2.88	0.624	85.2	19.3	-	228	524	304	14	4	28	26	1150	497		
7	35-39		3.08	0.613	60.7	22.4	55.2	243	525	304	4	10	48	24	1200	582		

JARS t = 73 days
Medium Temp.
DATE: 30-XI-78

*

1	0-2		5.73	0.566	431.9	25.1	9.77	579	868	266	6	3	-37	91	2250	863		
2	2-4		5.54	0.588	243.8	32.9	13.2	458	828	-65	6	-1	-110	69	2200	889		
3	4-6		5.25	0.632	140.3	75.5	6.8	349	740	31	8	-2	-25	54	2150	924		
4	6-10		5.00	0.828	182.6	47.5	6.1	328	634	40	3	-4	-56	46	2000	840		
5	10-14		3.40	0.721	87.4	21.9	9.7	257	541	148	10	-1	-36	24	1350	603		
6	14-18		3.02	0.666	70.4	18.6	8.3	227	647	146	7	0	-28	24	1150	537		
7	35-39		3.53	0.718	62.2	19.3	11.9	233	596	104	7	0	-47	29	1250	682		

JARS t = 72 days
High Temp.
DATE: 29-XI-78

*

1	0-2		8.22	0.607	631.6	56.2	22.6	1092	1087	138	46	-1	-72	137	2900	1143		
2	2-4		7.78	0.618	404.0	55.4	14.6	953	1072	86	69	8	-14	96	2850	1185		
3	4-6		7.22	0.638	315.8	76.4	20.5	579	1028	187	24	-4	-34	88	2800	1123		
4	6-10		6.09	0.639	206.3	77.7	35.2	335	894	170	40	0	20	57	2500	996		
5	10-14		5.67	0.622	42.9	43.8	22.6	450	749	143	31	-8	-15	50	2100	967		
6	14-18		3.95	0.666	109.7	24.5	19.9	334	804	237	51	-1	2	34	1500	685		
7	35-39		3.67	0.637	19.7	3.7	35.7	413	659	133	133	-9	-53	27	1300	720		

*Frozen and run 1 month later.

Table 3. Jar Experiment Data (cont'd).

JARS t = 143 days
Low Temp.
DATE: 8-II-79

Sample No.	I.W. Depth (cm)	pH	Carb. Alk. meq/l	Cl^- meq/l	Fe(II) µg-at/l	SRP µg-at/l	NO_2-NO_3 µg-at/l	NH_4^+ µg-at/l	SiO_2 µg-at/l	Zn ng-at/l	Cd ng-at/l	Pb ng-at/l	Cu ng-at/l	Mn µg-at/l	Ca µg-at/l	Mg µg-at/l	Na µg-at/l	K µg-at/l
1	0-2	7.35	7.31	0.720	364.5	31.8	9.9	429	847	60	-5	-2	-68	91	2350	917		
2	2-4	7.33	8.90	0.888	340.4	23.6	13.2	722	784	121	4	1	16	76	2500	1057		
3	4-6	7.42	7.35	0.790	156.6	59.5	12.9	563	647	254	-6	-4	-88	57	2300	997		
4	6-10	7.40	6.46	0.684	156.8	46.4	14.3	297	549	130	1	5	25	45	2050	872		
5	10-14	7.42	5.06	0.690	82.5	20.5	20.0	285	578	112	-2	1	11	32	1600	686		
6	14-18	7.39	3.99	0.684	68.1	14.7	21.4	238	573	259	-4	10	51	26	1350	630		
7	35-39	7.46	4.25	0.672	48.4	15.2	26.5	260	532	201	6	-3	5	22	1350	627		

JARS t = 142 days
Medium Temp.
DATE. 7-II-79

1	0-2	7.25	9.90	0.716	543.2	42.7	6.5	1011	916	50	6	7	-116	123	2750	1100		
2	2-4	7.34	8.87	0.629	379.3	47.7	9.6	725	875	98	7	6	-88	93	2500	1094		
3	4-6	7.39	6.94	0.673	452.7	68.8	7.0	175	804	80	1	1	-50	64	2250	935		
4	6-10	7.43	6.90	0.662	394.0	33.2	19.0	298	735	127	4	3	-15	61	2300	911		
5	10-14	7.24	6.45	0.646	398.5	34.0	12.4	310	896	322	7	9	29	57	2050	858		
6	14-18	7.26	5.12	0.716	281.0	23.1	24.0	306	714	77	-2	-5	-59	42	1600	674		
7	35-39	7.51	5.49	0.678	161.4	23.8	24.0	488	553	-22	0	-4	-40	45	1600	804		

JARS t = 143 days
High Temp.
DATE: 8-II-79

1	0-2	6.98	14.18	0.733	832.3	74.3	12.4	2483	1289	0	6	-2	-71	172	3750	1351		
2	2-4	7.06	11.56	0.672	553.8	73.3	15.6	1139	1667	-76	6	0	-57	117	3300	1292		
3	4-6	7.15	10.65	0.695	351.7	72.3	17.1	740	1157	-45	8	3	-51	95	3100	1258		
4	6-10	7.16	9.95	0.697	350.0	88.2	18.6	419	1215	73	6	-3	-72	87	3050	1244		
5	10-14	7.10	7.66	0.700	269.4	39.0	19.4	349	1376	108	6	3	-40	61	2400	971		
6	14-18	7.47	5.13	0.710	31.38	14.5	31.9	389	916	245	14	4	97	45	1700	760		
7	35-39	7.50	5.72	0.697	73.47	19.4	20.6	416	927	33	-6	1	29	45	1700	841		

Table 3. Jar Experiment Data (cont'd).

JARS t = 197 days
Low Temp.
DATE: 3-IV-79

Sample No.	I.W. Depth (cm)	pH	Carb. Alk. meq/l	Cl^- meq/l	Fe(II) µg-at/l	SRP µg-at/l	NO_2-NO_3 µg-at/l	NH_4^+ µg-at/l	SiO_2 µg-at/l	Zn ng-at/l	Cd ng-at/l	Pb ng-at/l	Cu ng-at/l	Mn µg-at/l	Ca µg-at/l	Mg µg-at/l	Na µg-at/l	K µg-at/l
1	0-2	7.30	8.26	0.714	488.3	41.3	13.5	772	832	-80	-5	3	-32	111	2350	917		
2	2-4	7.38	8.60	0.711	390.5	32.8	13.8	864	822	96	4	5	5	85	2550	1059		
3	4-6	7.54	7.87	0.678	239.9	46.9	16.0	565	649	246	1	3	-20	70	2450	956		
4	6-10	7.54	5.85	0.629	129.4	30.9	16.5	304	497	268	0	-1	-8	55	2100	875		
5	10-14	7.51	5.55	0.685	148.1	31.9	29.5	269	564	240	7	6	69	34	1850	710		
6	14-18	7.45	4.67	0.733	123.3	24.9	24.5	335	537	176	14	0	6	42	1500	590		
7	35-39	7.58	5.01	0.665	98.7	21.1	23.1	307	490	155	6	0	-35	46	1600	688		

JARS t = 198 days
Medium Temp.
DATE: 4-IV-79

1	0-2	7.13	11.01	0.708	740.4	45.9	40.4	1510	785	222	5	5	-47	142	3000	1156		
2	2-4	7.30	9.36	0.675	429.3	44.3	39.2	1060	793	-10	13	5	-49	96	2750	1040		
3	4-6	7.29	8.75	0.678	294.3	59.3	40.0	692	766	161	9	5	34	83	2800	1064		
4	6-10	7.32	7.58	0.650	290.0	74.7	39.7	360	694	13	2	-1	73	71	2600	1053		
5	10-14	7.36	8.31	0.667	184.9	32.2	56.9	321	650	154	3	16	106	44	1900	737		
6	14-18	7.24	3.58	0.672	170.2	21.1	57.1	378	723	300	5	3	189	45	1700	666		
7	35-39	7.38	5.54	0.656	99.5	28.1	44.1	443	629	255	3	5	355	39	1650	727		

JARS t = 197 days
High Temp.
DATE: 3-IV-79

1	0-2	6.92	14.06	0.823	683.3	70.8	7.9	2540	1198	145	5	3	-29	169	3650	1385		
2	2-4	7.09	13.12	0.815	849.9	73.5	22.5	1630	1185	214	6	7	-16	137	3950	1468		
3	4-6	7.30	11.01	0.703	453.6	77.6	20.6	952	1160	276	7	16	23	103	3650	1322		
4	6-10	7.29	8.77	0.677	316.2	83.6	21.6	397	1020	43	3	2	-90	78	2900	1133		
5	10-14	7.04	9.08	0.685	384.2	29.3	15.9	441	914	152	5	10	-101	83	2950	1127		
6	14-18	7.28	6.09	0.707	183.0	23.7	19.6	377	932	199	5	12	44	60	2050	773		
7	35-39	7.41	6.19	0.707	94.0	19.0	36.8	421	872	175	6	14	1	44	1850	831		

Table 3. Jar Experiment Data (cont'd).

IV. FLUX EXPERIMENT DATA

CORE R
FLUX EXPERIMENT
DATE: 20-XII-78

Sampling Interval (cm)	Water Content %	Total C %	Organic C %	Kjeldahl N µM/g	Total P µM/g	Total S µM/g	Acid Volatile S µM/g	Ca µM/g	Mg µM/g	Fe µM/g	Mn µM/g	Zn µM/g	Cd µM/g	Pb µM/g	Cu µM/g
0-1	59.9	2.17	1.12	0.92	22.8			476	657	480	6.75	1.29			0.17
1-2	58.3	2.16	1.14	0.93	22.2			495	676	510	5.42	1.83			0.41
2-3	56.0	2.30	1.11	1.01	21.9			511	682	480	5.95	1.47			0.60
3-4	56.3	2.08	1.37	1.02	21.2			399	687	460	5.78	1.47			0.31
4-5	55.5	2.05	0.99	0.94	21.1			472	669	460	5.34	1.42			0.31
5-6	54.6	2.11	1.31	1.00	21.7			455	672	520	5.05	1.36			0.39
8-10															
14-18	52.7	2.12	1.41	1.02	22.8			433	647	490	5.46	1.67			0.48
22-26	51.8	1.87	1.36	0.95	23.1			506	683	510	5.43	1.36			0.19

CORE 6
FLUX EXPERIMENT
DATE: 23-VII-79

0-1		3.53	2.70	2.49	31.0			956	716	600	16.1	3.41			0.52
1-2		3.41	2.47	2.29	28.6			692	704	530	9.27	3.02			0.52
2-3		3.25	2.35	2.01	27.8			1027	735	550	6.62	2.90			0.71
3-4		2.64	1.84	1.45	25.6			939	775	470	4.77	2.48			0.51
4-5		2.69	1.81	1.25	23.0			570	684	470	5.46	2.40			0.39
5-6		2.70	2.06	1.62	25.7			753	727	480	7.01	2.80			0.68
6-8		2.35	1.64	1.22	24.4			477	708	500	6.03	2.72			0.93
8-10		2.18	1.58	0.96	22.9			427	647	520	5.44	1.59			0.34
14-18		1.59	1.02	0.66	21.0			496	660	510	5.16	0.88			0.12
22-26		1.51	0.82	0.61	20.1			514	631	480	5.25	1.29			0.13

Table 4. Flux Experiment Data.

CORE T
FLUX EXPERIMENT
DATE: 27-111-79

Sampling Interval (cm)	Water Content %	Total C %	Organic C %	Kjeldahl N µM/g	Total P µM/g	Total S µM/g	Acid Volatile S µM/g	Ca µM/g	Mg µM/g	Fe µM/g	Mn µM/g	Zn µM/g	Cd µM/g	Pb µM/g	Cu µM/g
0-1	59.8	1.84	0.88	1.07	20.7			511	681	470	6.71	1.30			0.20
1-2	57.5	2.05	1.09	1.10	18.2			510	660	480	6.23	1.52			0.36
2-3	56.8	1.94	1.15	1.08	19.8			480	668	500	6.26	1.71			0.25
3-4	56.2	1.99	1.11	1.04	21.7			462	667	480	6.96	1.50			0.03
4-5	55.6	2.01	1.20	1.04	20.84			462	666	480	5.28	1.37			0.37
5-6	54.4	1.78	1.17	1.06	18.8			461	670	500	5.91	1.30			0.37
6-8	54.4	1.88	0.95	1.04	20.5			498	676	480	5.88	1.36			0.53
8-10	53.2	2.02	1.25	1.04	21.3			500	647	490	5.67	1.23			0.34
14-18	52.1	1.83	1.20	1.03	19.6			487	658	460	5.00	1.20			0.12
22-26	51.3	1.85	1.12	0.95	21.8			510	659	510	6.04	1.53			0.31

Table 4. Flux Experiment Data (cont'd)

Core: HMC-G (Worms present)
Days after preparation: 71

Sample Number	I.W. Depth (cm)	pH	Carb Alk. Meq/l	Cl^- Meq/l	Fe(II) µg-at/l	SRP µg-at/l	NH_4^+ µg-at/l	SiO_2 µg-at/l	Mn^{+2} µg-at/l	Ca^{+2} µg-at/l	Porosity %
0	0.W.		0.61	.102	3.5	0.1	3	137	0	200	
1	0-1		1.95	.202	40.5	81.6	182	513	27	800	
2	1-2		2.27	.236	74.1	114.8	194	627	31	850	
3	2-3		2.58	.276	78.4	71.2	168	730	33	900	
4	3-4		2.81	.316	96.0	61.5	209	820	38	1200	
5	4-5		3.02	.376	82.0	64.0	214	886	35	1050	
6	5-6		3.28	.395	99.3	63.6	202	924	39	1250	
7	6-8		3.53	.447	96.7	69.8	174	951	44	1350	
8	8-10		5.77	.511		60.0	167	957	48	1500	
9	10-14		2.10	.570	98.1	62.0	236	976	48	1600	
10	14-18		4.11	.651	130.3	59.0	259	959	48	1750	

Core: HMC-R (no worms)
Days after preparation: 72

0	0.W.		0.63	.097	0	0.4	0	105	1	200	
1	0-1		2.25	.419	64.3	9.0	293	717	28	1100	
2	1-2		2.67	.376	96.1	39.1	239	741	33	1100	
3	2-3		3.00	.462	83.3	51.7	265	778	38	1400	
4	3-4		3.21	.477	79.8	54.3	274	943	37	1300	
5	4-5		3.30	.550	88.1	70.0	294	968	39	1350	
6	5-6		3.40	.595	77.3	70.6	302	989	40	1400	
7	6-8		3.59	.581	122.4	70.0	293	1010	42	1450	
8	8-10				113.2	74.5		1029			
9	10-14		3.91	.823	122.3	81.3	300	1111	44	1650	
10	14-18		4.01	.693	133.2	73.2	308	1220	46	1550	

Table 4. Flux Experiment Data (cont'd)

Core: HMC-A (worms present)
Days after preparation: 100

Sample Number	I.W. Depth (cm)	pH	Carb Alk. Meq/l	Cl^- Meq/l	Fe(II) µg-at/l	SRP µg-at/l	NH_4^+ µg-at/l	SiO_2 µg-at/l	Mn^{+2} µg-at/l	Ca^{+2} µg-at/l	Porosity %
0	O.W		1.33		0	3.0	34	116			
1	0-1		2.81		99.1	57.4	224	603			
2	1-2		3.15		137.7	63.4	213	740			
3	2-3		3.42		132.5	71.2	187	824			
4	3-4		3.68		145.3	73.2	207	904			
5	4-5		4.00		155.9	82.9	199	933			
6	5-6		4.14		149.3	65.0	203	963			
7	6-8		4.18		157.4	65.9	200	991			
8	8-10		4.32		169.3	65.8	199	1004			
9	14-18		4.43		156.5	60.0	194	952			
10	22-26		4.68		191.0	70.5	217	984			

Core: HMC-N (no worms)
Days after preparation: 99

0	O.W.	7.14	0.58	.144	8.8	6.2	8.4	114			
1	0-1	7.23	2.49	.400	115.3	90.2	94.5	791			
2	1-2	7.37	2.79	.499	98.1	93.9	109.5	817			
3	2-3	7.36	3.06	.434	100.7	87.2	122.1	877			
4	3-4	7.34	3.21	.468	125.4	81.1	127.5	906			
5	4-5	7.40	3.37	.480	119.0	79.8	136.5	915			
6	5-6	7.31	3.46	.525	112.5	73.4	141.3	954			
7	6-8	7.25	3.46	.539	143.9	75.6	155.7	950			
8	8-10	7.26	3.75	.590	138.7	76.3	164.1	970			
9	14-18	7.52	3.96	.722	166.4	71.3	188.1	968			
10	22-26	7.40	4.00	.784	155.1	69.7	183.9	959			

Table 4. Flux Experiment Data (cont'd)

Core: HMC-S (no worms)
Days after preparation: 113

Sample Number	I.W. Depth (cm)	pH	Carb. Alk. Meq/l	Cl^- Meq/l	Fe(II) µg-at/l	SRP µg-at/l	NH_4^+ µg-at/l	SiO_2 µg-at/l	Mn^{+2} µg-at/l
0	O.W.	7.20	0.72	.070	2.9	1.1	7	198	
1	0-1	7.36	1.42	.179	19.3	9.0	52	1515	
2	1-2	7.10	1.67	.373	35.8	13.3	59	466	
3	2-3	7.13	2.07	.418	91.0	28.8	84	601	
4	3-4	7.15	2.42	.440	83.6	32.2	99	742	
5	4-5	7.19	2.72	.493	126.7	49.4	116	817	
6	5-6	7.23	2.98	.508	133.2	55.6	133	875	
7	6-8	7.23	3.33	.552	140.1	60.4	138	934	
8	8-10			.552				986	
9	14-18	7.26	4.39	.764	189.4	62.5	190	966	
10	22-26	7.16	4.60	.874	180.2	51.5	194	984	

Core: HMC-B (no worms)
Days after preparation: 120

0	O.W	7.14	1.0		4.8	11.7	18	133	
1	0-1	7.14	2.26		76.3	97.8	104	1050	
2	1-2	7.27	2.78		78.7	109.0	117	881	
3	2-3	7.24	3.22		79.4	113.4	133	985	
4	3-4	7.28	3.54		71.7	106.3	144	1029	
5	4-5	7.53	3.44		83.2	54.4	150	501	
6	4-6	7.30	3.93		106.9	105.7	163	1051	
7	6-8	7.22	4.20		108.3	98.5	176	1046	
8	8-10	7.29	4.48		118.0	105.9	186	1072	
9	14-18	7.20	5.00		115.1	94.2	212	1466	
10	22-26	7.22	5.15		110.1	93.9	217	1064	

Table 4. Flux Experiment Data (cont'd)

Core: HMC-Q (worms present)
Days after preparation: 120

Sample Number	I.W. Depth (cm)	pH	Carb Alk. Meq/l	Cl^- Meq/l	Fe(II) µg-at/l	SRP µg-at/l	NH_4^+ µg-at/l	SiO_2 µg-at/l	Mn^{+2} µg-at/l	Ca^{+2} µg-at/l	Porosity %
0	O.W.	7.06	0.78		7.8	17.7	14	188			
1	0-1	7.06	2.39		99.8	128.9	256	819			78.7
2	1-2	7.23	2.69		53.7	116.3	259	749			77.3
3	2-3	7.22	2.96		78.3	109.5	201	828			76.8
4	3-4	7.25	3.17		76.2	92.7	179	906			76.0
5	4-5	7.31	3.30		71.1	102.1	201	968			76.4
6	5-6	7.22	3.46		73.9	105.9	154	1011			76.0
7	6-8	7.23	3.89		103.7	102.1	179	1035			75.2
8	8-10	7.23	4.22		107.6	106.9	221	1043			74.7
9	14-18	7.24	4.64		112.5	100.2	193	1048			74.2
10	22-26	7.25	4.97		119.7	104.2	218	1064			73.8

Core: HMC-O (worms present)
Days after preparation: 133

0	O.W.	6.83	0.85		28.6	6.1	118	161			
1	0-1	7.14	3.24		150.3	58.8	389	737			79.0
2	1-2	.	3.48		44.9	33.4	357	878			76.8
3	2-3	7.18	4.28		188.2	86.5	364	933			76.8
4	3-4	7.17	4.83		186.6	84.8	362	1002			75.7
5	4-5		4.89		147.7	91.5	352	1034			75.7
6	5-6	7.18	5.33		191.6	80.3	340	1036			75.5
7	6-8	7.19	5.74		190.6	80.6	312	1069			75.0
8	8-10	7.18	6.02		239.2	72.8	293	1058			74.8
9	14-18	7.23	6.43		209.8	50.3	287	1065			73.6
10	22-26	7.25	6.39		222.0	69.7	271	1078			73.8

Table 4. Flux Experiment Data (cont'd)

Core: HMC-H (no worms)
Days after preparation: 134

Sample Number	I.W. Depth (cm)	pH	Carb Alk. Meq/l	Cl^- Meq/l	Fe(II) µg-at/l	SRP µg-at/l	NH_4^+ µg-at/l	SiO_2 µg-at/l	Mn^{+2} µg-at/l	Ca^{+2} µg-at/l	Porosity %
0	O.W.	6.85	0.83		27.5	12.4	10	175			
1	0-1	7.34	2.96		139.5	77.7	123	811			79.5
2	1-2	7.33	3.61		149.3	80.9	122	956			76.8
3	2-3	7.31	4.07		166.2	87.4	131	1016			76.8
4	3-4	7.30	4.43		159.9	94.6	118	1015			75.7
5	4-5	7.43	4.52		162.8	80.9	145	1067			75.7
6	5-6	7.19	4.87		183.7	88.1	160	1078			75.5
7	6-8	7.21	5.26		186.4	85.7	168	1156			75.0
8	8-10	7.22	5.39		197.7	98.9	175	1100			74.8
9	14-18	7.14	5.89		187.6	63.3	189	1123			73.8
10	22-26	7.17	6.02		216.0	80.0	197	1123			73.8

Core: HMC-C (worms present)
Days after preparation: 148

0	O.W.	7.16	1.46		13.1	4.2	77	173	11	550	
1	0-1	7.11	2.00		22.8	6.7	110	417	16	650	82.0
2	1-2	7.17	2.43		15.6	4.3	141	504	32	750	81.4
3	2-3	7.13	2.82		13.9	3.8	136	564	23	900	82.3
4	3-4	7.20	3.14		14.2	8.2	147	642	27	1000	81.0
5	4-5	7.14	3.44		40.5	22.9	149	742	29	1100	76.8
6	5-6	7.16	3.81		53.6	29.4	162	854	32	1100	66.7
7	6-8	7.22	4.13		73.1	42.5	170	961	40	1350	75.2
8	8-10	7.18	4.41		89.2	53.4	185	1031	43	1400	7.53
9	14-18	7.13	5.12		88.1	52.2	180	1104	49	1650	7.53
10	22-26	7.13	5.31		60.6	49.6	194	1118	51	1700	7.41

Table 4. Flux Experiment Data (cont'd)

Core: HMC-J (no worms)
Days after preparation: 147

Sample Number	I.W. Depth (cm)	pH	Carb Alk. Meq/l	Cl^- Meq/l	Fe(II) µg-at/l	SRP µg-at/l	NH_4^+ µg-at/l	SiO_2 µg-at/l	Mn^{+2} µg-at/l	Ca^{+2} µg-at/l	Porosity %
0	O.W.	6.74	0.60		2.2	3.2	9	139	0	150	
1	0-1	7.19	2.58		63.0	43.3	110	711	20	700	78.8
2	1-2	7.34	2.92		57.8	43.5	135	857	26	950	77.0
3	2-3	7.38	3.31		64.9	42.2	142	961	32	900	76.8
4	3-4	7.34	3.53		74.1	48.4	142	951	33	1100	74.9
5	4-5	7.35	3.87		77.0	53.7	149	995	38	1250	75.9
6	5-6	7.30	4.13		74.8	56.7	167	1042	39	1250	77.0
7	6-8	7.60	4.26		75.3	48.5	174	1042	43	1300	76.3
8	8-0	7.44	4.58		90.4	61.4	184	1056	45	1400	75.2
9	14-18	7.54	5.12		104.2	61.4	213	1064	50	1700	74.3
10	22-26	7.33	5.42		108.8	38.4	206	1082	54	1750	73.7

Core: HMC-E (worms present)
Days after prepration: 169

0	O.W.	7.00	0.85		11.0	6.3	22	156	0	350	
1	0-1	7.10	3.54		199.7	60.0	287	626	28	1100	78.6
2	1-2	7.33	4.07		239.9	72.1	319	727	34	1300	76.3
3	2-3	7.39	4.52		236.2	70.5	330	800	43	1450	76.2
4	3-4	7.24	5.11		252.2	67.3	334	851	47	1600	75.7
5	4-5	7.36	5.28		238.6	70.9	340	875	47	1850	75.7
6	5-6	7.35	5.76		237.6	79.5	325	879	54	1800	74.5
7	6-8	7.12	6.24		264.9	75.7	304	885	57	2000	74.5
8	8-10	7.14	6.59		301.8	91.9	296	898	59	2100	73.9
9	14-18	7.19	7.26		276.6	69.1	255	892	64	2350	73.8
10	22-26	7.24	7.28		301.4	70.8	309	890	66	2400	73.9

Table 4. Flux Experiment Data (cont'd)

Core: HMC-T (no worms)
Days after preparation: 169

Sample Number	I.W. Depth (cm)	pH	Carb Alk. Meg/l	Cl^- Meg/l	Fe(II) µg-at/l	SRP µg-at/l	NH_4^+ µg-at/l	SiO_2 µg-at/l	Mn^{+2} µg-at/l	Ca^{+2} µg-at/l	Porosity %
0	O.W.	7.36	0.74		3.6	3.8	9	136	1	300	
1	0-1	7.16	3.00		132.6	51.1	145	530	25	1000	79.4
2	1-2	7.25	3.43		144.9	69.9	179	705	32	1200	77.8
3	2-3	7.26	3.78		152.4	61.2	166	759	33	1300	77.3
4	3-4	7.25	1.85		141.7	51.1	168	793	33	1400	76.9
5	4-5	7.24	6.52		152.1	51.1	171	823	41	1500	76.4
6	5-6	7.18	4.63		175.1	52.0	194	845	41	1500	75.6
7	6-8	7.28	7.15		172.9	45.3	220	877	46	1700	75.5
8	8-10	7.28	3.11		179.7	49.4	234	855	47	1750	74.6
9	14-18	7.29	6.13		182.9	52.6	271	866	51	2000	73.8
10	22-26	7.28	5.98		208.6	45.3	290	866	54	2150	73.2

Table 4. Flux Experiment Data (cont'd)

Core: LCE-8
Days after collection: 66

Sample Number	I.W. Depth (cm)	pH	Carb. Alk. meq/l	Cl^- meq/l	Fe (II) µg-at/l	SRP µg-at/l	NH_4^+ µg-at/l	SiO_2 µg-at/l
0	O.W.		2.17	.539	1.1	1.3	2	
1	0-1		2.34	.702	5.3	7.5	89	471
2	1-2		2.87	.727	107.9	50.2	121	684
3	2-3		3.36	.677	139.4	77.7	143	897
4	3-4		3.72	.689	128.8	86.8	160	975
5	4-5		4.38	.652	143.2	93.8	172	975
6	5-6		4.34	.664	74.1	59.3	154	858
7	6-8		4.30	.689	60.3	39.0	154	747
8	8-10		4.49	.664	23.8	12.9	174	607
9	14-18		3.83	.677	40.6	14.3	175	665
10	22-26		3.38	.702	39.3	22.5	320	742

Core: LCE-9
Days after collection: 84

0	O.W.		2.04	.548	0.4	1.4	2	316
1	0-1		2.42	.536	17.9	5.0	68	513
2	1-2		3.03	.536	136.2	33.9	115	743
3	2-3		3.58	.512	179.8	69.0	152	874
4	3-4		4.00	.524	183.6	76.9	166	907
5	4-5		4.24	.500	163.7	66.3	173	874
6	5-6		4.55	.524	167.6	73.2	155	841
7	6-8		4.81	.489	115.2	50.5	149	792
8	8-10		4.84	.536	103.5	24.3	123	710
9	14-18		4.00	.500	92.0	16.6	155	792
10	22-26		3.54	.548	75.6	15.8	153	841

Table 4. Flux Experiment Data (cont'd)

Core: LCE-12
Days after collection: 92

Sample Number	I.W. Depth (cm)	pH	Carb. Alk. meq/l	Cl^- meq/l	Fe (II) µg-at/l	SRP µg-at/l	NH_4^+ µg-at/l	SiO_2 µg-at/l
0	O.W.		2.22	.614	0.1	3.0	1	263
1	0-1		3.33	.476	190.8	64.9	172	1288
2	1-2		3.87	.476	279.0	65.7	223	1513
3	2-3		4.31	.501	189.3	63.0	274	1513
4	3-4		4.62	.489	141.3	52.1	243	1457
5	4-5		4.89	.501	94.8	50.9	240	1288
6	5-6		5.20	.514	70.7	43.2	217	1232
7	6-8		5.29	.501	59.6	21.5	178	1176
8	8-10		4.82	.526	60.9	14.1	178	1064
9	14-18		3.87	.501	42.2	7.9	194	1232
10	22-26		3.00	.501	36.1	7.9	232	1176

Table 4. Flux Experiment Data (cont'd)

Core: LCE-6
Days after collection: 13

Sample Number	I.W. Depth (cm)	pH	Carb. Alk. meq/l	Cl^- meq/l	Fe (II) µg-at/l	SRP µg-at/l	NH_4^+ µg-at/l	SiO_2 µg-at/l
0	O.W.		1.96	.489	0.0	0.8	8	127
1	0-1		2.27	.575	3.0	4.5	35	386
2	1-2		2.73	.546	69.6	25.8	73	674
3	2-3		3.07	.546	57.8	36.5	96	770
4	3-4		3.33	.575	32.2	26.7	104	770
5	4-5		3.44	.561	20.2	13.1	75	706
6	5-6		3.22	.574	11.6	7.4	63	626
7	6-8		3.53	.546	8.6	22.1	59	546
8	8-10		3.51	.575	12.7	7.0	63	530
9	14-18		2.67	.561	27.2	8.8	97	679
10	22-26		2.53	.546	19.2	10.1	117	785

Core: LCE-7
Days after collection: 29

0	O.W.	7.60	2.19	.547	14.6	15.8	39	203
1	0-1	7.56	2.96	.547	25.6	57.6	150	707
2	1-2	7.48	3.59	.560	34.3	79.0	149	919
3	2-3	7.65	3.96	.521	157.9	76.1	154	952
4	3-4	7.94	4.18	.573	120.9	60.1	167	883
5	4-5	7.40	4.69	.508	132.9	53.3	118	818
6	5-6	7.49	4.66	.547	101.3	28.5	124	740
7	6-8	7.38	4.74	.521	68.8	10.2	89	609
8	8-10	7.41	4.34	.521	101.0	20.1	115	661
9	14-18	7.45	3.53	.534	90.0	17.3	105	694
10	22-26	7.61	2.91	.508	74.4	25.1	115	772

Table 4. Flux Experiment Data (cont'd)